

**NUMERICAL TOOL FOR FATIGUE LIFE
PREDICTION OF CORRODED STEEL RIVETED
CONNECTIONS USING VARIOUS DAMAGE MODELS**

Ihab El Aghoury

A Thesis

in

The Department of
Building, Civil and Environmental Engineering

Presented in Partial Fulfillment of the Requirements
for the Degree of Doctorate of Philosophy (Civil Engineering) at

CONCORDIA UNIVERSITY
Montréal, Québec, Canada

April 2012

© Ihab El Aghoury, 2012

**CONCORDIA UNIVERSITY
SCHOOL OF GRADUATE STUDIES**

This is to certify that the thesis prepared

By: Ihab El Aghoury

Entitled: Numerical Tool for Fatigue Life Prediction of Corroded Steel Riveted Connections Using Various Damage Models

and submitted in partial fulfillment of the requirements for the degree of

DOCTOR OF PHILOSOPHY (Civil Engineering)

complies with the regulations of the University and meets the accepted standards with respect to originality and quality.

Signed by the final examining committee:

Chair

Dr R Raut

External Examiner

Dr. J. J. Cheng

External to Program

Dr. R. Sedaghati

Examiner

Dr. O. Pekau

Examiner

Dr. A. Bagchi

Thesis Supervisor

Dr. K. Galal

Approved by _____
Dr. K. Ha-Huy, Graduate Program Director

April 5, 2012 _____ Dr. Robin A.L. Drew, Dean
Faculty of Engineering & Computer Science

ABSTRACT

Fatigue of structural elements has been a major cause of many catastrophic failures of steel bridges. Corrosion is considered to be an influential factor that significantly contributes to the reduction of the fatigue life of steel structures. The objective of this research is to develop a numerical tool that is capable of predicting the fatigue life of steel members and connections while accounting for the effects of corrosion. To reach this goal, the research is divided into three phases.

In the first phase, a stress-life damage accumulation model (called the VTLC, for Virtual Target Life Curves) is proposed and validated using the experimental work available in the literature. The model has the advantage of including the effect of overloading. The VTLC model was verified using a case study of a riveted railway bridge.

In the second phase, a numerical tool is developed (named CorrFLP for Corrosion Fatigue Life Predictor). It acts as an add-on and uses available FEM packages as solvers. This tool is useful in predicting the fatigue life of railway or roadway steel bridges with riveted or bolted connections. CorrFLP uses the strain-life approach along with the theory of critical distances. CorrFLP is validated using several test results in the literature with and without the effect of corrosion.

To account for corrosion, a new fatigue strain-life model based on the Smith-Watson-Topper model is proposed in the third phase of this research. The model takes into account the corrosivity of the environment, the stress level, and the corrosive behaviour of the material used. A method is proposed to standardize a testing protocol to evaluate some new material constants that describe its behaviour in corrosive

environments. The proposed strain-life method is implemented in CorrFLP and the resulting fatigue life predictions matched well with reported experimental results of twenty-four steel beams subjected to various fatigue and weathering conditions.

It is seen that the developed numerical tool, along with the corrosion-fatigue strain-life based model, would help structural engineers by generating several stress-life design charts to predict the fatigue life of several commonly-used structural components while accounting for different levels of corrosion.

To my beloved wife, son, daughter, and family

ACKNOWLEDGEMENTS

I would like to express my sincere gratitude to my supervisor, Dr. Khaled Galal, for his guidance, encouragement and patience during my research. I believe that this research wouldn't have been completed without his continuous support. His efforts in reviewing and correcting this thesis drafts are greatly appreciated.

The financial support of the Canadian National Railway (CN) through their awards is greatly appreciated. Encouraging awards from Concordia University are also acknowledged.

Of course I wouldn't have reached this stage without the continuous help, guidance, support and care of my wife, my mother and father in every single stage of my life. I would like to thank all my professors in Ain Shams University, Cairo, Egypt. Their great help and support during my undergraduate study really helped me to have a strong academic background and to continue my studies here in Canada to achieve what I aimed for. I want to thank my friend Wael El-Haddad for continuously inspiring me during our studies together. I would like to thank my friend Ahmed Eweda for helping me so much on the final stages of presenting this thesis. I would also like to thank all my friends in Montréal for their support for me during my study.

Finally, I dedicate this thesis to my wife, my mother and my father, my sisters and all my friends and fellow colleagues for their invaluable support during my study. I also dedicate it to my lovely son and my newly born daughter. Their presence in my life was the main motivator for me to work hard on my research and achieve my goals.

TABLE OF CONTENTS

CHAPTER 1 INTRODUCTION	1
1.1 Background, problem definition, and need for research	1
1.2 Deterioration of Structures and the Need for Fatigue Life Prediction	2
1.2.1 Methods of Determining Fatigue Life	3
1.2.2 The Need for a Fatigue Life Prediction Software with Corrosion	4
1.2.3 Fatigue of Metals	4
1.2.4 Corrosion of Metals	5
1.2.4.1 Introduction	5
1.2.4.2 Corrosion-Fatigue	7
1.2.4.3 Factors Influencing Corrosion	8
1.2.4.4 Effects of Corrosion on Structural Components	9
1.3 Motivations for this Research	10
1.4 Objective and Scope of Research	12
1.5 Thesis Organization	13
CHAPTER 2 LITERATURE REVIEW	14
2.1 History of Fatigue	14
2.2 Fatigue Testing Approaches	15
2.2.1 Fatigue Evaluation of Riveted Connections	15
2.2.1.1 Fatigue testing without corrosion	16
2.2.1.2 Fatigue testing with corrosion	18
2.2.3 Evaluation of corrosion	21
2.3.1 Corrosion damage functions	21
2.3.2 Time of Wetness (TOW)	22
2.4 Fatigue Life Prediction Approaches	23
2.4.1 Stress-life method	24
2.4.2 Strain-life method	25
2.4.2.1 Principal strain criterion:	27
2.4.2.2 Von Mises equivalent strain criterion:	28
2.4.2.3 Smith-Watson-Topper relationship:	29
2.4.2.4 Maximum shear strain criterion:	29
2.4.2.5 Brown-Miller combined strain criterion:	30

2.4.2.6	Universal Material Method:	31
2.4.3	Energy-based method	32
2.4.4	Fracture Mechanics Approach	32
2.4.5	Theory of Critical Distances	33
2.5	Cycles Counting	34
2.5.1	Level-Crossing Counting	35
2.5.2	Peak Counting	35
2.5.3	Simple Range Counting	35
2.5.4	Rainflow Cycle Counting	35
2.6	Corrosion fatigue Life Prediction	36
2.7	Review on cumulative fatigue damage models	37
2.8	Review of Current Standards	38
2.9	Remaining Fatigue Life	41
2.10	Review on available finite element fatigue software	42
2.10.1	Introduction	42
2.10.2	Object Oriented Programming	43
2.10.3	Fe-Safe™ (2011)	43
2.10.3.1	MSC.Fatigue™ (2011)	44
2.10.3.2	FemFat™ (2011)	44
2.10.3.3	Ansys™ nCode Design Life (2011)	45
2.10.3.4	Comparison and Proposed tool	46
CHAPTER 3	DEVELOPMENT OF A FATIGUE ACCUMULATIVE-DAMAGE MODEL	48
3.1	Introduction	48
3.2	Review on Cumulative Damage Models	49
3.2.1	Miner's Linear damage Rule (LDR)	49
3.2.2	Marco-Starkey theory	50
3.2.3	Damage theories based on endurance limit reduction	51
3.2.3.1	Corten and Dolan theory	52
3.2.3.2	Manson's theories	53
3.2.3.3	S-N Curve modification theories	54
3.3	Factors Affecting Damage Models	55
3.3.1	Mean Stress Effects	55
3.3.2	Effect of Frequency	56

3.3.3	Effect of temperature	56
3.3.4	Effect of corrosion	56
3.3.5	Other effects from previous damage models	57
3.4	Proposed Damage Model	57
3.4.1	Discussion	57
3.4.2	Derivation	60
3.4.3	Overloading effect	65
3.4.4	Proposed procedure	66
3.5	Remaining life calculations	67
3.6	Validation	67
3.6.1	Introduction	67
3.6.2	Observations and Conclusions	70
3.7	Extending the methodology	71
3.8	Case Study	71
3.8.1	Geometry	72
3.8.2	Formation of the stress range spectrum	73
3.8.3	Fatigue Life Prediction using VTLC	76
3.8.4	Discussion and Conclusions	77
CHAPTER 4	NUMERICAL FORMULATION OF THE FATIGUE LIFE PREDICTION TOOL	79
4.1	Introduction	79
4.2	Pre-Processing Module	81
4.2.1	Model Preparation Section	81
4.2.2	Simulation Section	82
4.2.3	CorrFLP's User Interface	83
4.2.4	Material Editor	85
4.2.5	Spectrum Editor	86
4.3	Analysis Section	87
4.3.1	CorrFLP's Object Oriented Structure	87
4.3.2	Main Mesh Object	87
4.3.2.1	Fatigue Management Object	88
4.3.2.2	Corrosion Management Object	89
4.3.2.3	Temperature Management Object	89
4.3.2.4	Interaction Management Object	90

4.3.2.5	Refinement Management Object	90
4.3.2.6	Element Damage Management Object	91
4.3.2.7	Spectrum Management Object	91
4.3.2.8	Input/Output Management Object	91
4.3.2.9	FE Components Object	92
4.3.2.10	FE Containers Object	93
4.3.2.11	Searching Management Object	93
4.3.2.12	Statistics Management Object	94
4.3.2.13	Mesh Info Management Object	94
4.3.3	Cycle Jumps	94
4.3.3.1	The cycle jump concept	95
4.3.3.2	Calculation of Local Cycle jump	96
4.3.3.3	Choice of the Global Cycle jump	97
4.3.4	CorrFLP's Fatigue calculations:	98
4.3.4.1	Fatigue Life Prediction	98
4.3.4.2	Analysis Procedure	101
4.4	Post-Processing Phase	102
4.5	Verification with experimental results	102
4.5.1	Case Study 1: Plate with a circular hole	103
4.5.1.1	Test Description	103
4.5.1.2	Specimen Dimensions and Material Properties	103
4.5.1.3	Finite Element Model	104
4.5.1.4	Fatigue Life Prediction	105
4.5.2	Case Study 2: Riveted plates with staggered circular holes	107
4.5.2.1	Test description and geometry	107
4.5.2.2	Materials and Properties	107
4.5.2.3	Finite Element Model	109
4.5.2.4	Interaction surfaces	109
4.5.2.5	Fatigue Life Prediction	111
4.5.2.6	Discussion of results	115
4.5.3	Case Study 3: Built-up beams	116
4.5.3.1	Introduction	116
4.5.3.2	Experimental Tests	117
4.5.3.3	Materials	119

4.5.3.4	Experimental Test Procedure	120
4.5.3.5	Finite Element Model	120
4.5.3.6	Boundary Conditions and Loading	121
4.5.3.7	Modeling material properties	122
4.5.3.8	Fatigue Life Prediction	122
4.5.3.9	Summary	125
4.6	Discussion	125
CHAPTER 5	EFFECT OF CORROSION ON FATIGUE LIFE	127
5.1	Introduction	127
5.2	Implementing the effect of corrosion	128
5.2.1	Geometrical representation of corrosion	128
5.2.2	Proposed corrosion fatigue strain-life model	131
5.2.3	Calibration of the proposed model	135
5.2.4	Implementation in CorrFLP	139
5.3	CorrFLP (Corrosion Module) Verification	140
5.3.1	Introduction	140
5.3.2	Material	142
5.3.3	Finite Element Model	143
5.3.4	Fatigue Life Prediction	145
5.3.5	Discussion of results	147
5.3.5.1	Discussion of group 1 results	149
5.3.5.2	Discussion of group 2 results	149
5.3.5.3	Discussion of group 3 results	150
5.3.5.4	Conclusions	150
5.3.6	Standardizing a procedure for determining new material constants	152
5.3.7	Summary	152
5.4	Guidelines for developing corrosion-fatigue design charts	153
5.4.1	Introduction	153
5.4.2	Method for generating environmental S-N curves for various riveted details	154
5.4.3	Splice Plates	155
5.4.4	Angles connected to Gusset Plates	157
5.4.5	Angles in built-up Plate Girders	158
5.5	Future work	160

CHAPTER 6 CONTRIBUTIONS, CONCLUSIONS AND RECOMMENDATIONS	161
6.1 Summary and Contributions of this research	161
6.2 Features of the developed numerical tool:	163
6.2.1 CorrFLP Applications:	163
6.2.2 CorrFLP Advantages:	163
6.2.3 CorrFLP Current Limitations:	164
6.3 Significance of this Research	165
6.4 Conclusions	166
6.5 Recommendations for future work	168
REFERENCES	169
APPENDIX A	177
APPENDIX B	187
APPENDIX C	189

LIST OF FIGURES

Figure 2.1 Stable cyclic stress-strain hysteresis loops using Ramberg-Osgood equation (Dowling, 1999)	26
Figure 2.2 Cycle closure and material memory effect (Drapper, 2008)	27
Figure 2.3 Fatigue life of several riveted fatigue details from literature (adopted from Kulak (2005))	40
Figure 3.1 Possible trends in fatigue damage models (Hwang et al., 1986)	49
Figure 3.2 Load sequence effect in Marco-Starkey theory (1954)	51
Figure 3.3 Corten's hypothesis of the progress of fatigue damage (Corten et al., 1956) ..	52
Figure 3.4 Modified S-N curve approach	54
Figure 3.5 The proposed Virtual Target Life Concept	58
Figure 3.6 Comparison between the proposed VTLC and previous S-N curve modification approaches	59
Figure 3.7 VTLC as a measure of deterioration of structures	60
Figure 3.8 Change in slope in multi-stress level loading using a linear trend	63
Figure 3.9 VTLC as a measure of deterioration of structures	64
Figure 3.10 Schematic curve for the expected loss in life at each stress level	64
Figure 3.11 Testing Loading Pattern (Corten et al., 1956)	67
Figure 3.12 Analytical predictions of fluctuating stress amplitude experiments with high stress of 96,000 psi using three methods: VTLC, Corten, and Miner.	69
Figure 3.13 Analytical predictions of fluctuating stress amplitude experiments with high stress of 86,000 psi using three methods: VTLC, Corten, and Miner.	69
Figure 3.14 Structural System of the truss bridge showing the investigated member D-36	72
Figure 3.15 VTL curves for the investigated member D-36 showing the deterioration in fatigue life with years (assuming the detail is category D)	76
Figure 3.16 VTL curves for the investigated member D-36 showing the deterioration in fatigue life with years (assuming the detail is category C)	77
Figure 4.1 Illustration for the three main modules of CorrFLP and the interaction between applying damage and cycle jumps	80
Figure 4.2 Schematic drawing for the CorrFLP and ABAQUS TM communication process	83
Figure 4.3 CorrFLP's user interface snapshot	84
Figure 4.4 CorrFLP's material editor (showing the list of built-in materials library)	85
Figure 4.5 CorrFLP's spectrum editor (a) Input window, and (b) History graph window ..	86
Figure 4.6 Schematic drawing for the mesh managers in CorrFLP	88
Figure 4.7 Supported formats for the Input Output Management Object	92
Figure 4.8 Components managed by the FE Components Management Object	92
Figure 4.9 Containers managed by the FE Containers Management Object	93
Figure 4.10 The super cycle and cycle jump concept Paepelgem et al. (2001)	95
Figure 4.11 Damage extrapolation and corresponding cycle jump	96
Figure 4.12 Choice of global cycle jump based on frequency distribution (Paepelgem et al., 2001)	97

Figure 4.13 Sub-meshing of critical (parent) elements into fine (children) elements	99
Figure 4.14 Propagation of Damage in (children) elements	100
Figure 4.15 Schematic flow chart for the analysis process showing the “Management Object” responsible for each task	101
Figure 4.16 Test specimens from Sehitoglu (1983)	103
Figure 4.17 The finite element model (Loading on the left, meshing on the right) using CorrFLP	104
Figure 4.18 Damage during the crack initiation life using CorrFLP	105
Figure 4.19 Predicted lives using CorrFLP vs. experimentally observed by Sehitoglu (1983) using three different criteria	106
Figure 4.20 Test specimens of Josi et al. (1999).....	108
Figure 4.21 The Finite Element model for series (S0) from Josi et al. (1999) (Meshing on the left and boundary conditions on the right) using CorrFLP	109
Figure 4.22 Locations of interaction surfaces in the Finite element model.....	111
Figure 4.23 Section cut in the CorrFLP FE model showing the stress distribution and the relative sliding between interaction surfaces (Scaled deformed shape for illustration) .	112
Figure 4.24 Damage during the crack initiation life using CorrFLP surfaces (Scaled deformed shape for illustration).....	112
Figure 4.25 Predicted lives using CorrFLP vs. experimentally observed by Josi et al. (1999) using three different criteria	115
Figure 4.26 Riveted Girders tested by Fisher et al. (1988).....	118
Figure 4.27 Cross-Section of tested girders Fisher et al. (1988)	118
Figure 4.28 Extraction of modeled part in CorrFLP analysis.....	121
Figure 4.29 Finite Element Model for Santa Fe Girders (Loading and boundary conditions on the left, meshing on the right)	122
Figure 4.30 Plot for Fatigue crack initiation lives for Santa Fe Girders from the NCHRP report 302 (1988) vs. those from CorrFLP simulation	123
Figure 4.31 Reported crack initiation and propagation (Fisher et al., 1988) vs. CorrFLP damage initiation for specimen SF-2	124
Figure 5.1 Stress concentration factor due to pitting corrosion depending on pit shape (Cerit et al., 2009)	129
Figure 5.2 Assigning corrosion rate factors for mesh surfaces in CorrFLP	130
Figure 5.3 Simulation of corrosion thickness loss on selected critical surfaces	130
Figure 5.4 Relationship between total strain amplitude and endurance in a non-corrosive environment	132
Figure 5.5 Relationship between total strain amplitude and endurance in a highly corrosive environment	133
Figure 5.6 Plot for the proposed relation between the log of the penetration versus the proposed corrosion factor γ_{corr}	136
Figure 5.7 Fatigue strength of two year weathered plain rolled SMA steel specimens (Kunihiro et al., 1972).....	137
Figure 5.8 Kunihiro et al. (1972) data points converted into strain-life data points and fitted	138
Figure 5.9 Corrosion of weathering steel compared with copper-bearing and mild steels (Albrecht, 1983).....	139
Figure 5.10 Configurations of tested beams (Albrecht et al., 1994).....	141

Figure 5.11 Test matrix and corrosion rates table adapted from Albrecht et al. (1994).	141
Figure 5.12 Finite element model for the girder (loading and boundary conditions in the top, meshing and cross-section in the bottom).....	143
Figure 5.13 Plot of γ_{corr} γ_σ values versus σ_{max} / σ_u	145
Figure 5.14 Predicted lives using CorrFLP vs. experimentally observed by Albrecht et al. (1994).....	148
Figure 5.15 Sample S-N curves for a studied detail for several corrosion rates.....	155
Figure 5.16 The finite element model for “Splice Plate” series	156
Figure 5.17 Schematic drawing for the test variables.....	156
Figure 5.18 The finite element model for the “Angles connected to Gusset Plates” series	157
Figure 5.19 Schematic drawing for the test variables.....	158
Figure 5.20 The finite element model for the “Built-up Beam” series	158
Figure 5.21 Schematic drawing for the test variables.....	159

LIST OF TABLES

Table 2.1	TOW categories according to ISO standard 9223 (1992)	23
Table 2.2	Coefficients for deriving the cyclic coefficients using the Universal Material Method.....	31
Table 2.3	A comparison of features offered by commercial fatigue postprocessors and the proposed tool CorrFLP. (Maximum is marked with five stars, whereas No stars corresponds to no implementation).....	46
Table 3.1	Tables reported by Kühn, et al. (2008) for estimated damage from (a) 1895-1980, and (b) 1980-2000	74
Table 3.2	Chronologically ordered data from Kühn et al. (2008) report	75
Table 4.1	Observed Results from Josi et al. (1999) vs. minimum and maximum expected cycles to crack initiation from CorrFLP	114
Table 4.2	Selected Specimens in this study from NCHRP Report 302 (1988).....	119
Table 4.3	Material properties of NCHRP report 302 (1988).....	119
Table 4.4	Fatigue Crack initiation lives for Santa Fe Girders from the NCHRP report 302 (1988) and from CorrFLP simulation.....	123
Table 5.1	Correlation between and the ISO-9224 categories.....	136
Table 5.2	Input data for the finite element model	144
Table 5.3	Derived Corrosion factors and estimated number of cycles to failure	146

LIST OF SYMBOLS

a	[-]	Universal Material method factor
b	[-]	Fatigue strength exponent
b'	[-]	Fatigue strength exponent in an NaCl 3.5% corrosive environment
b_v	[-]	Virtual life curve slope
b_{vi}	[-]	Virtual life curve slope at stress level i
c	[-]	Fatigue ductility exponent
c'	[-]	Fatigue ductility exponent in an NaCl 3.5% corrosive environment
C	[-]	Marco-Starkey power exponent
C_L	[-]	Load cycles per truck
D	[-]	Accumulated fatigue damage
D_0	[-]	Previous damage state
e	[-]	Normal strain on given plane
E	[MPa]	Elasticity modulus in tension
F	[N]	External force
g	[-]	Shear strain on given plane
g_r	[-]	Traffic growth rate
G	[MPa]	Elasticity modulus in torsion
K'	[MPa]	Cyclic strength coefficient
K_C	[MPa.m ^{1/2}]	Critical stress intensity factor
L	[m]	Critical length
m	[-]	Slope of S-N curve
n'	[-]	Cyclic strength exponent
n_i	[-]	Number of cycles applied under the i^{th} constant-amplitude loading level
N	[MPa]	Normal stress on given plane
N'_i	[-]	Modified life in Leipholtz's model
N_f	[-]	Number of cycles to failure
N_{fl}	[-]	Cycles to failure under constant-amplitude loading level for high stress level
N_{f2}	[-]	Cycles to failure under constant-amplitude loading level for low stress level
N_{acc}	[-]	Total accumulated cycles
N_{fi}	[-]	Number of cycles to failure under the i^{th} constant-amplitude loading level
N_{VTL}	[-]	Number of cycles to reach the virtual target life
p	[-]	Material constant for overstress effect
p_a	[-]	Average annual penetration due to corrosion
r_b	[-]	Ratio of S_2/S_1
R	[-]	Stress ratio (low to high stress)
R_L	[-]	Remaining life of a detail
S_1	[MPa]	High stress level
S_2	[MPa]	Low stress level
S_u	[MPa]	Ultimate strength
S_y	[MPa]	Yield strength
Y	[-]	Number of years
α	[-]	Corten's high to low stress level number of cycles ratio
α_b	[-]	Ratio of b'/b
α_c	[-]	Ratio of c'/c
β_i	[-]	Frequency of cycles in Leipholtz's model
Δb_i	[-]	Change in virtual life curve slope in cycle block i .
Δb_{Di}	[-]	Change in virtual life curve slope due to overstress loading
Δb_{vo}	[-]	Total expected change in virtual life curve slope under constant amplitude loading
$\Delta N_{\text{expected}}$	[-]	Difference between the VTL and the S-N curve life at a certain stress level
$\Delta \varepsilon$	[-]	Strain range
$\Delta \varepsilon_l$	[-]	Principal strain range
$\Delta \varepsilon_{EFF}$	[-]	Effective Von Mises strain range
$\Delta \varepsilon_N$	[-]	Nominal strain range perpendicular to the plane of maximum shear strain range

$\Delta\gamma_{max}$	[MPa]	Maximum shear strain range
ΔK_{th}	[MPa.m ^{1/2}]	Fatigue threshold stress intensity factor
$\Delta\sigma$	[MPa]	Stress range in fatigue
$\Delta\sigma_0$	[MPa]	Critical stress range in fatigue
ε'_f	[-]	Fatigue ductility coefficient
ε_n	[-]	Normal strain
γ	[-]	Shear strain
γ_{corr}	[-]	Environment corrosivity intensity factor
γ_σ	[-]	Correction factor depending on the maximum applied stress
ν	[-]	Poisson's ratio
ν^*	[-]	Equivalent Poisson's ratio
σ_0	[MPa]	Fatigue limit in repeated tension
σ_a	[MPa]	Stress amplitude
$\sigma_{l,max}$	[MPa]	Maximum principal stress
σ_{max}	[MPa]	Maximum normal stress
σ_n	[MPa]	Normal stress
σ'_f	[MPa]	Fatigue strength coefficient
σ_H	[MPa]	Hydrostatic stress
τ	[MPa]	Shear stress

NOMENCLATURE

AASHTO	American Association of State Highway and Transportation Officials
ADT	Average Daily Traffic
ADTT	Average Daily Truck Traffic
AREA	American Railway Engineering Association
DCA	Damage Curve Approach
DDCA	Double Damage Curve Approach
DLLR	Double Linear Damage Rule
ECCS	European Convention for Constructional Steelwork
EPFM	Elastic Plastic Fracture Mechanics
FE	Finite Element
FEA	Finite Element Analysis
FEM	Finite Element Method
FT	Percentage of Truck traffic
FL	Percentage of Trucks in the main lane in highways
HCF	High-Cycle Fatigue
LCF	Low-Cycle Fatigue
LCM	longest chord method
LDR	linear damage rule
LEFM	Linear Elastic Fracture Mechanics
LHS	left hand side of equation
LPM	longest projection method
MD	critical plane set according to Maximum Damage criterion
MS	mean stress
MSE	mean stress effect
SWT	Smith, Watson & Topper method of uniaxial fatigue damage calculation
TOW	Time Of Wetness
VTL	Virtual Target Life
VTLC	Virtual Target Life Curves

CHAPTER 1

INTRODUCTION

1.1 Background, problem definition, and need for research

North America has a large inventory of riveted railway and roadway steel bridges' infrastructure that is rapidly aging and is in continuous need for regular inspection, monitoring and maintenance. One of the main components of an effective structural evaluation of steel bridges is to determine the remaining fatigue life of the structure. Corrosion is considered to be an influential factor that significantly contributes to the reduction of the fatigue life. The corrosion process is highly accelerated in cold climate regions where de-icing salt is regularly used. Laboratory fatigue testing is the most accurate method for determining the fatigue life of structural elements or small assemblages. The drawback is that such tests are costly, time consuming, usually based on constant amplitude loading, and being specific to a certain detail. Moreover, simulating corrosion experimentally along with fatigue loading is challenging, expensive, and has several limitations. On the other hand, the other alternative for fatigue life prediction is to carry out stress or strain analysis using the finite element method (FEM) along with selecting an appropriate damage law. Unfortunately, there is a limitation in the damage models that account for fatigue-corrosion interaction, thus the fatigue life prediction using the finite element is limited to cases where there is no severe corrosion.

The following sections provide a brief description on the amount of deterioration in the existing infrastructure, as well as the needs and means for fatigue life prediction taking into account the effect of corrosion.

1.2 Deterioration of Structures and the Need for Fatigue Life Prediction

Recent survey reported by the American Society of Civil Engineers (ASCE, 2005) estimates that almost one-quarter of the North America's bridge inventory are rated structurally deficient or functionally obsolete. Over 40% of Canada's Bridges are over 40 years old and a significant percentage of them are structurally or functionally deficient (Lounis, 2007). Existing bridges are experiencing accelerated deterioration due to increasing traffic demands, higher loads, harsh environment, along with inadequate maintenance funding.

Fatigue has consistently been a major source of many bridge catastrophic failures throughout history. On the other hand, corrosion resulted in similar catastrophic failures of bridges. Back in 1967, Ohio silver bridge collapsed due to a miniature crack caused by stress corrosion cracking in one of its main eye-bar connections. It is worth mentioning that the loads at the time of collapse were tripled with respect to the service loads at the time of construction in a period of 39 years.

There are several initiatives for predicting the fatigue life of different structural details, yet they are -until now- uni-dimensional, with serious limitations in incorporating the interaction between sources of fatigue, such as: loading amplitude, loading sequence, mean stress, stress gradients, residual stresses, temperature, corrosion, and metallurgy of the metal, pre-existence of micro-cracks. Although fatigue life is affected by several factors, corrosion is considered to be one of the factors that significantly contribute to the reduction of the fatigue life. The corrosion process is highly accelerated in snowy regions where there is excessive use of de-icing salt like Canada. Therefore, there is a need to

have an accurate methodology to determine the remaining fatigue life of deteriorating structures.

1.2.1 Methods of Determining Fatigue Life

Traditionally, fatigue life prediction is determined experimentally, but the drawback is that fatigue tests are costly, time consuming, and are usually based on constant amplitude loading and specific to a certain detail. Moreover, experimental work is generally neither timely nor statistically comprehensive for a majority of designers.

Modern structural design codes of practice usually refer to well-known damage accumulation rules such as Miner's rule (Miner, 1945) to predict the fatigue life of specific details, by knowing its expected loading history in a simplified empirical way. All civil engineering codes use the “stress-life” approach, which is based on the net section stresses and fatigue category of the structural detail in study. That method could be conservative in some cases or it could be detrimental if the engineer does not know the rationale behind the choice of the code fatigue limits, or does not have detailed data regarding the real/expected loading history of the structure. Moreover, codes of practice do not have detailed provisions or guidelines for the predicting fatigue life of corroding structural components.

Another alternative approach is to predict the fatigue life of a specific structural critical component (e.g. a connection) by a strain analysis using the finite element method. This could be achieved by applying the actual loading along with selecting an appropriate damage law based on the “strain-life” method, or stress analysis along with applying the “theory of critical distances”. Currently (2012), the software packages that

are capable of such analyses are not widely available and have several limitations that will be discussed in details in Chapter 2.

1.2.2 The Need for a Fatigue Life Prediction Software with Corrosion

The advancements in the field of numerical simulations of structures using the finite element method (FEM) in the last few decades encouraged engineers and researchers to develop post-processing programs to estimate the fatigue life of structural components. Despite this advancement, there is still a need for more research in the field of fatigue life prediction of structural components using the FEM. A literature survey of the advancements and limitations of fatigue life prediction tools will be discussed in Chapter 2. Until now, up to the author's knowledge, there is no evaluation tool that accounts for the structural response under the combined effects of fatigue and corrosion using the finite element method. Corrosion is known to accelerate the fatigue process and reduce the fatigue life of a given detail depending on the severity of corrosion and the corrosion type (Du, 1998). Hence, there is a need to develop a fatigue life prediction numerical tool that accounts for the effects of corrosion.

1.2.3 Fatigue of Metals

Fatigue cracking occurs even if the maximum applied stress is less than the elastic limit of the metal. A fatigue crack usually originates at a location of stress concentration, such as an existing material/manufacturing flaw or an abrupt geometrical discontinuity in the material. While almost all metals can exhibit fatigue cracking, structural engineers are often concerned with the fatigue performance of structural steel as most of fatigue-critical structures such as bridges, offshore structures and towers are usually made of steel. The

dominant variables that influence the fatigue strength of structural steel are the applied stress range, the number of cycles of applied stress, and the type of structural detail (Fisher, 1977).

Fatigue failures typically involve minimal levels of plastic deformation. Consequently, it can be difficult to detect fatigue cracks before fracture of the remaining cross-section occurs. Many examples of catastrophic failures caused by fatigue cracking have been documented by Fisher et al. (1987) illustrating that structural engineer must have a firm understanding of the phenomenon of fatigue. Many civil engineering structures, such as bridges, cranes or offshore structures are required to withstand the effects of high cycle fatigue because of the nature of the moving or repeated loads that they must carry.

1.2.4 Corrosion of Metals

1.2.4.1 Introduction

Corrosion is a process of degradation of a metal by an electrochemical reaction with its environment. This means a loss of electrons of metals reacting with water and oxygen. For example, weakening of iron due to oxidation of the iron atoms is a well-known example of electrochemical corrosion which is commonly known as rust. This type of damage usually affects metallic materials, and typically produces oxide(s) and/or salt(s) of the original metal. Corrosion could be categorized into several types (USACE(EM), 2001):

1- General atmospheric corrosion: is defined as a slow uniform corrosive attack that results in a uniform thinning spread over a wide area that is not likely to cause

significant structural degradation in a short period of time. This type of corrosion can be easily measured.

2- Crevice corrosion: occurs in narrow openings between two contact surfaces, such as between adjoining plates or angles in a connection. It can lead to blistering and failure of the paint system, which further promotes corrosion

3- Pitting corrosion: occurs on bare metal surfaces as well as under paint films. It is characterized by small cavities penetrating into the surface over a localized area (at a point). If pitting occurs, it can rapidly accelerate the fatigue damage.

4- Galvanic corrosion: can occur in when steels with different electrochemical potential (dissimilar metals) are in contact. The corrosion typically causes blistering or discoloration of the paint and failure of the paint system adjacent to the contact area of the two steels and decreases as the distance from the metal junction increases.

5- Stray current corrosion: may occur when sources of direct current (i.e., welding generators) are attached to the structure, or unintended fields from cathodic protection systems are generated.

6- Filiform corrosion: occurs under thin paint films and has the appearance of fine filaments emanating from one or more sources in random directions.

7- Erosion corrosion: is caused by removal of surface material by action of numerous individual impacts of solid or liquid particles and usually has a direction associated with the metal removal.

8- Cavitation corrosion: is caused by cavitations associated with turbulent flow. It can remove surface films such as oxides or paint and expose bare metal, producing rounded micro craters.

9- Fretting corrosion: is a combination of wear and corrosion in which material is removed between contacting surfaces when very small amplitude motions occur between the surfaces.

10- Stress Corrosion: Corrosion can cause many types of surface micro-cracking, for example: Stress corrosion cracking (SCC) is the cracking induced from the combined influence of tensile stress and a corrosive environment. The impact of SCC on a material usually falls between dry cracking and the fatigue threshold of that material. The required tensile stresses may be in the form of directly applied stresses or in the form of residual stresses (KTS, 2010).

In civil engineering applications, there are some common causes for corrosion; next sections will briefly discuss them.

1.2.4.2 Corrosion-Fatigue

Corrosion-fatigue is the result of the combined action of an alternating or cycling stresses and a corrosive environment. The fatigue process is thought to cause rupture of the protective passive film, upon which corrosion is accelerated. If the metal is simultaneously exposed to a corrosive environment, the failure can take place at even lower loads and shorter time. The fatigue fracture is brittle and the cracks are most often transgranular, as in stress-corrosion cracking, but not branched. Usually corrosion-fatigue cracks are widened by a secondary corrosion reaction. The corrosive environment can cause a faster crack growth at a lower tension level than in dry air. Even relatively mild corrosive atmospheres can reduce the fatigue strength of aluminum structures considerably, down to 75% (or even 25%) of the fatigue strength in dry air (KTS, 2010). Fatigue cracks usually nucleate from the surface (Argon, 1971). In case of metals in a

corrosive environment, the environment produces surface roughening (Hunsche et al., 1988). Moreover, it is known that pitting is the most common and important form of corrosion and it was observed that fatigue cracks initiate on surfaces roughened by pitting corrosion (Kawahara et al., 1988).

Corrosion is among the major factors affecting durability and service life of bridges, particularly those located in cold regions where de-icing salts and other aggressive chemicals are used that accelerate the corrosion process. This is common in Canada.

1.2.4.3 Factors Influencing Corrosion

Many factors could affect the corrosion rate such as the design details, material properties, maintenance, operation, environment, and coating system. In general, the primary influencing factors are the local environment and the protective coating system. The following is brief description of the most important factors.

The pH value of the surrounding environmental significantly affects the corrosion rate. Corrosion usually occurs at low pH (highly acidic conditions) or at high pH (highly alkaline conditions). At intermediate pH, a protective oxide or hydroxide often forms. Deposits of film-forming materials such as oil and grease, and sand and silt can also contribute to corrosion by creating crevices and ion concentration cells.

The most important substance involved in the atmospheric deterioration of metals is sulphur dioxide (NACE, 2011). Also, steel structures that are near the sea would be significantly affected by the presence of chlorides. The corrosion rate of ferrous metals is determined by two factors, namely the time of wetness and the rate of sulphur deposition. The corrosion itself is an electrochemical process that operates in the presence of water.

Any dissolved air pollutant ions that may be present increase the conductivity and, therefore, the rate of corrosion (Boden, 1989).

Corrosion of steel increases significantly when the relative humidity is greater than 60%. Corrosion is also aggravated by alternate wet and dry cycles, where it was found that longer periods of wetness tends to increase the effect (USACE(EM), 2001).

Paint and other protective coatings are the primary preventive measures against corrosion on hydraulic steel structures. Sharp corners, edges, crevices, weld terminations, rivets, and bolts are often more susceptible to corrosion since they are more difficult to coat adequately. Any variation in the paint system can cause local coating failure, which may result in corrosion under the paint (USACE(EM), 2001).

Snow fighting has a long history. However, the first use of salt for de-icing roads can only be traced back to the 1930s and it was not until the 1960s that the use of salt in conjunction with blowing became widespread after winter maintenance personnel learned of its effectiveness (KTS, 2010).

1.2.4.4 Effects of Corrosion on Structural Components

Corrosion can seriously weaken a steel structure or impair its integrity as it affects the strength, stability, and serviceability of the structure. A study on the cost and preventative strategies mandated by the U.S. Congress estimated the total direct cost of metal corrosion in 26 industrial sectors to be US\$276 billion per year (Koch et al., 2002). The major degrading effects of corrosion on structural members are a loss of cross section leading to increase in stress levels. Also, accumulation of corrosion products (rust) at structural connections, for example between the web and the adjacent plates or

angles of a built-up section, would cause prying action. This is referred to as corrosion pack out and results from expansion during the corrosion process. Also localized pitting corrosion can form notches that may serve as fracture initiation nodes. Also, notching is known to reduce the fatigue life of a steel member significantly.

1.3 Motivations for this Research

Due to the difficulty and limitations of fatigue life prediction tests, the author was motivated to develop a numerical tool to predict the fatigue life for any steel assembly (riveted or bolted) using the finite element method. Although corrosion can drastically reduce the fatigue life of structural components, this effect has not been thoroughly studied by researchers in the field of structural engineering and is not explicitly quantified in almost all design codes of practice. The methodology that the author adopted to address this shortage is by modifying the strain-life fatigue life prediction method to account for the effects of corrosion. This can enable designers to estimate the fatigue life of any structural component in any corrosive environment. This research will approach the corrosion problem geometrically by modelling the thickness loss and numerically by the newly proposed strain-life model.

On the other hand, structural engineers normally use the stress-life method along with the constant amplitude S-N curves for fatigue life prediction. It is not feasible for most of structural engineers to perform a detailed strain analysis of a structural component. Moreover, most structural engineers may not have enough detailed knowledge of the details of the fatigue phenomenon nor the concepts of fracture mechanics. Thus, for design purposes, the developed numerical tool is intended to bridge

the gap between civil engineering and fracture mechanics by being able to generate several fatigue design charts taking into account the effects of corrosion.

Most of the current structural engineering codes of practice recommend the use of Miner's linear damage accumulation rule in fatigue life calculations due to its simplicity. It will be further discussed in Chapter 3 that this approach can be sometimes detrimental to the safety of the bridge structure. Thus, a new stress-based fatigue damage accumulation model is proposed and verified using experimental test results from literature.

1.4 Objective and Scope of Research

The objective of this research is to develop a numerical tool that is capable of predicting the fatigue life of steel members, connections, and assemblages while accounting for the effects of corrosion, and real complex loading patterns. In order to reach this objective, the scope of this study is to:

1. Propose a new stress-life damage accumulation model based on the review the existing stress-life based fatigue damage accumulation models.
2. Develop a numerical tool using the finite element method and utilising the strain-life fatigue life prediction approach along with the Theory of Critical Distances to predict the remaining fatigue life of different structural details.
3. Verify results obtained from the finite element tool against experimental data and classical linear fracture mechanics.
4. Extend the numerical tool's capabilities to include the geometrical effect of corrosion.
5. Propose a new strain-life corrosion-fatigue model and propose a standardized experimental methodology for determining the newly proposed corrosion material properties.
6. Perform several validation examples versus experimental tests for fatigue and corrosion to verify the developed numerical tool.
7. Providing guidelines for developing S-N design charts for structural engineers for predicting the fatigue life of various important riveted and bolted structural details while accounting for the effect of corrosion.

1.5 Thesis Organization

The thesis is arranged as follows: Chapter 2 is a literature review on fatigue life prediction approaches, available fatigue analysis software, limitations in current codes of practice. Chapter 3 reviews different stress-life fatigue damage accumulation models and proposes a new model. Chapter 4 discusses the implementation of a proposed numerical tool using the strain-life methods and its technical details in addition to three verification examples. The verification examples highlight the ability of the proposed tool to predict crack initiation life of any plane or riveted component. Chapter 5 proposes a new strain-life corrosion fatigue model that incorporates the mean stress effects and also proposes new corrosion material properties along with an experimental methodology for determining the newly proposed corrosion material properties. Chapter 5 extends the features of the numerical tool to include the effect of corrosion in the finite element simulation with a validation example that highlights the capabilities of the proposed numerical tool in simulating corrosion. Different conclusions and recommendations are drawn. Consequently, qualitative guidelines are proposed for deriving environmentally dependant design charts for several commonly used riveted connection details under different corrosion levels based on the stress-life approach. Finally, Chapter 6 summarizes this research, its applications and limitations, as well as the conclusions and recommendations for future work.

CHAPTER 2

LITERATURE REVIEW

2.1 History of Fatigue

For more than 150 years, numerous research studies were conducted by mechanical engineers, material scientists, physicists, chemists and mathematicians to understand the fatigue phenomenon. In 1870, Wohler published his results of fatigue tests of railway axles and constructed the S-N curves concept. In 1899, Goodman developed a method for fatigue life calculation at different levels of cyclic stresses. Later in 1924, Palmgren provided a simple criterion for predicting the extent of fatigue damage induced by various stress blocks and was later formulated by Miner in 1945 (Miner, 1945), which was thereafter known as Palmgren-Miner cumulative damage law. In 1970, Elber (1970) first introduced the crack closure phenomenon which is still a challenging and controversial topic until now. In 1965, studying of fatigue crack propagation was first embraced by Paris et al. (1961) namely, the Paris law which relates the rate of advancing of the fatigue crack width per stress cycle, da/dN , to the range of the stress intensity factor ΔK . More than 10 years after Paris law, the cyclic J-integral range was proposed by Dowling and Begley (1976) characterizing the advance of crack under elastic-plastic conditions. Since then, hundreds of researchers added to the body of knowledge. More details about fatigue study history are described in (Schutz, 1996). One of the latest advances in the fatigue and fracture mechanics is the development of the “Theory of Critical Distances” (TCD) (Taylor, 2008) which sums up the pioneering work done by Neuber (1958), Peterson (1959) and El Haddad et al. (1979).

2.2 Fatigue Testing Approaches

This section describes the fatigue testing as pertinent to structural engineering applications without getting into the applications within fracture mechanics context. Many fatigue tests that were reported in literature helped shaping the current S-N curves (Stress range – Number of cycle's relationship) in various codes of practice. Many of these experimental results were reporting tests of either welded details or riveted details. As this thesis focuses on the fatigue behaviour of riveted details, a review of previous tests on riveted connections only will be conducted. For a more detailed review of other fatigue tests in literature, refer to the survey done by El-Sisi (2009). Fatigue tests reported in the literature will be divided into two main groups; fatigue tests without studying corrosion and fatigue tests with corrosion.

2.2.1 Fatigue Evaluation of Riveted Connections

Connections (either riveted or bolted) are the most essential components in non-welded bridges. It is important to adequately design these connections for fatigue. Although it is usual in contemporary design for fatigue resistance of bolted connections to use slip-critical joints, many existing bridges are more likely to have bearing-type joints that use either rivets or high-strength bolts that usually have staggered holes' patterns. Fatigue fracture of tension members with bearing-type joints that use staggered holes is observed to take place on a plane perpendicular to the axis of the member. The $s^2/4g$ rule set by Cochrane (1922) (where s and g are the spacings between the bolt rows in the direction of the loading and the perpendicular direction, respectively), commonly used for static strength design of bolted tension members, is not applicable for this case.

Moreover, according to Josi et al. (1999) there is no clear definition for what net section is to be used to calculate the stress range in fatigue. Literature reports many tests that were conducted to evaluate the fatigue life of riveted connections, as will be discussed in the next two sections.

2.2.1.1 Fatigue testing without corrosion

Reemsnyder (1975) investigated full scale specimens of gusset plate connections from an “ore bridge” under fatigue loading. Tests showed that specimens which originally had rivets that were replaced with high strength bolts at locations of observed or anticipated cracking, experienced an increase in the fatigue life of about 2 to 6 times and retarded the crack growth and prevented crack initiation. An increase in bolt clamping force from 70% to 90% of the bolts yielding strength slightly increased the fatigue life. Baker et al. (1985) investigated the fatigue life of riveted connections by conducting fatigue tests on 11 riveted girders. High strength bolts were used to replace missing rivets. Riveted connections had a fatigue life greater than the referred detail category D in AASHTO.

Fisher et al. (1989) published a report on fatigue evaluation of riveted bridges with an extensive review of previous fatigue data on riveted shear splices and full-scale members. They concluded that differences between riveted details were not significant and that category D provided a lower bound for crack detection. They also noted that the failure of the cross section and the loss in loading capacity did not happen until category C was reached. The results obtained from testing various riveted details were very scattered and it would be very conservative to assign them all to category D, knowing that these categories were first created for welded details which are different in behaviour

than riveted and bolted details. Mang et al. (1993) investigated methods to determine the remaining life of riveted structures. They conducted fatigue tests on thirteen full scale main girders from bridges taken out of service. It was noticed that the previous load history of the tested specimens did not seem to affect the fatigue life. Tests with high strength bolts provided positive response of the fatigue performance.

Zhou et al. (1995) investigated the effect of clamping force of rivets and the influence of hole preparation on fatigue capacity. Tests with constant amplitude limit were performed at stress levels under 70 MPa. Investigations concerning the cut off limit were performed with stress ranges from 44.1 MPa to 54.4 MPa with a stress spectra provided by the Canadian National (CN) North America Railway. A total of 20 tests were performed, 12 at constant amplitude and 8 with a varied stress range. The result showed that rivet holes were the most frequent origin for crack initiation and was depending on the surface of the hole. Other factors were corrosion and welding. Girders with punched holes provided lower fatigue endurance than drilled or sub punched and reamed. The fatigue limit where no fatigue damage occurred was determined to be 41 MPa. The fatigue detail category D of the American Railway Engineering Association (AREA) (AREA, 1987) provided a lower bound for riveted girders in general and wrought iron girders exhibited lower fatigue endurance than steel. Category C is equivalent to category 71 in Eurocode (Eurocode3, May 2003).

Al-Emrani (2002) investigated the fatigue endurance of stringers. The fatigue threshold was investigated at a stress range of 60 MPa. The European design curve $C = 71$ provided a lower bound estimation for the fatigue life of the tested stringers at the stress range of 100 MPa. The stringers showed structural redundancy and a slow and steady

crack propagation, with a rather “ductile” fracture scenario. A total of six stringers were used in the investigation of the fatigue threshold.

2.2.1.2 Fatigue testing with corrosion

Out et al. (1984) investigated the fatigue resistance of four riveted stringers. The tests focused on the corroded region of flange angles and the riveted connection between the web and the angle. Measurements on the girders that were still in service at that time showed that 1% of the stress cycles exceeded the detail category C. The extreme life endurance of riveted connections between web and flange were situated near the detail category C. Fatigue damage from service was found to be negligible. The resistances of the corroded sections lied between AASHTO detail category E and C depending on loss of cross section. Riveted beams showed redundancy behaviour due to that stresses distributed to nearby parts. Tests performed at reduced temperatures at periodic intervals did not result in unstable crack growth.

Abe (1989) studied the fatigue performance of plates and stringers with a varying state of corrosion. The fatigue investigations were conducted in tension, with a stress range varying from zero to the yield strength of the material. The details tested were 5 small scale tests including riveted connections and the tension part of webs and flanges of 9 riveted beams. The investigation concluded that the effect of slight corrosion on riveted connections did not shorten the fatigue life. Severe corrosion in the riveted connections shortened the fatigue life. This was believed to be a result of reduced net area contributing to higher stress concentrations at rivet holes. The effect of the rough surface due to corrosion was also believed to influence the results. The previous loading history did not affect the fatigue life of the investigation.

Fisher et al. (1990) conducted an extended literature survey with results from over 1200 fatigue tests. Fourteen full-scale tests on riveted girders fatigue endurance were performed with test conditions varying from room temperature to -73 °C. Despite the low test temperatures, crack growth or premature fracture did not seem to be affected. The literature survey showed that tests with high stress range seemed to provide low fatigue life endurances, because of yielding in the material. Plates with empty holes had a better ability to endure fatigue than riveted joints. Results from the investigation on full-scale tests were that girders without severe corrosion, developed cracks in the net section at a rivet hole. Corrosion notch effects made the beams develop fatigue cracks at the gross cross section. The cracks usually formed at rivet holes unless more than 20% of the gross cross section was decreased due to corrosion.

Forsberg (1993) investigated the fatigue life of corroded steel plates. Tests were retrieved from corroded 55 beams with varying state of corrosion. In service stage, the stress range was between 20 to 30 MPa and the beams had endured approximately 10^7 cycles. Fatigue tests were done under both varied and constant stress range. Six specimens were included in the investigation, retrieved from the tension flange. The state of corrosion varied from light to heavy, with very rough surfaces. The effect of minor corrosion didn't seem to affect the fatigue life, but a more severe state of corrosion made the fatigue performance drop drastically, below the detail category C.

Adamson et al. (1995) investigated the fatigue behaviour of stringers retrieved from a bridge built in 1911. It was concluded from the load history and strain measurements that the fatigue damage was negligible. Presence of corrosion on stringers was also believed to have a negligible effect on the fatigue performance. The

investigation included five full scale tests on stringers. None-bearing riveted details showed a tendency of having fatigue resistance higher than riveted connections designed to act in bearing. The redundancy of riveted structures added significantly to its fatigue resistance. The results of the fatigue endurance of the stringers were covered by the detail category D in American Association of State Highway and Transportation Officials (AASHTO). DiBattista et al. (1995) investigated the fatigue performance of tension members from the truss girder bridge investigated by Adamson et al. (1995). A uniform corrosion existed on all tension members. Stress ranges in the tests were selected to provide information near the category C and D fatigue limit American Association of State Highway and Transportation Officials (AASHTO). A total of seven full scale tests were performed. No accumulated fatigue damage was present due to previous load history, based on measured strains while in service and from inspections. The tests showed that the fatigue resistance of diagonals and their connections to the bottom chord panel could be evaluated by detail category D American Railway Engineering Association (AREA, 1987), depending on definition of net section area. Repair of cracked tension members to the gusset plate with preloaded bolts extended the life of the connection significantly.

Xiulin et al. (1996) investigated fatigue tests on plates with removed rivets. The investigation included tests of 28 small scale samples. The plates were retrieved from tension chords in a bridge. Results from the investigation were comparable with results available in literature. The initiation phase of the fatigue cracking occupied the major part of the fatigue life of the material investigated.

DeJong et al. (2009) recently investigated the corrosion-fatigue resistance of coupons of MMFX microcomposite and 316 LN stainless steel. They performed several cyclic tension tests with overloads both in air and in an aqueous 3.5% NaCL solution to compare the fatigue resistance of these materials. They showed that corrosion fatigue reduced the periodic overload performance of both materials although they retained their intrinsic fatigue limit. Under constant amplitude loading, MMFX had a reduced performance in corrosive environment while the 316 LN stainless steel did not show much reduction (except for high loads).

2.3 Evaluation of corrosion

Corrosion and fatigue are two major factors that contribute to aging of structures. These two factors can act separately, sequentially or simultaneously (Du, 1998). Few approaches were done by Doyle et al. (1990) using Laser-based profilometry to locate and measure corrosion fatigue cracking or using Laser speckle sensors to measure surface roughness to study corrosion fatigue crack initiation. The influence of corrosive environment on fatigue has been studied by many researchers such as Gangloff (1990) and can be further referred to by the state-of the-art review by Duquette (1998).

2.3.1 Corrosion damage functions

The term "damage function" denotes a mathematical dose-response function connecting material damage to the factors involved in the damaging process. Many of these damage functions are listed by Boden (1989). The input of such damage functions is the concentration of harmful substances, time of wetness, temperature, etc. The output of such functions can have many forms such as weight loss, loss in thickness, etc). These

damage functions are widely used to describe atmospheric corrosion and atmospheric deterioration. Moreover, the ISO standard 9223 classifies the corrosivity of an atmosphere based on measurements of time of wetness (TOW), and pollution categories (sulphur, airborne chlorides). The standard was not intended to be used in extreme service atmospheres such as those within chemical or metallurgical processing facilities or where there is direct contact with salt spray (NACE, 2011).

Only airborne chlorides and sulphur dioxide are considered in terms of classifying the pollution, this gives good coverage of rural, urban, industrial and marine atmospheres. Based on these measures an atmosphere is classified as being in one of five categories in terms of its corrosivity using two types of units, i.e. short term corrosion rate (CR) of steel as $\text{g} \cdot \text{m}^{-2} \cdot \text{year}^{-1}$ (one year) or $\mu\text{m}/\text{year}$ (twenty years):

2.3.2 Time of Wetness (TOW)

From the fundamental theory, the time of wetness (TOW) of a corroding surface is a key parameter, directly determining the duration of the electrochemical corrosion processes. This is a complex variable, since all the means of formation and evaporation of the surface electrolyte solution must be considered. The TOW refers to the period of time during which the atmospheric conditions are favourable for the formation of a surface layer of moisture on a metal or alloy (KTS, 2010). This moisture film is extremely important from the point of view of the chemical mechanisms of the corrosion process. For the purposes of the standard this has been defined as the time period during which the relative humidity is in excess of 80% and the temperature is above 0 degrees Celsius. This measure can either be determined from weather data or measured directly through various means.

TOW categories range from "Internal microclimates (T_1) with climatic control" to "Part of damp climates, unventilated sheds in humid conditions (T_5)."
TOW units are hours per year when relative humidity (RH) > 80% and the temperature > 0°C.

Table 2.1 lists the different TOW categories.

Table 2.1 TOW categories according to ISO standard 9223 (1992)

Time of Wetness (TOW)	Designation
$TOW \leq 10$	T_1
$10 < TOW \leq 250$	T_2
$250 < TOW \leq 2,500$	T_3
$2,500 < TOW \leq 5,500$	T_4
$5,500 < TOW$	T_5

The TOW is strongly dependent on the critical relative humidity. Apart from the primary critical humidity (associated with clean surfaces); secondary and even tertiary critical humidity levels may be observed where the corrosion rate increases abruptly. Hygroscopic corrosion products and capillary condensation of moisture in corrosion products are thought to account for these effects. Other sources of surface electrolyte include chemical condensation (by chlorides, sulphates and carbonates), adsorbed molecular water layers and direct moisture precipitation (ocean spray, dew, rain).

2.4 Fatigue Life Prediction Approaches

Numerical techniques for fatigue life prediction could be classified into two major approaches: empirical correlation approach, and fracture mechanics approach (Ellyin, (1997); and Dowling (1999)). In the empirical correlation approach, a damage parameter 'D' is used to present actual fatigue test results, in which fatigue life calculation is generally performed with respect to either final fracture or crack initiation. The

application of fracture mechanics approach is widespread, especially for crack propagation life (Chen et al., 2005). In order to predict the fatigue life under a specified condition, different empirical damage parameters, D , have been proposed to correlate with the fatigue life (number of cycles to failure, N_f). The empirical correlation approach is generally divided into three categories, i.e., “stress-life” method, “strain-life” method and energy-based method, where stress, strain or energy is used as the damage parameter D , respectively, for each method.

2.4.1 Stress-life method

The “stress-life” method uses the alternating stress amplitude to predict the number of cycles to failure. This method is based on comparing the stress amplitude to a stress versus fatigue life curve (S-N curve), which comprises the influence of material, geometry and surface condition (Radaj et al., 1998). The S-N curves are based on empirical formulas derived from experimental data. The “stress-life” method is generally used for high cycle fatigue (HCF) where the material response is mostly elastic such as in case of the analysis of bridges.

The “stress-life” method emphasizes nominal stresses, rather than local stresses and strains, and it normally employs elastic stress concentration factors and empirical modifications to account for the concentration effect of notches (Leis et al., 1973). However, the accuracy of life prediction depends heavily on an accurate evaluation of the nominal stress range and the stress concentrations at the fatigue detail. It has been shown that, in some cases, “stress-life” methods predict fatigue lives that differ from test values by more than two orders of magnitude (Everett, 1992).

2.4.2 Strain-life method

The “strain-life” method uses true strain to predict the number of cycles to failure. When components are under high load and/or have critical locations (notches and/or bolted holes), the stress-strain relationship is no longer linearly related. In such situations, the plastic strain becomes a significant part of the deformation. Since the primary mechanism in fatigue is plastic deformation, an elastic model is not appropriate. The “strain-life” method has found wide applications in fatigue analysis, especially for fatigue crack initiation life calculation. This method is currently considered as a comprehensive method that can be used instead of “stress-life” methods (Dowling, 1999). In contrast to the “stress-life” method, the “strain-life” method considers the plastic deformation that may occur in localized regions where fatigue cracks initiate. The strain-based method assumes the material in highly strained areas, such as at a notch root, behaves similarly to material in a smooth specimen under cyclic strain controlled loading with the same strain (Morrow et al., 1981). Thus, this method can account directly for the difference in stress concentrations among different fatigue details through an inelastic finite element evaluation of the strain distribution. Dowling (1982) has reported that the estimated life is not very sensitive to the calculated strain, thus making the use of the local strain method a useful tool for the prediction of crack initiation life.

The strain-based method uses a cyclic stress versus strain curve and a strain versus life curve instead of the $S-N$ curve used in “stress-life” method. The coefficients and exponents that define these curves are treated as fatigue properties of the material. At the early developmental stages for the technique, there were insufficient fatigue data to quantify the fatigue properties of many engineering metals and various equations were

proposed to correlate the fatigue properties to the tensile properties (Morrow et al., 1981). The widespread adoption of closed-loop mechanical testing systems and the development of the “strain-life” method have largely eliminated the need for these empirical equations and there is an abundance of data defining the fatigue properties of numerous engineering metals (Rice et al., 1988). For engineering materials at room temperature (same as the case in laboratory tests), cyclic hardening or softening is usually rapid at first and then approaches a stable condition. The stable cyclic stress versus strain curve is often defined using the Ramberg-Osgood equation (Dowling, 1999). Figure 2.1 shows how the stable cyclic stress-strain passes through the tips of the hysteresis loops.

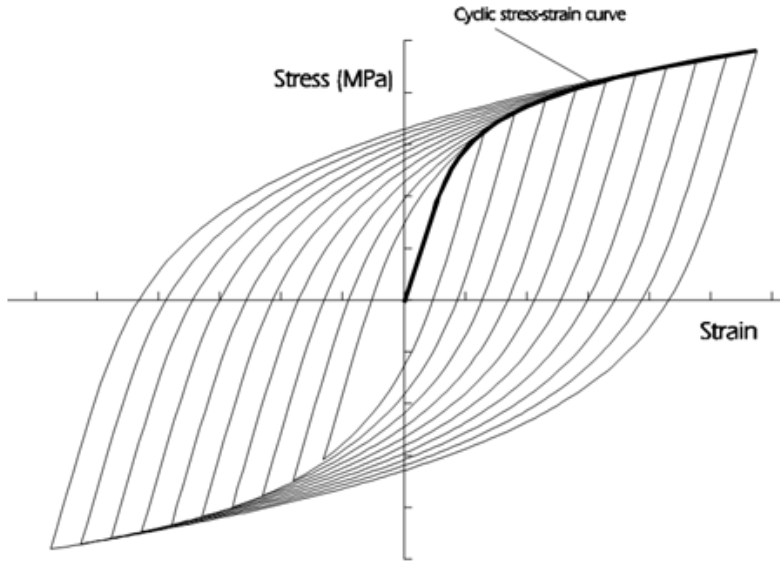


Figure 2.1 Stable cyclic stress-strain hysteresis loops using Ramberg-Osgood equation (Dowling, 1999)

Whenever a smaller range cycle follows a bigger one, this causes a closed loop that doesn't affect the main stable cyclic curve; this is what is sometimes referred to as the material memory effect (Drapper, 2008), this phenomenon is illustrated in Figure 2.2.

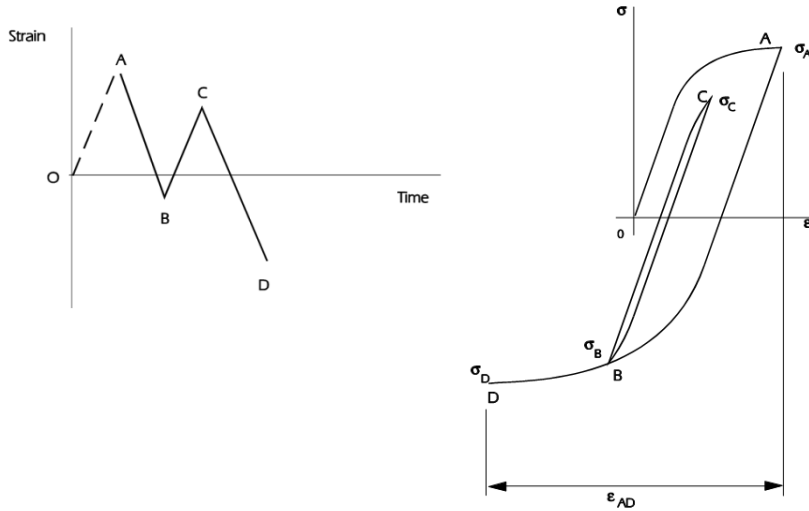


Figure 2.2 Cycle closure and material memory effect (Drapper, 2008)

The following sections introduce several fatigue life criteria based on the strain-based method.

2.4.2.1 Principal strain criterion:

This criterion proposes that fatigue cracks initiate on the planes experiencing the largest principal strain amplitude. This criterion is recommended for the analysis of brittle metals like cast iron and some very high strength steels. In general, it tends to give unsafe life estimates for ductile metals (Drapper, 2008). The endurance using the principal strain criterion can be obtained from equation (2-1):

$$\frac{\Delta\epsilon_1}{2} = \frac{\sigma'_f}{E} (2N_f)^b + \epsilon'_f (2N_f)^c \quad (2-1)$$

where $\Delta\epsilon_1$ is principal strain range, σ'_f is the fatigue strength coefficient, ϵ'_f is the fatigue ductility coefficient, E is the elastic modulus, b is the fatigue strength

exponent (Basquin's exponent) and c is the fatigue ductility exponent (Coffin-Manson exponent).

2.4.2.2 Von Mises equivalent strain criterion:

Since the von Mises criterion provides an estimate of the onset of yielding, this criterion has been proposed for fatigue life estimation. The major problem with the von Mises criteria is that the effective von Mises strain ε_{EFF} is always positive. Some approximations have been proposed to assign the sign based on hydrostatic stress or strain which makes this criterion named signed von Mises. The endurance using the principal strain criterion can be obtained from equation (2-2):

$$\frac{\Delta\varepsilon_{EFF}}{2} = \frac{\sigma_f'}{E} (2N_f)^b + \varepsilon_f' (2N_f)^c \quad (2-2)$$

where

$$\varepsilon_{EFF} = \beta \left((\varepsilon_1 - \varepsilon_2)^2 + (\varepsilon_2 - \varepsilon_3)^2 + (\varepsilon_3 - \varepsilon_1)^2 \right)^{0.5} \quad (2-3)$$

where β is a proposed term based on an equivalent value of Poisson's ratio ν^* based on elastic and plastic strains and Poisson ratios.

$$\beta = \frac{1}{(1+\nu^*)\sqrt{2}} \quad \text{where} \quad \nu^* = \frac{\nu_E \varepsilon_E + \nu_P \varepsilon_P}{\varepsilon_T} \quad (2-4)$$

Von Mises criterion correlates poorly with test data, especially for biaxial stresses when the two in-plane principal stresses change their orientation during the fatigue loading (Drapper, 2008).

2.4.2.3 Smith-Watson-Topper relationship:

As an approach to include the effect of mean stresses, Smith-Watson-Topper (1970) modified the principal strain criterion to include the mean stress as shown in equation (2-5):

$$\frac{\Delta \varepsilon}{2} \sigma_{\max} = \frac{(\sigma_f^{'})^2}{E} (2N_f)^{2b} + \sigma_f^{'} \varepsilon_f^{'} (2N_f)^{b+c} \quad (2-5)$$

This method was extended by Socie and Bannantine (1989) for brittle metals and shown in equation (2-6):

$$\frac{\Delta \varepsilon_1}{2} \sigma_{1,\max} = \frac{(\sigma_f^{'})^2}{E} (2N_f)^{2b} + \sigma_f^{'} \varepsilon_f^{'} (2N_f)^{b+c} \quad (2-6)$$

where $\Delta \varepsilon_1$ is principal strain range, $\sigma_{1,\max}$ is the maximum principal stress, $\sigma_f^{'}$ is the fatigue strength coefficient, $\varepsilon_f^{'}$ is the fatigue ductility coefficient, E is the elastic modulus, b is the fatigue strength exponent (Basquin's exponent) and c is the fatigue ductility exponent (Coffin-Manson exponent).

2.4.2.4 Maximum shear strain criterion:

The maximum shear strain criterion proposes that the crack will initiate on planes which experience the maximum shear strain amplitude (causing the slip bands). The principal strain criterion would be rewritten to replace the principal strain with the

maximum shear strain γ_{\max} . This criterion tends to give conservative life estimates for ductile metals, but can give unsafe life estimates for brittle metals (Drapper, 2008). The criterion is shown in equation (2-7):

$$\frac{\Delta\gamma_{\max}}{2} = 1.3 \frac{\sigma'_f}{E} (2N_f)^b + 1.5 \varepsilon'_f (2N_f)^c \quad (2-7)$$

where $\Delta\gamma_{\max}$ is maximum shear strain range, σ'_f is the fatigue strength coefficient, ε'_f is the fatigue ductility coefficient, E is the elastic modulus, b is the fatigue strength exponent (Basquin's exponent) and c is the fatigue ductility exponent (Coffin-Manson).

2.4.2.5 Brown-Miller combined strain criterion:

Same as the maximum shear strain criterion, the Brown-Miller criterion (Kandil et al., 1982) assumes that the fatigue damage occurs on the plane which experiences the maximum shear amplitude, but additionally this function incorporates both shear strain and strain normal to this plane. The Brown-Miller criterion gives realistic life estimates for ductile metals and tends to be non-conservative for brittle metals. The criterion is shown in equation (2-8):

$$\frac{\Delta\gamma_{\max}}{2} + \frac{\Delta\varepsilon_N}{2} = 1.65 \frac{\sigma'_f}{E} (2N_f)^b + 1.75 \varepsilon'_f (2N_f)^c \quad (2-8)$$

where $\Delta\gamma_{\max}$ is maximum shear strain range, $\Delta\varepsilon_N$ is the normal strain range perpendicular to the plane of maximum shear strain range, σ'_f is the fatigue strength coefficient, ε'_f is the fatigue ductility coefficient, E is the elastic modulus, b is the

fatigue strength exponent (Basquin's exponent) and c is the fatigue ductility exponent (Coffin-Manson exponent).

2.4.2.6 Universal Material Method:

If the cyclic properties of a steel material or an aluminum material are not present, the Universal material method can be used to obtain cyclic properties from static properties. Baumel and Seeger (1990) have published this method for plain carbon and low to medium alloy steels and also for aluminum and titanium alloys. Experience shows that this method generally gives satisfactory agreement with measured materials properties (Drapper, 2008). The method can be summarized as shown in Table 2.2.

Table 2.2 Coefficients for deriving the cyclic coefficients using the Universal Material Method.

Plain Carbon Steels	Aluminum and Titanium alloys
$\dot{\sigma}_f = 1.5\sigma_u$	$\dot{\sigma}_f = 1.67\sigma_u$
$\dot{\varepsilon}_f = 0.59a^*$	$\dot{\varepsilon}_f = 0.35$
$b = -0.087$	$b = -0.095$
$c = -0.58$	$c = -0.69$
$n = 0.15$	$n = 0.11$
$K' = 1.65\sigma_u$	$K' = 1.61\sigma_u$

* $a = 1.0$ for $\sigma_u/E < 0.003$, otherwise $a = 1.375 - 125\sigma_u/E$

2.4.3 Energy-based method

Experimental observations have confirmed the significant role that plastic deformation plays in the fatigue damage process. As cyclic plastic deformation is related to slip along crystallographic planes and dislocation movement, cyclic stress is related to the resistance to such movement at the microscopic level and strain energy is dissipated during such irreversible deformations (Ellyin, 1997). The energy-based method uses energy as a damage parameter to characterize fatigue, emphasizing the interrelation between stress, strain, and the fatigue damage process. It unifies high and low cycle fatigue, and has the potential to bridge fatigue data obtained in different laboratories using specimens of different geometry and size and tested under different controls. This method is not in the scope of this research.

2.4.4 Fracture Mechanics Approach

The use of fracture mechanics in fatigue propagation life prediction became widespread since it was first applied to fatigue crack growth about 50 years ago (Paris et al., 1961). For many structures, the major portion of the fatigue life is expended in propagating a crack from an existing flaw, that is, only the fatigue crack propagation life needs to be determined.

The parameter describing the stress field around the advancing crack tip is an important component in the fracture mechanics approach. The stress intensity factor, K , is used in Linear-Elastic Fracture Mechanics (LEFM) when the nominal stress versus strain response is essentially elastic. When plasticity effects are considered, various parameters have been proposed, among which Crack Tip Opening Displacement ($CTOD$) and J -integral are the most commonly used in Elastic-Plastic Fracture Mechanics (EPFM). In

highly ductile materials and where the crack tip plastic zone is large, EPFM may be more appropriate. Crack propagation life calculations are carried out from a specific initial crack size to a final crack size at failure, which may be determined from the material fracture toughness. However, a number of parameters are difficult to determine in practice, especially the initial crack size and shape. The problem is that concepts of LEFM are not accurate for short cracks (usually less than 1mm). Thus the crack initiation phase cannot be accurately captured (Taylor, 2008). The theory of critical distances bridges the gap between the short crack regime and long crack regime that can be predicted by LEFM.

2.4.5 Theory of Critical Distances

One of the latest advances in the fatigue and fracture mechanics is the development of the “Theory of Critical Distances” (TCD) (Taylor, 2008) which sums up the pioneering work done by Neuber (1958), Peterson (1959) and El Haddad et al. (1979). The theory applies for short cracks and assumes that there is an intrinsic characteristic critical length “L” for each material, where if the average stresses at a distance L/2 away from the surface crack or notch exceeds a material constant stress which is usually near its ultimate stress, the crack would propagate, otherwise it can be considered as a non-propagating crack. Moreover, if the surface crack length is less than this critical distance “L”, LEFM would not accurately apply. The critical distance “L” can be expressed as follows:

$$L = \frac{1}{\pi} \left(\frac{K_c}{\sigma_o} \right)^2 \quad (2-9)$$

where K_c is the critical stress intensity factor of the material in case of static loading and σ_o is the critical stress which is usually equal to the strength of the material as measured on unnotched samples. The same equation can be extended to fatigue loading as follows:

$$L = \frac{1}{\pi} \left(\frac{\Delta K_{th}}{\Delta \sigma_o} \right)^2 \quad (2-10)$$

where ΔK_{th} which is the fatigue threshold intensity factor in case of fatigue loading. $\Delta \sigma_o$ is the critical stress range which is usually equal to the fatigue limit. This is true for metal fatigue and for static fracture of brittle ceramics (Taylor, 2008). The current availability of robust FEA solvers, makes this method a promising method for fatigue crack initiation and propagation analysis.

2.5 Cycles Counting

Counting the number of cycles in a given loading history is very important for fatigue life calculations. Because the stress pattern obtained from traffic data does not have a constant amplitude, a systematic manner of counting stress cycles is needed. Various cycle-counting algorithms have been developed for the purpose of reducing complex histories into a finite number of variable amplitude cycles. Among the earliest of these are the level-crossing counting, peak counting, and simple range counting techniques and the rain flow analysis. The following subsections explain these counting methods.

2.5.1 Level-Crossing Counting

Level-crossing counting involves dividing the stress axis into an arbitrary number of equal increments. A reference stress is initially chosen, and each time a positively sloped portion of the stress record crosses an increment above the reference stress a count is recorded for that particular increment value. Likewise, each time a negatively sloped portion of the stress history crosses an increment value below the reference stress, a count is recorded. Then, the counts are combined to form full cycles. Usually this is done by combining the counts to form the largest possible cycle, and the remaining counts are combined to form the next largest possible cycle. When all counts have been assigned to a cycle, the process is completed.

2.5.2 Peak Counting

Peak counting also involves dividing the stress axis into increments and choosing a reference stress. All local maxima above the reference stress and all local minima below the reference stress are recorded. Then, these counts are combined by sequentially grouping the greatest maxima with the least minima to form complete cycles.

2.5.3 Simple Range Counting

Simple range counting involves recording the range between successive stress reversals and counting each range as one half-cycle.

2.5.4 Rainflow Cycle Counting

There are certain limitations to the cycle-counting techniques described above. Mainly, each of these methods disregards the actual sequence of applied stress cycles.

Consequently, in the late 1960s, a new type of cycle counting algorithm was introduced. It attempted to identify closed hysteresis loops in the stress-strain response of a material under cyclic-loading. The term *rainflow counting* has been applied to the general family of such algorithms. Each stress record from the field testing must be processed through a rainflow cycle-counting algorithm.

The current rainflow cycle counting algorithm used in engineering is originally attributed to Downing et al. (1982). Some pre-processing of the field stress history data is required before this algorithm can be applied. As with all rainflow counting algorithms, it is first necessary to re-arrange the stress record so that it begins and ends with the stress value of the greatest magnitude. This ensures that no half-cycles are counted. This method is the most commonly used method in all fatigue signal processing software.

2.6 Corrosion fatigue Life Prediction

Corrosion-fatigue behaviour of a given material-environment system refers to the characteristics of the material under fluctuation loads in the presence of a particular environment. Corrosion-fatigue damage occurs more rapidly than would be expected from the algebraic sum of the individual effects of fatigue, corrosion, or stress corrosion cracking. Fatigue crack initiation threshold ΔK_{th} in a non-corrosive environment can be related to the yield strength of some materials (Barsom et al., 1999). In corrosive environments, the fatigue threshold varies and can be related to the yield strength too, but not all experimental evidences on all tested materials support this observation. Novak (1983) has investigated the corrosion fatigue crack initiation (CFCI) behaviour for four types of steel (the A36, A588-A, A517-F, and V-150 steels). His main observation was

that there is no clear corrosion fatigue crack initiation threshold ΔK_{th} for the four types of steel after corrosion, in contrast to fatigue crack initiation thresholds clearly obtained in non-corrosive environment.

Further research is needed to establish the relationships, if any, between the properties of the material and the corrosion-fatigue threshold at different corrosive environments. It is important to mention that the corrosion fatigue threshold ΔK_{th} varies with the applied stress ratio R , loading frequency, for each environment-material system which makes the corrosion fatigue phenomenon more complex and needs further experimental investigations.

2.7 Review on cumulative fatigue damage models

Fatigue damage increases with applied load cycles in a complex cumulative manner. Cumulative fatigue damage analysis plays a key role in the fatigue life prediction of components and structures subjected to field load histories such as bridges. Due to the complexity of the fatigue phenomenon and in order to assist designers in considering the several factors involved in the fatigue process such variable loading histories, mean stress effects, effects of multi-axial loading, many fatigue damage model were proposed throughout the past few decades. Since the introduction of damage accumulation concept by Palmgren (Palmgren, 1924) about 70 years ago and ‘linear damage rule’ by Miner (Miner, 1945) about 50 years ago, the treatment of cumulative fatigue damage has received increasingly more attention. Consequently, many damage models have been developed. A more detailed and comprehensive review will be presented in Chapter 3. A new damage model will be proposed and compared with other approaches.

Due to the previously mentioned difficulties of the variable amplitude fatigue testing, results of constant amplitude fatigue testing are to be extrapolated towards variable amplitude loading using cumulative damage laws. For further state-of-the-art reviews on different fatigue damage models, refer to the comprehensive work done by Fatemi and Yang (1998), and Hwang and Han (1986).

2.8 Review of Current Standards

The American Association of State Highway and Transportation Officials (AASHTO) produced a guide for fatigue evaluation of existing steel bridges based upon an extensive report by Moses et al. (1987). It was intended that the guide eventually be included in the AASHTO Manual for Maintenance Inspection of Bridges (AASHTO, 1989). The guide focused on highway bridges and traffic loadings, and it provides guidelines for calculating the remaining fatigue life as either the remaining mean fatigue life or as the remaining safe fatigue life. The remaining mean life has a 50% probability of being exceeded, and it is considered the best estimate of the remaining fatigue life. It is generally used for cost comparisons and estimates.

The final section of the AASHTO guide (AASHTO, 1989) provides alternative solutions if the calculated remaining fatigue life is inadequate. The solutions provided can be either to restrict the traffic that uses the bridge, to modify the bridge to eliminate or extend the life of the critical detail, or to institute inspections of the critical details so as to enable timely discovery of any crack growth. The AASHTO guide recommends using the fatigue resistance category D for the base metal at the net section of a riveted connection. Fisher et al. (1987) recommended changes to the 1983 version of the AASHTO Manual for Maintenance Inspection of Bridges to the effect that riveted steel

members that resist net section tensile stress by three or more components (e.g., one web and two flange angles) can be checked according to category C for fatigue resistance. This is based upon their conclusions that category D identifies fatigue crack development and category C characterizes fatigue resistance, defined as the ability of a member to carry load with one or two cracked components.

Fatigue evaluation of existing railway bridges is covered in the AREA (American Railway Engineering Association) standard (AREA, 1987) which is now recognized as the American Railway Engineering and Maintenance-of-Way Association (AREMA). AREMA (AREMA, 2011) recommends the use of category D for members with riveted or bolted connections with low slip resistance. However, this may be increased to category C if the engineer can verify that the rivets have developed normal clamping force. No guidance is provided for making such verification. The reasoning behind this benefit is that category D was defined with riveted connections that had low clamping force, and that rivets with high clamping force are better designed by category C. Hence a higher fatigue resistance is permissible for rivets with normal clamping force.

More stringent fatigue category requirements are specified for fracture critical members. i.e. members whose failure would make the bridge unable to fulfill its intended service. Riveted members are not considered to be this type of member because of their internal cross-sectional redundancy. However, if the riveted members do not satisfy the fatigue category requirements, the requirements may be waived if it can be deemed that the members have adequate structural redundancy to redundancy the load when one of the components cracks. Inspections must be frequent enough to discover the local failure and to perform repairs. There is no specific category for the riveted members or the

riveted connections. category D can be used as a lower bound for the evaluation of riveted members. There are no S-N curves for fatigue in corrosive environments in the aforementioned codes of practice.

The Canadian Highway Bridge Design Code (CHBDC S6, 2006) also uses detail category D for riveted connections, but there is a big scatter in the results that were used for choosing this detail category as shown in Figure 2.3.

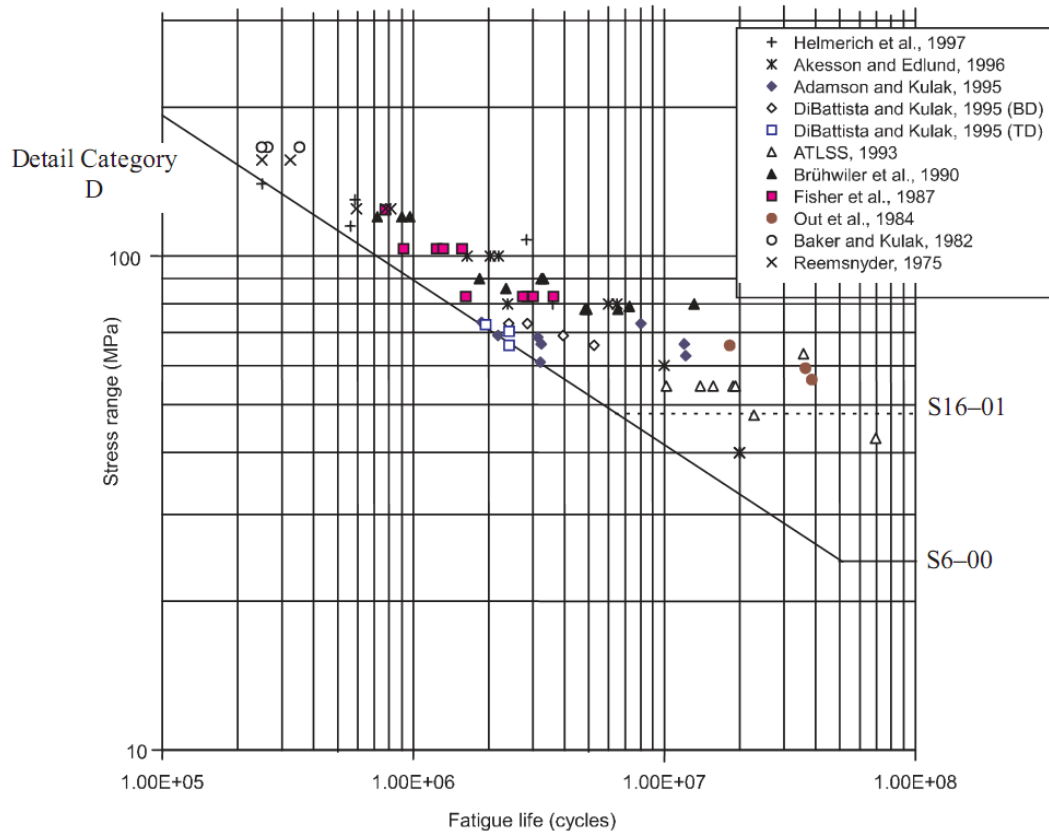


Figure 2.3 Fatigue life of several riveted fatigue details from literature (adopted from Kulak (2005))

2.9 Remaining Fatigue Life

This section discusses how the remaining fatigue life is calculated in years from the fatigue life in load cycles. The first step in calculating the remaining fatigue life is to ascertain the traffic over the bridge. The average daily traffic (ADT) and the traffic growth rate on the bridge can be obtained from the reports published by ministries of transportation. The ADT can be determined by using equation (2-11).

$$ADT(Y) = G + g_r \cdot Y \quad (2-11)$$

where G is the current predicted ADT , g_r is the growth rate and Y is the number of years starting from the year of construction. The percent truck traffic of the traffic should be obtained. Average daily truck traffic (ADTT) for the main lane is determined using equation (2-12):

$$ADTT(Y) = ADT(Y) \times FT \times FL \quad (2-12)$$

where FT is the percentage of truck traffic and FL is the percentage of trucks of main lane in case of roadway road. To determine the number of load cycles to failure, the following relationship is used:

$$N_f = 365 \times C_L \int_A^{R_L} ADTT(Y) \cdot dY \quad (2-13)$$

where N_f is the number of load cycles to failure (remaining fatigue life in cycles), C_L is the load cycles per truck, R_L is the remaining life of the detail, and A is the current age of the structure. The remaining life can be found by integrating and solving for R_L .

2.10 Review on available finite element fatigue software

2.10.1 Introduction

In the past two decades, the computer advancement revolutionized engineering analysis methodologies, and gave better confidence in accomplishing lengthy numerical analyses that were previously difficult to carry out and needed several simplifications with many assumptions. The prior availability of the Finite Element Method (FEM) in mechanical and structural engineering assisted such numerical tools; it helped in performing complex stress analysis on complex structural and mechanical components. One of the fields that were greatly affected by the advancement in FEM and numerical tools is the field of fracture mechanics. This contributed significantly to the advancement of aerospace technology. Also, it enabled researchers in the field of fracture mechanics to verify their analytical closed-form solutions for different fracture mechanics problems. Advancement in computer technology and parallel processing helped in simulating difficult phenomena such as crack propagation problems, flow of plasticity and even micro-structural inter-granular interactions and sliding.

The main challenge for design of a structural steel element for fatigue is to incorporate all parameters that would affect the fatigue life computation. Such requirement is not currently implemented in the available commercial fatigue load postprocessors. Several approaches were made in the literature to develop finite element programs or adapt existing software for fatigue evaluation purposes. More details on these approaches can be found in Hanq et al. (2000), Engelstad et al. (2001) and Cojocaru et al. (2008).

2.10.2 Object Oriented Programming

Since this research involves the development of a numerical tool, a quick review for the Object-oriented programming (OOP) methodology used is explained. OOP concepts began developing since the 1960s but it developed as the dominant programming methodology in the early and mid-1990s when programming languages supporting the OOP techniques became widely available. Before that, the procedural programming was the dominant methodology where procedures can be represented as a network of routines which call one another, i.e., "call tree". Whereas in the OOP approach, there is a collection of discrete classes (objects) that incorporate data structures and combined with it, the procedures which apply to that data structure. An object oriented program is composed of objects, each with a number of attributes that define the state of the object and methods (functions) that define the behaviour of an object for changing or returning the state of the object.

Since the scope of this study focuses on developing a numerical tool for fatigue life prediction utilizing the FEM, several commercially fatigue postprocessors that are available at the time of writing this thesis are reviewed in the following sections. Detailed review of different fatigue software can be found in Papuga (2005).

2.10.3 Fe-SafeTM (2011)

Fe-SafeTM is developed by Safe Technology in Sheffield, England (Fe-Safe, 2011). Fe-Safe is distributed via the ABAQUS distribution network; this is besides it being a stand-alone product as well. Fe-SafeTM incorporates another product of Safe Technology, which is the Safe4FatigueTM aimed at signal processing and damage computation without

FE-data. They added new modules, namely, “Rotate” for solution of axis-symmetric components and “TMF” for thermo-mechanical fatigue solution including creep effects.

The multi-axial fatigue solution incorporates both the stress based (S-N) and the strain based (e-N) approaches. A representative of combined criteria Brown-Miller Brown et al. (1973) with normal and shear strains is implemented too. The program is not capable of representing corrosion simulation.

2.10.3.1 MSC.Fatigue™ (2011)

The program is highly modular. It is fully integrated into the Nastran™ environment, which is an interesting feature. The multi-axial fatigue module is separated as well as modules *Vibration*, *Welds*, *Fracture* and *Utilities*.

The *Weld* module has its limitations in specific requirements on modelling of weld area, which considerably complicate work. Thus, e.g. the fillet weld of two perpendicular components has to be modelled with a row of elements connecting both sheets under 45°. The *Fracture* module is the only module of commercial products described, which computes the crack growth phase as well. This is in accordance with the Nastran's focus towards aviation industry. The program offers nearly all solutions except for the thermo-mechanical fatigue with creep. The only thermal effect incorporated is the change of S-N curves under specific high temperature. The program does not have corrosion simulation features.

2.10.3.2 FemFat™ (2011)

The program is highly modular. FemFat™ (FemFat, 2011) is entirely based on the S-N solution. Even the multi-axial method is based on S-N curves, which are evaluated

over specific planes. FemFat™ does not offer complete clarification of its approach and leaves it as its know-how (black box).

Another advantage of FemFat™ is the existence of the *Heat* module with embedded thermal fatigue and creep model. The *Visualiser* module enables graphic inspection of results on FE-mesh, but it has only very basic functions.

2.10.3.3 Ansys™ nCode Design Life (2011)

ANSYS™ created a Fatigue Powerful Module in collaboration with HBM nCode (2011) engine incorporating both stress-life and strain-life analyses with a variety of mean stress correction methods, including Morrow, Smith-Watson-Topper (SWT) and many other criteria, the ANSYS™ Fatigue Module provides contour plots of fatigue life, damage, factor of safety and bi-axial stresses. Additional results include rainflow matrix, damage matrix, fatigue sensitivity and hysteresis. The drawback of this powerful program is that it does not alter the mesh to simulate corrosion penetration or run any crack propagation analysis. It is worthy to mention that this program has significantly improved from 2010 and added many features compared to its state at the beginning of this thesis.

2.10.3.4 Comparison and Proposed tool

From the previous review of the available known software packages, it can be found that most of these programs:

- Do not allow adding custom damage laws (for research purpose), they are like a black box with fixed features.
- Do not allow altering the mesh progressively and simulating corrosion effects on the mesh (which is a contribution of this research).
- User can not add custom interaction laws that correlates input parameters together such as (corrosion with temperature, corrosion with fatigue ...etc).

One of the objectives of this research is to develop a numerical tool that helps in overcoming the previously mentioned drawbacks of available fatigue software. The numerical tool will be called CorrFLP (CORRosion Fatigue Life Predictor). Table 2.3 shows a quick comparison between existing software and the proposed numerical tool.

Table 2.3 A comparison of features offered by commercial fatigue postprocessors and the proposed tool CorrFLP. (Maximum is marked with five stars, whereas No stars corresponds to no implementation).

Criterion	ZenCrack	Fe-Safe	Ansys. Fatigue	MSC.Fatigue	FemFat	Proposed CorrFLP
Corrosion Simulation (Geometric)						*****
Corrosion-Fatigue (Strain-life model)						***
Thermal fatigue	*	*****	**	*	*****	*
Creep		***			***	
Multiaxial solution	*****	*****	***	*****	***	***
Post Processing FE results	**	*****	*****	*****	*****	***
Transient solution (sequence of FE-calc.)	***	***	***	*****	*****	***
Load history operation	***	*****	***	**	**	***
Crack growth	*****			*****		**
Internal visualiser			*****	*****	***	****
Adding Custom Damage Rules		***	*	**	*	**
Adding Interaction Rules						***
Seam welds	*	**		***	***	
Spot welds		*		*****	*****	

From Table 2.3 it can be seen that CorrFLP is the only tool that incorporates the simulation of corrosion. CorrFLP also incorporates the concept of programmable interaction rules, which enables any researcher as a user to test any theory and apply any damage model that interacts with all input factors. On the other hand, it should be mentioned that CorrFLP is not powerful in thermal fatigue and fatigue in welds, which could be a point for future research. Also, Zencrack and MSC.Fatigue are powerful in crack propagation analysis, while CorrFLP has limited crack propagation features (out of the scope of this research). Next chapters will illustrate the methodology used in this research.

CHAPTER 3

DEVELOPMENT OF A FATIGUE ACCUMULATIVE-DAMAGE MODEL

3.1 Introduction

Most of the available data regarding fatigue life is based on experimental work conducted on specimens subjected to constant amplitude cyclic loading (stress or strain). As a matter of fact, during the service life of any structure, it is expected that the structure would be subjected to various random loads that could have a constant- or random-loading pattern. The current practice for quantifying the accumulated damage at each stress (or strain) level, and consequently the fatigue life of the structural element, is to use these available constant amplitude experimental data. Unfortunately, experiments using variable amplitude loading are expensive, time-consuming and having much uncertainties about the in-service loading spectrum (Paepegem et al., 2002). This is the reason that studying multi-stress level fatigue has always been a challenge for researchers and engineers and much more difficult to formulate than constant amplitude stress fatigue.

Many damage models were proposed in the literature to explain the multi-stress level fatigue phenomena and predict its life by cumulative damage model approaches. Cumulative damage model approach could be classified as damage models defined by number of fatigue cycles, material characteristic variables, the applied stress levels, temperature, frequency of loading, moisture content and the geometric shape of the specimens (Du, 1998). In general, cumulative damage function can have either trend A, B or C as shown in Figure 3.1.

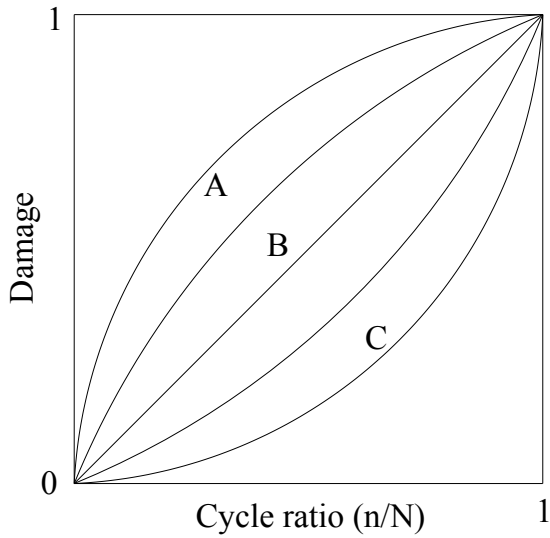


Figure 3.1 Possible trends in fatigue damage models (Hwang et al., 1986)

3.2 Review on Cumulative Damage Models

In this section, a more comprehensive and technical review on several available damage models is conducted. The purpose of this review is to highlight the points of strength and weakness in these damage models. Moreover, a quick inspection of the common phenomena traced by these models will give a clearer picture of fatigue damage and paves the way to propose a new fatigue damage model. In the following subsections, a detailed review on some of the most important fatigue damage models is presented.

3.2.1 Miner's Linear damage Rule (LDR)

In 1945, Miner (Miner, 1945) expressed the concept of damage accumulation in a very simple linear trend (trend B in Figure 3.1). Miner expressed this damage law (also known as Palmgren-Miner's Law) in the following mathematical form:

$$D = \sum \frac{n_i}{N_{fi}} \quad (3-1)$$

Where D denotes the damage, n_i and N_{fi} are the applied cycles and the total number of cycles to failure under the i^{th} constant-amplitude loading level, respectively. This rule is still the most popular rule used due to its simplicity. Unfortunately, this damage model has many deficiencies. This rule fails to predict the effect of load history sequence. Experimental data indicate that the sequence in which various stress levels are applied has significant influence on the fatigue behaviour of materials. It is also widely known that Miner's damage sum to failure is greater than unity for low-to-high tests and less than unity for high-to-low tests (Hwang et al., 1986). Another major limitation of Miner's rule is that it is stress level independent, in that its damage trend follows only one function (which is linear) for any stress level.

3.2.2 Marco-Starkey theory

In 1954, and as a remedy to the deficiencies of Miner's LDR, Marco and Starkey (1954) proposed the first non-linear load-dependent damage theory. This damage model is based on (D-r) curves, where 'r' represents different stress levels. This model has the form:

$$D = \left(\frac{n_i}{N_{\hat{f}}} \right)^C \quad (3-2)$$

where 'C' depends on the stress level and has a value greater than unity, which means it always follows the trend 'C' in Figure 3.1. Although this rule is stress dependent, but its main disadvantage is the possibility of having the damage sum greater or less than unity depending on the load sequence as shown in Figure 3.2.

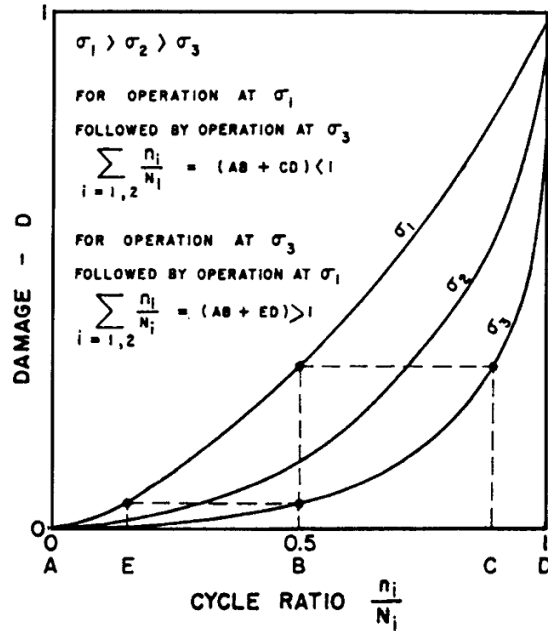


Figure 3.2 Load sequence effect in Marco-Starkey theory (1954)

3.2.3 Damage theories based on endurance limit reduction

One of the deficiencies of the previous damage models that they always correlate to the Number of cycles to failure N_f of a virgin material under constant amplitude loading. Many approaches were done to represent the accumulated damage as a reduction in the fatigue endurance limit of the material. Examples of these are theories proposed by Henry (1955), Gatts (1961) and Bluhm (1962). All these damage models are nonlinear and are able to account for the load sequence effects. However, the mathematical form of these models is complicated. Moreover, they do not take into account the load interaction effects.

3.2.3.1 Corten and Dolan theory

Corten et al. (1956) performed hundreds of experimental tests on cold-drawn steel wires by applying different loading blocks with different stress levels. Their experimental test program had several series of two-stress level loading sequences repeated until failure. They described damage in a phenomenological hypothesis that represents the nucleation of microscopic voids which develop into cracks. The damage is given in terms of number of damaged nuclei and the rate of damage propagation as a power function of the number of cycles as shown in Figure 3.3.

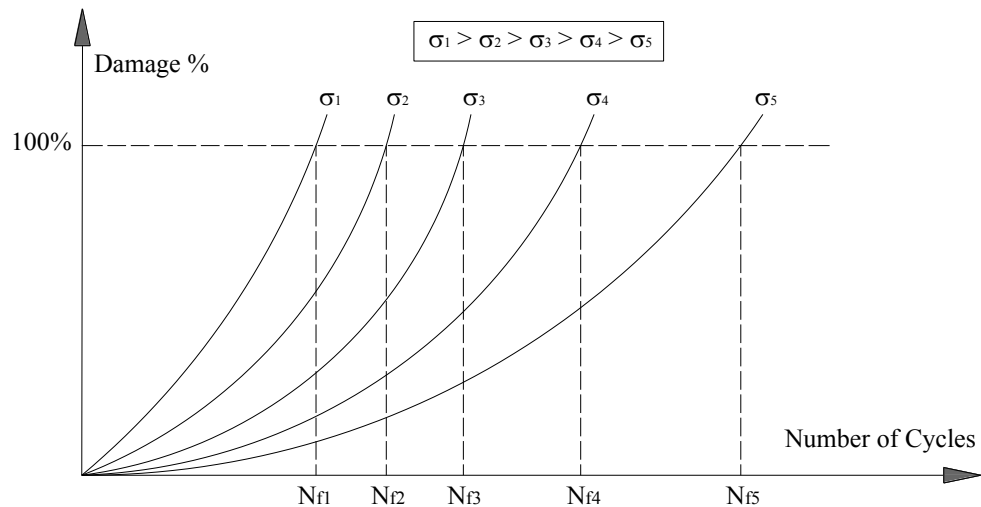


Figure 3.3 Corten's hypothesis of the progress of fatigue damage (Corten et al., 1956)

Corten et al. (1956) formulated the expected life in a two stress level loading block history in a simplified equation as follows:

$$N = \frac{N_1}{\alpha + R^{1/a}(1 - \alpha)} \quad (3-3)$$

where N is the total accumulated life, N_1 is the number of cycles to failure under constant amplitude loading under the high stress level, α is the ratio of the number of high stress level cycles to the low stress level cycles in one loading block, $R^{1/\alpha}$ is a factor that can be related to the stress ratio.

$$R^{1/\alpha} = \left(\frac{S_1}{S_2} \right)^{6.57} \quad (3-4)$$

where S_1 is the high stress level and S_2 is the low stress level. Results using this equation had a good agreement with their tests. Equation (3-3) is limited to a two-level stress block sequence loading history. The constant 6.57 in equation (3-4) was determined by fitting experimental results.

3.2.3.2 Manson's theories

With over 20 years of testing, Manson and his co-workers proposed several conceptually-different damage models, and continuously updated them to correlate with their considerable test result data. Manson et al. (1967) first introduced the concept of Double Linear Damage Rule (DLDR). After which, their work was extended to develop the concept of Damage Curve Approach (DCA) and later the Double Damage Curve Approach (DDCA) (Manson et al., 1981). These models were in good agreement with experimental work in low cycle fatigue under two loading levels. These damage models are all load-level dependent, but do not account for the load interaction effect and small amplitude cycle damage. Also determining the Knee point (which is a new concept introduced in Manson's work) is a tedious procedure that could be inconvenient.

3.2.3.3 S-N Curve modification theories

Many researchers agreed that the errors in the LDR life predictions are not necessarily due to the linear summation of damage but to the assumption of damage-rate independence of loading levels (Fatemi et al., 1998). Based on experimental results, Subramanyan (1976) introduced a modified damage model of several damage iso-lines having a knee point or pivot near the fatigue limit of the material. This approach has problems at stresses near the fatigue limit due to the singularity at the knee point. Later, Hashin et al. (1978) presented a discussion of the S-N curve rotation approaches and performed analytical calculations along with experimental work. The predicted results were in good agreement with test data. Later, Leipholtz (1986) revived the concept of a modified S-N curve as shown in Figure 3.4, named S-N' curve, which accounts for load interaction effects. Leipholtz's model is represented as:

$$N = 1 / \sum (\beta_i / N'_i) \quad (3-5)$$

where N is the total accumulated life, and β_i is the frequency of cycles and N'_i is the modified life with loading level σ_i .

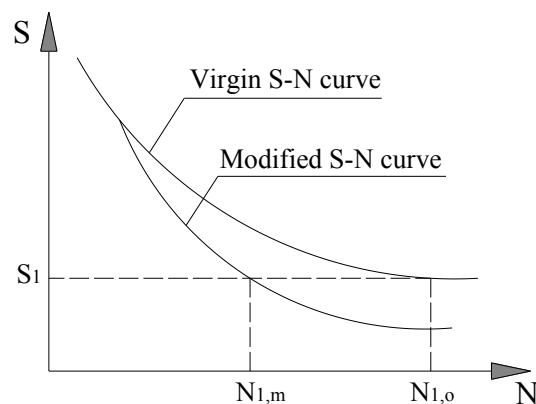


Figure 3.4 Modified S-N curve approach

3.3 Factors Affecting Damage Models

Based on available models, it could be said that, in general, damage state indicator of the material can be expressed as follows:

$$D = f(N, s, r, f, t, c, D_o, \dots) \quad (3-6)$$

where,

D = material damage state (0 for undamaged, 1 for completely damaged)

N = number of fatigue cycles

s = previously applied stress level

r = applied stress level

f = frequency

t = temperature

c = corrosion rate

D_o = Previous material damage state

In the following sections, a brief discussion on the influence of different parameters and their respective effects that need to be considered when formulating a comprehensive, yet simple, fatigue damage model.

3.3.1 Mean Stress Effects

Fatigue tests have shown that applying a tensile mean stress results in a shorter life than those test specimens that are subjected to a zero mean stress. Many equations were developed to take this into account, such as Goodman (1899), Morrow et al. (1981) and Smith-Watson-Topper (Kandil et al., 1982). The latter two equations showed the best agreement with many test data on different materials (Drapper, 2008).

3.3.2 Effect of Frequency

Developing a unified damage law that takes into account *all* factors might not be computationally effective; hence, some effects could be omitted from a damage model due to their insignificant influence. For example, many researchers reported that the frequency of loading does not significantly affect the fatigue behaviour if it is within the range of 1-200 Hz (Frost et al., 1974).

3.3.3 Effect of temperature

At elevated temperatures, mean stress effects become extremely complex to simulate because of the interactions among creep, fatigue and environment. Moreover, the linear elastic stress intensity factor has more limitations at elevated temperatures because of the appreciable plasticity (Cui, 2002). Fortunately, regular fatigue-sensitive structures are not usually designed for elevated temperatures. Thus, these effects could be neglected. It is important to mention that temperature fluctuation in snowy regions (which can reach -80 °C in some places) can have a minor effect on the ductility of metal and the mean stress. This could be easily taken into account when studying fatigue of a structural component.

3.3.4 Effect of corrosion

Fatigue in a corrosive environment is a very complex phenomenon known as corrosion-fatigue. It is important to differentiate between corrosion-fatigue and stress-corrosion-cracking which is the environmentally assisted fracture under static loading. Due to the experimental difficulty of simulating corrosion and measuring its effect on the fatigue behaviour, this topic needs more future investigation. Although the damage rule

that will be proposed later in this chapter does not take into account the effect of corrosion, it has the potential of being extended to account for the effect of corrosion provided that there is a huge amount of long-term experimental test results under several corrosion rates available.

3.3.5 Other effects from previous damage models

In order to have a comprehensive fatigue damage model, it has to take into account:

- Load interaction & load sequence effects.
- Stress-level dependency.
- Simplicity in its formulation and use by designers.

3.4 Proposed Damage Model

In this section, a new damage model is proposed. This damage model will aim to alleviate some of the shortcomings in the previously mentioned available damage models. The damage model will incorporate the effects of stress-level dependency and load sequence effects while still maintaining a simple form (which is the main reason designers still use the Palmgren-Miner rule).

3.4.1 Discussion

In this research, a phenomenological approach for estimating the level of fatigue damage will be used. Material damage can be described as the loss in expected life by accumulation of loading cycles under certain stress levels. A new concept is proposed which will be called the “Virtual Target Life Curves” (VTLC). In this approach, it will be

assumed that any material has a virtual (theoretically infinite) expected life that is, by definition, greater than the real failure life under constant amplitude loading. As constant amplitude fatigue loading proceeds, this expected life reduces in magnitude depending on the number of cycles, where the rate of deterioration keeps changing depending on the stress level. In cases of variable amplitude fatigue loading, some sudden jumps of damage (and consequently corresponding loss in expected life) will occur due to overloading effects resulting from the increase from low stress levels to high stress levels (and vice versa). The magnitudes of these jumps depend on the ratio of the two stress levels. Figure 3.5 shows that the concept of virtual target life curves –in case of constant amplitude loading– will lead to the regular S-N curve (which represents the number of constant amplitude cycles that leads to failure of a laboratory tested element).

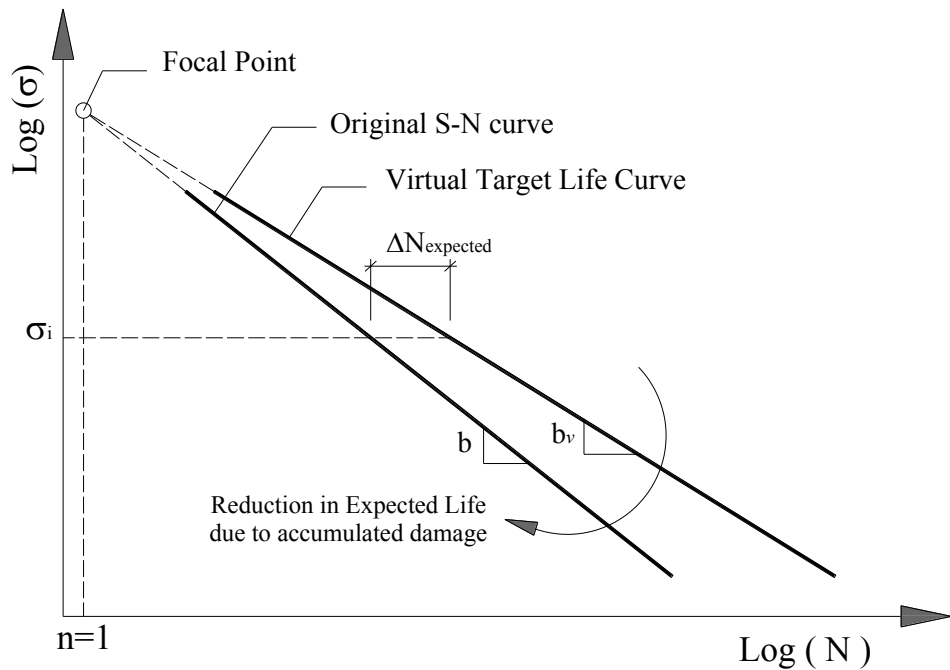


Figure 3.5 The proposed Virtual Target Life Concept

It is important to note the difference between the proposed approach and other approaches in the literature that are based on modifying the S-N curve. Previous approaches such as Manson's early work and Subramanyan (1976) were based on shifting the so-called virgin material curve as a starting point to account for cumulative damage in cases of variable amplitude loading. The author doesn't agree with the term *virgin material curve* to be used for the S-N curve as this curve represents in reality the failure of the specimen, whereas the term virgin material implies a totally unloaded material. In this research, a different approach is adopted; the material is supposed to endure until it reaches a virtual target life. The virtual life decreases as damage accumulates. The rate of decrease of this virtual life changes based on the loading history (including both: stress levels and loading sequences) and depends on the material. Figure 3.6 illustrates the difference between Manson's approach, Subramanyan's approach and the VTLC approach.

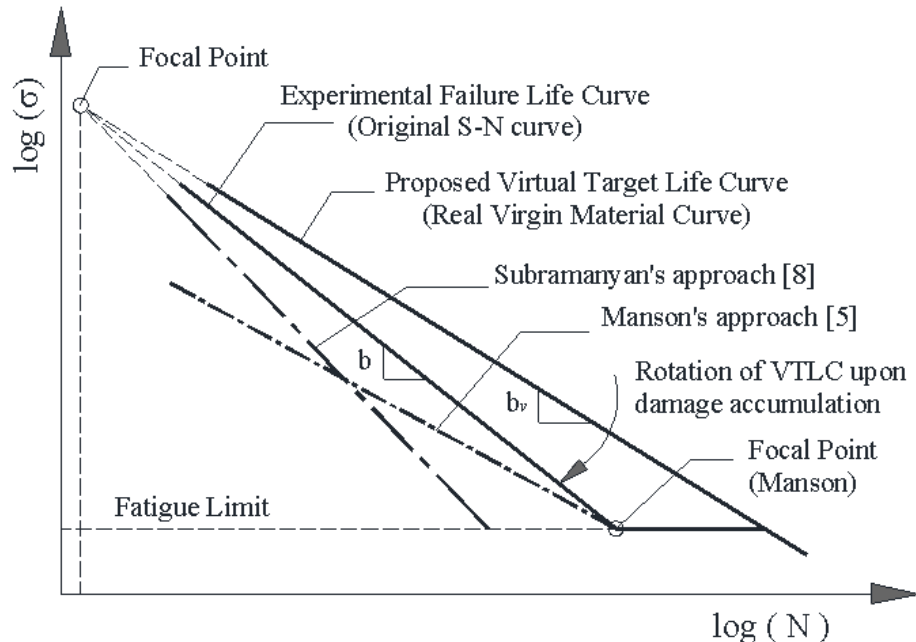


Figure 3.6 Comparison between the proposed VTLC and previous S-N curve modification approaches

The VTLC approach aims to give regular S-N curves (for constant amplitude excitations) a time- or loading- history dependency by making them dynamically moving according to the damage state. Moreover, it would be useful to have the S-N Curve as a way of monitoring the history of deterioration of a certain component in a structure as illustrated in Figure 3.7.

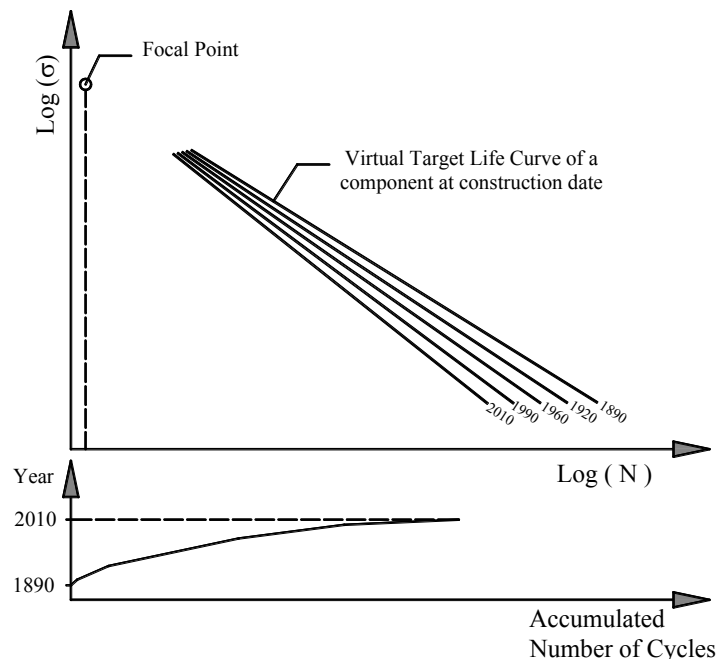


Figure 3.7 VTLC as a measure of deterioration of structures

3.4.2 Derivation

The concept of fatigue damage has always been challenging as it is not easy to set a clear definition for damage or provide a physical correlation to it. The VTLC approach doesn't use physical damage as a failure criterion. The VTLC approach gives a different perspective for the concept of damage. It views damage rather than being an accumulative sum of cycles up to failure, to being a concept of accumulated loss in the expected life. Unlike the regularly used criterion for failure when damage reaches unity,

the VTLC failure criterion is reached when the accumulated number of cycles reaches the current target life at a certain stress level.

Using S-N curves, at certain stress amplitude σ_a , the number of cycles to failure could be determined from the following equation:

$$N_f = \left(\frac{\sigma_a}{\sigma'_f} \right)^{1/b} = \left(\frac{\sigma'_f}{\sigma_a} \right)^{-1/b} \quad (3-7)$$

where b is the fatigue strength exponent and σ'_f is the fatigue strength coefficient of the material. Equation (3-7) can be re-written as :

$$\log(\sigma_a) = b \log(N_f) + \log(\sigma'_f) \quad (3-8)$$

To construct the virtual target life (VTL) curve from an existing S-N curve, we will assume another curve of slope b_v , which has to be less than b . All (VTL) curves are assumed to meet at the same intercept at $N = 1$ cycle which means the equation will have the same constant term: $\log(\sigma'_f)$. Thus, the equation for any Virtual Target Life Curve would be:

$$\log(\sigma_a) = b_v \log(N_{VTL}) + \log(\sigma'_f) \quad (3-9)$$

Therefore, the virtual target life (VTL) of a component at a certain stress level i can be expressed by the following equation:

$$N_{VTL_i} = \left(\frac{\sigma_i}{\sigma'_f} \right)^{1/b_{vi}} = \left(\frac{\sigma'_f}{\sigma_i} \right)^{-1/b_{vi}} \quad (3-10)$$

The rate by which the VTLC approaches the original S-N curve is important. Corten et al. (1956) proposed a stress dependency trend that schematically depends on the

stress level following a power law as shown in Figure 3.3. In order to simplify the damage calculation process, the trend in this research was selected to be linear. However, a new factor for excess overloading damage is introduced. Generally, the total change in slope Δb_i of VTL curve from the original initial slope b_v at stress level i , can be expressed as:

$$\Delta b_i = r_i N_i^a \quad (3-11)$$

where a is the power chosen for the trend, N_i is the total equivalent number of accumulated cycles under stress level i and r can be determined from:

$$r_i = \Delta b_{vo} / N_{fi}^a \quad (3-12)$$

where Δb_{vo} is the total expected change in slope of the VTL curve in case of constant amplitude loading and N_{fi} is the number of cycles needed for failure under constant amplitude loading at stress level i .

$$N_i = N_{i-1} \left(\frac{N_{fi}}{N_{fi-1}} \right) \quad (3-13)$$

where N_i, N_{i-1} are the total equivalent accumulated number of cycles under the current and previous stress levels i and $i-1$, respectively. N_{fi}, N_{fi-1} are the number of cycles to failure under the current and previous stress levels i and $i-1$, respectively.

Thus it can be easily proved that by adding n_i cycles:

$$\Delta b_i = r_i (N_i + n_i)^a = \frac{\Delta b_{vo}}{N_{fi}^a} \left(N_{i-1} \frac{N_{fi}}{N_{f,i-1}} + n_i \right)^a \quad (3-14)$$

To make the trend linear, taking $a = 1$ in equation (3-14)

$$\Delta b_i = \frac{\Delta b_{vo}}{N_{fi}} \left(N_{i-1} \frac{N_{fi}}{N_{f,i-1}} + n_i \right) \quad (3-15)$$

This equation can be formulated in terms of stress ratio

$$\Delta b_i = \frac{\Delta b_{vo}}{N_{fi}} \left(N_{i-1} \left(\frac{S_{f,i-1}}{S_{fi}} \right)^{-\frac{1}{b}} + n_i \right) \quad (3-16)$$

By using $a = 1$, the trend will become linear as shown in Figure 3.8.

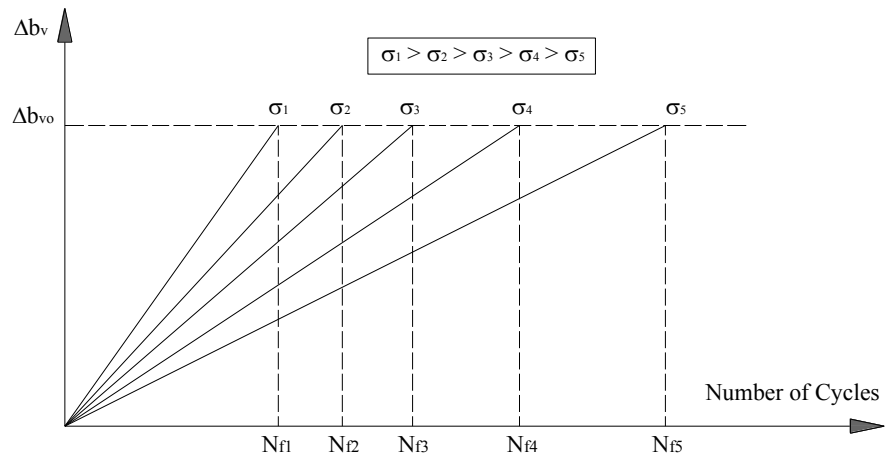


Figure 3.8 Change in slope in multi-stress level loading using a linear trend

In the VTLC method, the change in slope can be interpreted as being the loss in expected life. Applying a constant amplitude loading at a certain stress level should decrease the life by a well-known value $\Delta N_{\text{expected}}$ corresponding to a change in slope of

Δb_{v_0} such that the moving target life curve coincides with the original S-N curve as shown in Figure 3.9.

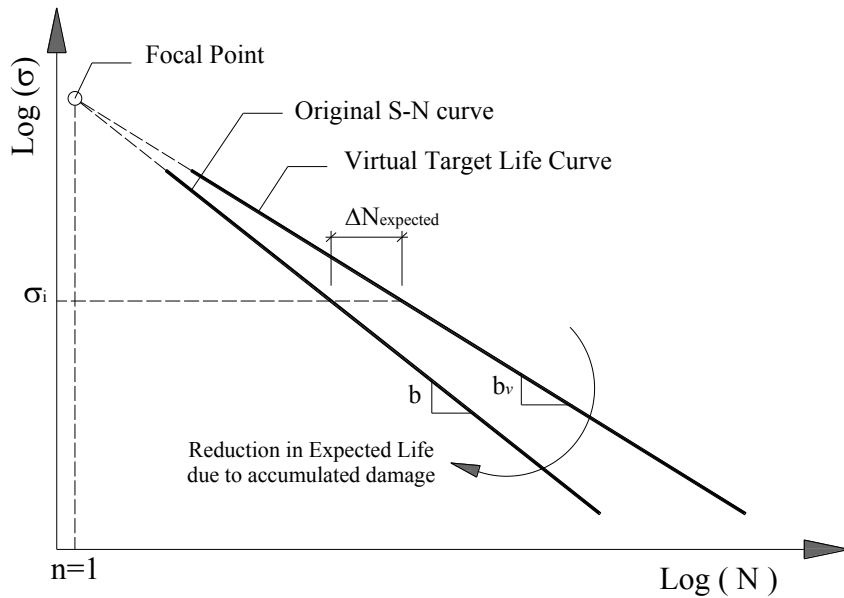


Figure 3.9 VTLC as a measure of deterioration of structures

Since both the original and VTL curves are linear on a log-log curve, then the expected loss in life curve should also be linear as shown in Figure 3.10.

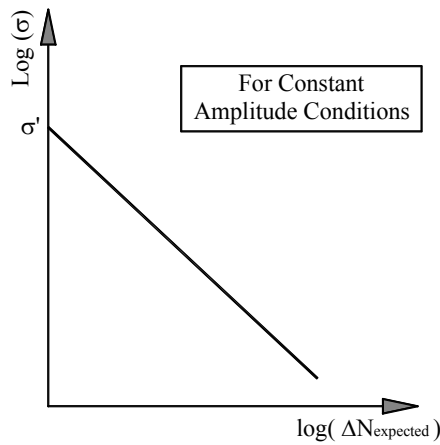


Figure 3.10 Schematic curve for the expected loss in life at each stress level

The total change in slope Δb_{vo} will be taken equal to the original S-N curve slope. This assumption is verified by the experimental results and validation examples that will be discussed later in the following sections.

3.4.3 Overloading effect

The effect of load sequence and interaction can be dealt with using two approaches (Li et al., 2001). The first approach is to account for the effect by evaluating an additional term of fatigue damage due to the effect of load interaction. The second approach is to account for the effect by obtaining an effective reduced fatigue life. The method adopted in this paper combines both approaches indirectly. It is important to take into account the overloading damage that occurs due to shifting from low stress level to high stress level (L-H). This damaging effect depends on the ratio between the two stress levels and the current damage level. A new term Δb_{Dj} is introduced, which is the j^{th} additional jump in slope due to changing the stress level. This overloading term must be introduced once the stress level changes from low stress level S_2 to high stress level S_1 . Δb_{Dj} depends on the ratio of stress amplitudes between consecutive blocks $r_b = S_2/S_1$ as in equation (3-17).

$$\Delta b_{Dj} = \frac{\Delta b_{vo}}{100} \left(1 - r_b^p \right) \quad (3-17)$$

where p could be a material constant that can be determined from experimental results and is a function in the ratio r_b .

3.4.4 Proposed procedure

Assuming that the element is subjected to a loading history with multiple stress levels, the fatigue life prediction procedure using the VTLC approach would be as follows:

1. For each cycle block, get the total change in slope Δb_i due to the additional number of cycles n_i from equation (3-16).
2. If the loading block i has a higher stress level, add the overstress term Δb_{Dj} to Δb_i from equation (3-17).
3. Calculate the new virtual target life at stress level i at loading block j from the following equation:

$$N_{VTL_{ij}} = \left(\frac{\sigma_i}{\sigma_f} \right)^{\frac{1}{b_v - \Delta b_j}} \quad (3-18)$$

4. Store the real total accumulated number of cycles.
5. Check that the equivalent total accumulated number of cycles $N_i < N_{VTL_{ij}}$.

Repeat from steps 1 to 5 until the condition in step 5 is violated. Then the total life would be the last value calculated from step 4.

If the total accumulated number of cycles is still less than the last calculated $N_{VTL_{ij}}$, then the tested specimen still has some fatigue life remaining. Next section will illustrate how to calculate the remaining fatigue life using the VTLC method.

3.5 Remaining life calculations

Using the VTLC method, the life curve is being reduced as the number of cycles keeps accumulating and increasing. This makes the prediction of the fatigue life an iterative problem. Using any programming script or a spreadsheet program could easily calculate the remaining life. Despite the iterative nature of the problem, it could still be solved manually by repeating steps 3 to 5 in the previous sub-section using small loading blocks until reaching failure. Counting these extra blocks and adding them up simply gives the expected remaining life. A sample object oriented C# computer code is provided in Appendix A

3.6 Validation

3.6.1 Introduction

In order to validate the proposed methodology, results from an intensive experimental investigation performed by Corten et al. (1956) were used. Over 700 steel wire specimens were tested in that investigation under several stress levels and different loading patterns. Corten et al. (1956) studied the specimens on three phases and noted them as Series A, B, and C. Figure 3.11 shows the loading pattern used in the tests.

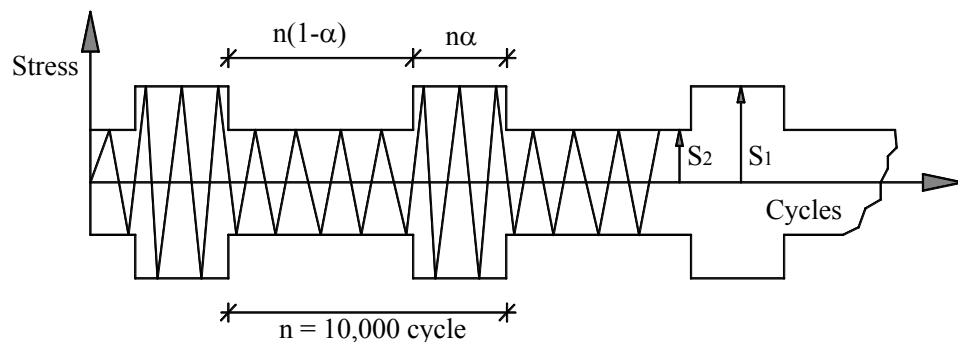


Figure 3.11 Testing Loading Pattern (Corten et al., 1956)

Results of the proposed damage model were compared to the commonly used Miner's Linear Damage rule (LDR) and Corten and Dolan's rule mentioned in section 3.2.4. The chosen value of p for equation (3-17) for the steel material used in Corten et al. tests was found by curve fitting to be as follows:

$$p = 100r_b^2 - 120r_b + 36 \quad (3-19)$$

Figure 3.12 and Figure 3.13 show a comparison between the results obtained using Miner's LDR, Corten et al.'s rule and the proposed VTLC method. It is convenient to combine the uncertainty in measurements by forming the ratio N/N_{fl} , which in terms of logarithm is equal to $\log(N)-\log(N_{fl})$. Each set of results represent 17 tested specimens. The round circles for each set in the figures represent the mean value, while the error range bars represent the 95 per cent confidence limits of the experimental results. By applying the VTLC approach procedure described in section 3.4.3, very good predictions of the experimental results were obtained.

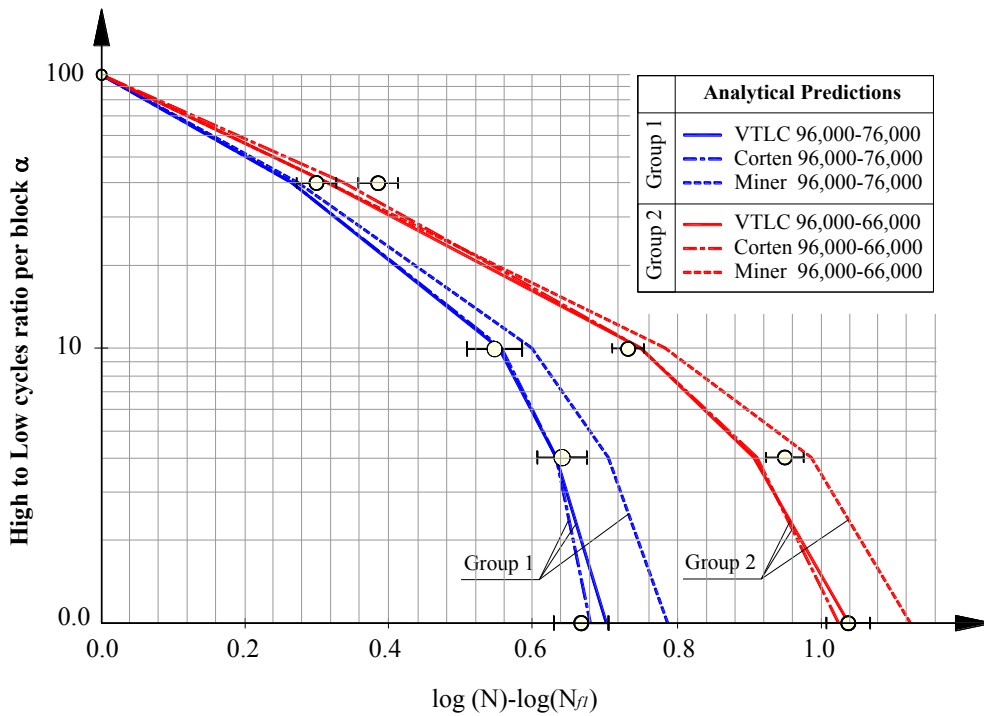


Figure 3.12 Analytical predictions of fluctuating stress amplitude experiments with high stress of 96,000 psi using three methods: VTLC, Corten, and Miner.
 (—○— Experimental results, Corten et al., 1956)

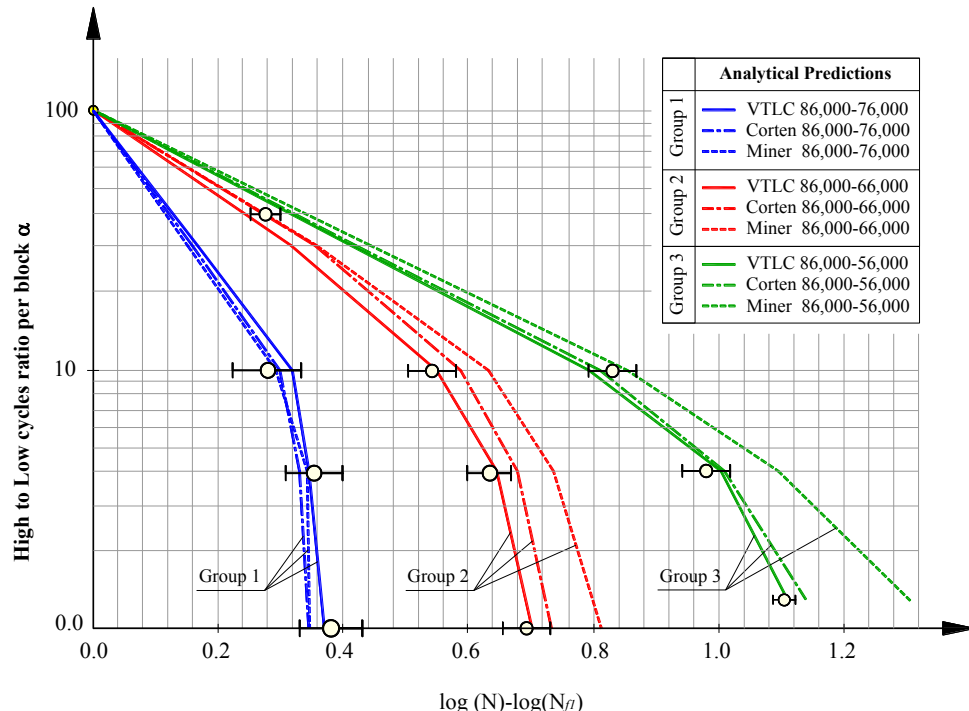


Figure 3.13 Analytical predictions of fluctuating stress amplitude experiments with high stress of 86,000 psi using three methods: VTLC, Corten, and Miner.
 (—○— Experimental results, Corten et al., 1956)

3.6.2 Observations and Conclusions

From the above results it could be seen that the VTLC approach captures different ratios of low to high (L-H) loading patterns with a relatively small error compared to the non-conservative results obtained using Miner's LDR rule. Miner's LDR rule has good predictions for loading patterns with block stress ratio $r_b = S_2/S_1$ that are very close to constant amplitude loading (close to unity). Although the VTLC method takes a linear (thus a more simple) trend in describing damage, it has very good agreement with life predictions that uses Corten's rule. This could be attributed to the fact that VTLC accounts for damage jumps that are caused by overloading through the term Δb_{Di} . As such, it could be said that the VTLC approach is a linear damage rule for measuring the loss in life that incorporates nonlinear effects arising from overloading in case of a variable fatigue loading pattern. It can be observed that for high values of the ratio α , the predicted life using either the Miner rule, Corten's rule or the VTLC method is usually more conservative. This might be attributed to the crack closure phenomenon reported by Elber (1970), which can be observed when the amount of high stress cycles becomes significantly more than the low stress cycles. This complex phenomenon could be further investigated and incorporated through the term Δb_{Di} in future work. Also, it should be noted that it is interesting to explore the model for case of both variable stress and variable frequency patterns, but there was no available experimental data in the literature to correlate the model with.

3.7 Extending the methodology

One of the interesting features of this method is that it could be extended to include the effect of corrosion-fatigue. As corrosion of a component increases, the damage increases, thus the slope of the VTL curve will automatically decrease. Finding a relation between the rate of corrosion and the change in slope is the challenging part as there is very limited experimental data available in literature to calibrate such model. In order to achieve this target, many experiments on several environmental-material systems should be done, to study the effect of such system on the rate of change in slope of the VTL curves. Moreover, an experimental program should be conducted to study the effect of overloads in several corrosive environments. Such a program should also evolve different frequencies of loading to account for different loading frequencies with time.

3.8 Case Study

As an example for the practical application of the developed damage model, the remaining fatigue life of a main member of a riveted single-track railway bridge built in Croatia in 1895 was investigated. This bridge was chosen because it was the only bridge (available to the authors during the course of this thesis) that had detailed data for its loading over about 100 years. Detailed bridge data and loading was acquired from the report provided by Kühn et al. (2008). No climate data or corrosion data have been reported.

3.8.1 Geometry

The bridge is composed of two equal trusses. The structural system of each truss is shown in Figure 3.14 . In year 2000, after over 100 years of service, there was a motivation for assessment since the bridge has reached the end of its design working life. Therefore, an assessment was carried out to determine the residual service life of the bridge. The actual traffic at that time has reached the maximum capability of the railway line. Construction of a new railroad is expected in the future (double track).

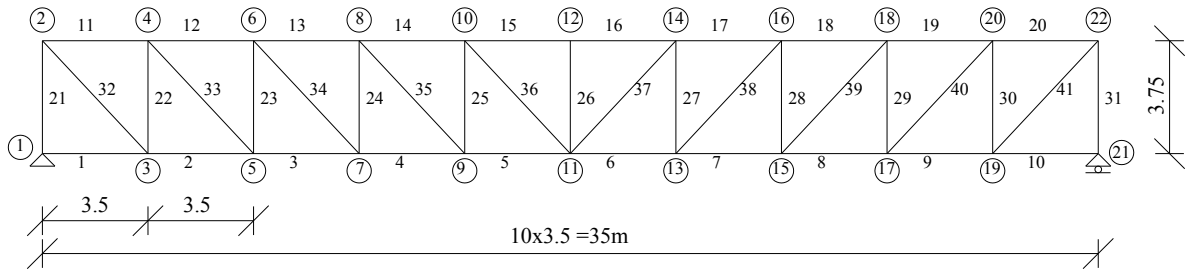


Figure 3.14 Structural System of the truss bridge showing the investigated member D-36

Concerning the number of locomotives and wagons involved, a detailed explanation is provided in the report prepared by Kühn et al. (2008). Since the bridge has been in use for 105 years, there is a higher probability of failure due to fatigue than due to static overloading. Data about traffic load and about materials were obtained from the railways archives. The structural system of the main truss is shown in Figure 3.14 . It should be noted that each specific structural element has a different fatigue life. The diagonal element in the middle of the span (D-36) was estimated as the most critical in fatigue. The highest number of cycles and the highest tensile stress range are expected to occur in this element (ordinates of the shear influence line are both positive and negative, and at their highest value). It was confirmed by reports of measurements that the highest

stress range was at this element (Kühn et al., 2008). Member (D-36) is 5.13m long and has a cross-section of 4L 80x10 with a gross area of 60.4 cm² and a net area of 52.0 cm². It is connected at its ends by a riveted connection using rivets 16mm in diameter. Detailed data on traffic such as number of trains each year, the type of trains and tons transported yearly was collected from the railways archives and available to do a Miner's sum. The analysed element was built using rivets, which corresponds to the detail category D in AASHTO (2007).

3.8.2 Formation of the stress range spectrum

On the basis of the data reported by Kühn et al. (2008), velocity measurements were taken along with corresponding stress ranges to calculate the dynamic amplification factor which was calculated to be about 1.17. The total secondary stresses that it could amount to were practically chosen to be 16% of the primary stresses. In that report, the calculations were based on the net cross-sectional area of the member D-36. The stress range spectrum for the time period from 1895 until 1980 was provided and corresponding fatigue damage was calculated using Miner's rule as shown in Table 3.1(a). Another stress range spectrum was done for each year from 1980 to 2000 and the corresponding number of crossings as shown in Table 3.1(b). Kühn et al. (2008) considered the studied detail having a fatigue category D according to AASHTO. Calculations showed that there is no remaining design fatigue life at 1985. The member chosen for the analysis cannot be considered safe anymore after 90 years of service, although the bridge was reported to still be in service for more than 105 years.

Table 3.1 Tables reported by Kühn, et al. (2008) for estimated damage from (a) 1895–1980, and (b) 1980–2000

a. For the time period 1895 – 1980

$\varphi \cdot \sum k \cdot \Delta \sigma$ [N/mm ²]	n _i	m	N _i	$\frac{n_i}{N_i}$
92.6	235 000	3	902 000	0.26053
82.8	369 000		1 261 000	0.29262
70.8	318 000		2 017 000	0.15766
64.3	18 000		2 693 000	0.00668
60.8	140 000		3 185 000	0.04396
45.9	880 000	5	9 615 000	0.09152
37.6	63 000		26 067 000	0.00242
34.7	481 000		38 939 000	0.01235
23.6	90 000	∞	∞	0.00000
20.4	784 000		∞	0.00000
16.8	18 000		∞	0.00000
	$\sum n_i = 3 396 000$			$\sum \frac{n_i}{N_i} = 0.86775$

b. For the time period 1980 – today

$\varphi \cdot \sum k \cdot \Delta \sigma$ [N/mm ²]	n _i	m	N _i	$\frac{n_i}{N_i}$ (for 1 year)
70.8	20 000	3	2 017 000	0.00992
45.9	65 000	5	9 615 000	0.00676
20.4	41 000	∞	∞	0.00000
	$\sum n_i = 126 000$			$\sum \frac{n_i}{N_i} = 0.01668$

m : represents the slope of the S-N curve

n_i : represents the actual number of cycles

N_i : represents the number of cycles to failure

The data from Kühn et al.'s report has been thoroughly investigated and rearranged chronologically year by year as shown in Table 3.2.

Table 3.2 Chronologically ordered data from Kühn et al. (2008) report

	Train Passing	$\varphi \cdot \sum k \cdot \Delta \sigma$	Number of cycles
1895-1913	Cargo wagon	23.6	90000
	S 123 Locomotive	60.8	140000
	Passenger wagon	20.4	173000
1914-1946	S 32	82.8	369000
	Cargo wagon	34.7	345000
	Passenger wagon	20.4	301000
1947-1959	S 38	92.6	235000
	Cargo wagon	34.7	136000
	Passenger wagon	20.4	119000
1960-1980	E 362	70.8	318000
	2E 362	64.3	18000
	Cargo wagon	45.9	880000
	E 320	37.6	63000
	Passenger wagon	20.4	192000
1980-Present (Yearly)	E 362	70.8	20000
	Cargo Wagon	45.9	65000
	Passenger wagon	20.4	41000

3.8.3 Fatigue Life Prediction using VTLC

By using the same detail category of the connection (category D) as reported by Kühn et al. (2008), the VTL curve for this member was constructed using an initial slope equal to double the original slope 3. By performing the procedure mentioned in section 0 several VTL curves were plotted showing the loss in fatigue life of the studied member (which has a detail category D) throughout the years of service as shown in Figure 3.15 . In order to compare the effect of considering the detail as category C on the predicted fatigue life, several VTL curves showing the loss in fatigue life were plotted as shown in Figure 3.16.

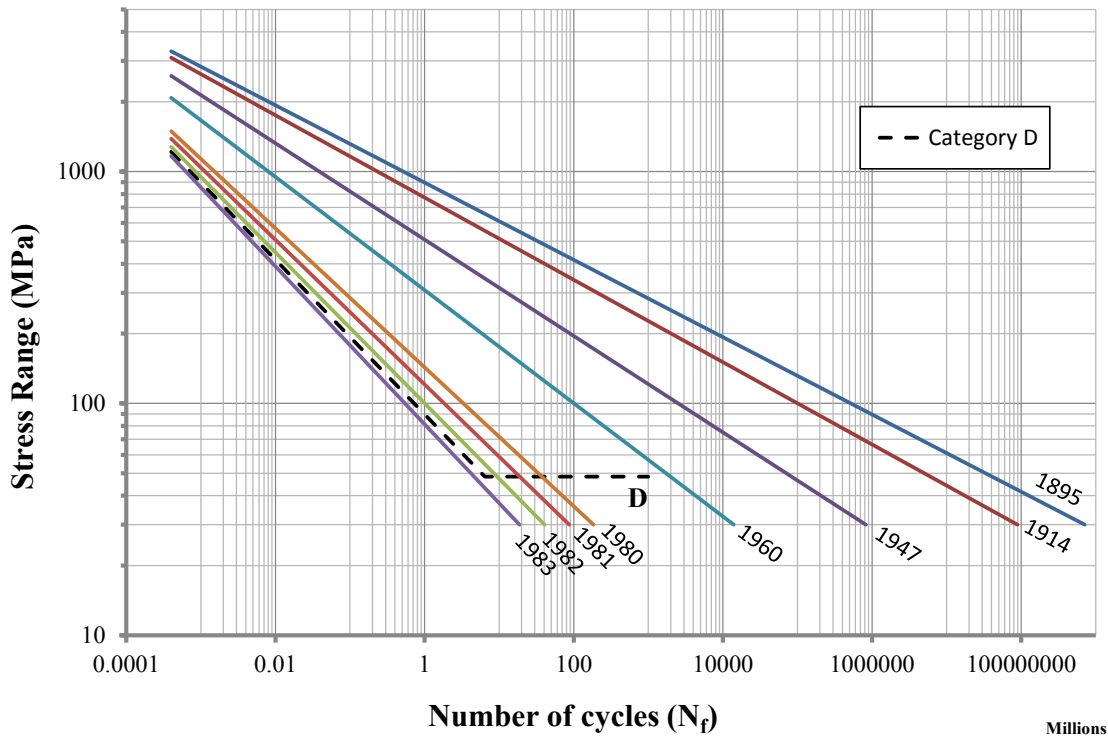


Figure 3.15 VTL curves for the investigated member D-36 showing the deterioration in fatigue life with years (assuming the detail is category D)

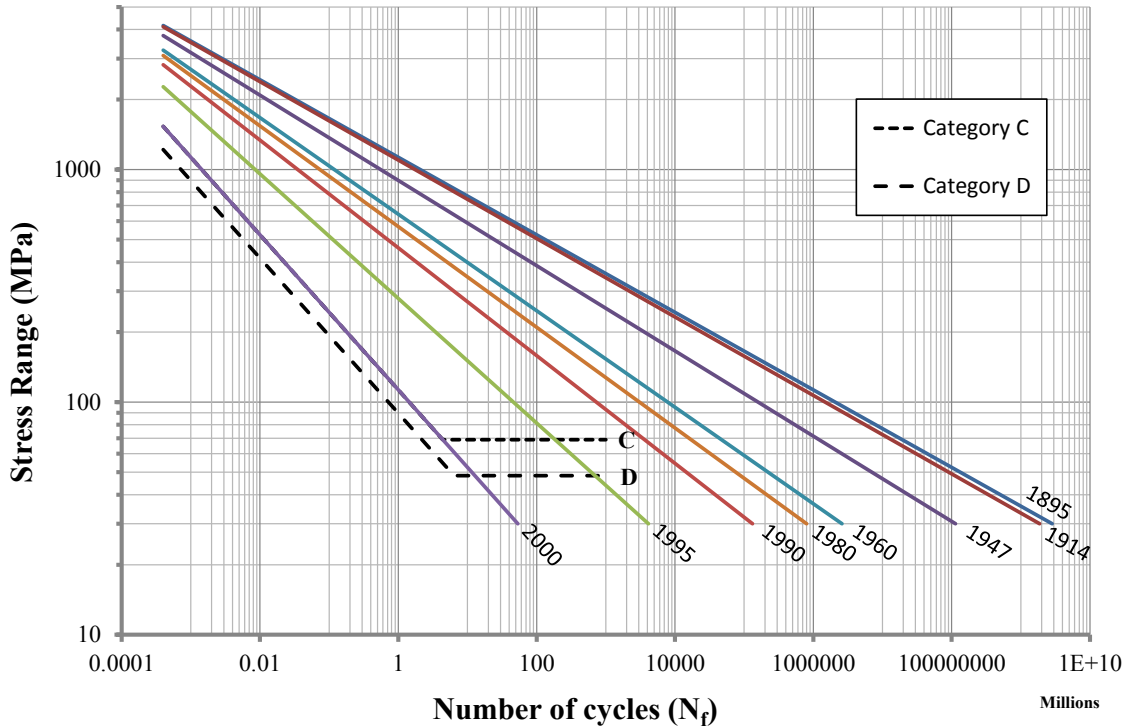


Figure 3.16 VTL curves for the investigated member D-36 showing the deterioration in fatigue life with years (assuming the detail is category C)

3.8.4 Discussion and Conclusions

The proposed VTLC method provides a simple and a visually illustrative method for predicting the fatigue life of a certain structural detail under variable amplitude loading. It has been shown that this method could be calibrated to take into account the effect of stress overloading. On the other hand, similar to all damage accumulation models, they need calibration with a wide range of real experimental data to become more accurate and reliable. The VTLC predictions showed that there is no remaining design fatigue life after year 1982, which is about 87 years of service. This estimation is more conservative than the 90 years predicted by Kühn et al. (2008) using Miner's cumulative damage rule.

It is important to mention that the bridge was reported to still be in service for more than 105 years, while the VTLC estimations were about 87 years. This difference could be attributed to the choice of detail category D for all riveted connections, which is—as mentioned before in the literature review—a lower bound for all riveted connections that could go up to detail category C or slightly more in some cases. If the same detail was to be considered as category C, the predicted life using the VTLC would have extended to the year 2000, which corresponds to 104 years of service life. This shows that there is a need to categorize riveted connections and further classify them into more categories. This point will be highlighted in a case study in Chapter 4.

CHAPTER 4

NUMERICAL FORMULATION OF THE FATIGUE LIFE PREDICTION TOOL

4.1 Introduction

Finite element method (FEM) is a vital tool for the analysis of various structural elements. The continuous rapid advancement in computing technology led to the development of several finite element software packages that facilitate solving large structural models in a relatively shorter time. This latter aspect (speed of executing the analysis) encouraged many researchers to simulate physical tests using FEM. Within the context of this thesis, the FEM has facilitated performing stress analyses along with implementing the concepts of linear fracture mechanics in order to predict the fatigue life of structural steel components. This approach provides a better alternative to experimental fatigue tests which are time consuming and costly. Moreover, a thorough literature review showed that only few fatigue tests were based on variable amplitude loading which represents the real in-service loading scenario. On the other hand, fatigue testing results using constant amplitude are affected by the frequency of loading, which, in most cases, is higher than reality (in order to complete the test in a relatively shorter duration).

An add-on program named CorrFLP (**C**orrosion **F**atigue **L**ife **P**redictor) is developed using the C# language. CorrFLP (about 40,000 lines of object oriented code) acts as an add-on that could be associated with several FE software packages, where it enables the fatigue analysis capabilities by providing many fatigue damage models. CorrFLP is capable of analyzing the input mesh and adding fatigue and corrosion

parameters to the regular FEM analysis. CorrFLP can simulate the crack propagation process along with the geometric simulation of corrosion by simulating the loss in thickness. CorrFLP can present the output in the form of contours of damage, stress concentrations or expected remaining life. The fatigue assessment process implemented in CorrFLP involves three main phases; pre-processing phase, analysis phase and post-processing phase. Figure 4.1 illustrates the whole process of the fatigue analysis as being modeled in CorrFLP. Sections 4.2, 4.3, and 4.4 elaborate on the details and features of the three main phases of CorrFLP, namely, pre-processing phase, analysis phase and post-processing phase, respectively.

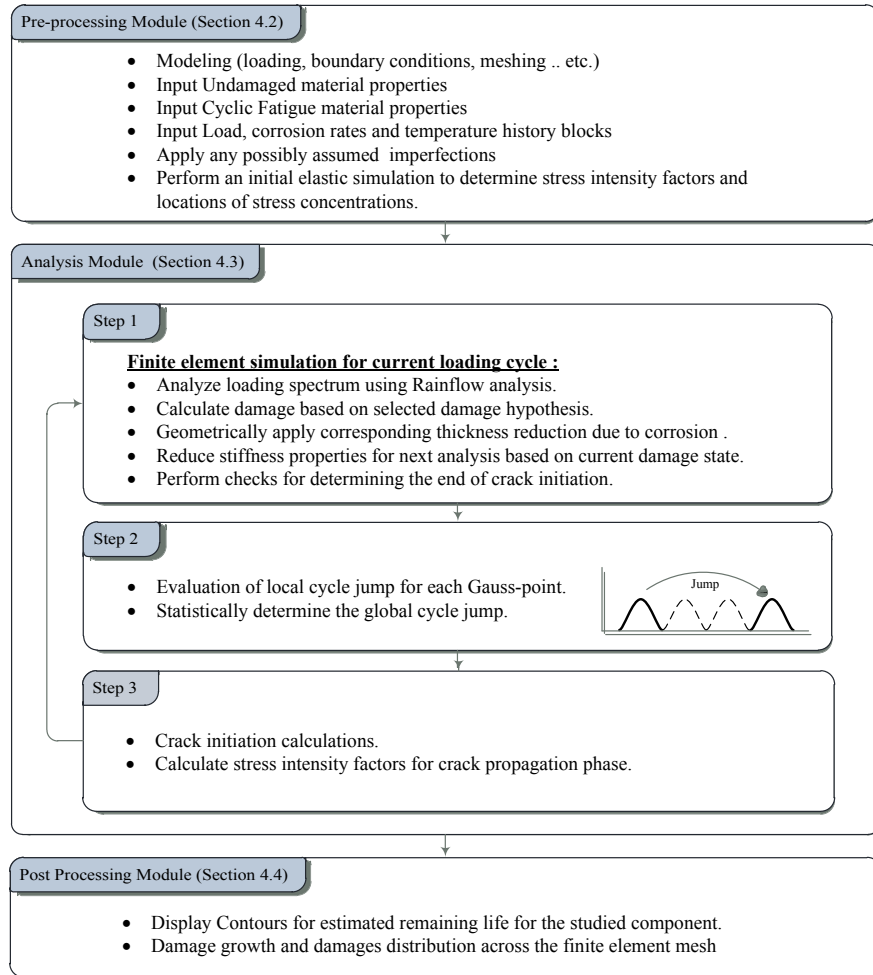


Figure 4.1 Illustration for the three main modules of CorrFLP and the interaction between applying damage and cycle jumps

4.2 Pre-Processing Module

4.2.1 Model Preparation Section

ABAQUSTM 6.10 (Dessault-Systems, 2010) was chosen as the finite element software package to be used for modeling and analyzing all the FE models in this research. In this research, CorrFLP acts as a fatigue analysis add-on for ABAQUSTM; it uses the finite element models created in ABAQUSTM. To simulate real-time environmental and loading effects on the studied component, CorrFLP accepts the following input:

1. Customized loading patterns (Load Cycle Block), to simulate the daily traffic loading intensity on the studied component per hour.
2. Corrosion rates expressed by the rate of loss of thickness in mm/year.
3. Monthly temperature change.
4. The damage model chosen for fatigue life prediction.
5. The user can also predefine any pre-existing damage in the model to simulate imperfections.

The user then specifies if the simulation is to proceed up until failure or if it is required for a certain time interval. The program also gives the option to choose the method of cycle jumps to reduce the total execution time. The concept of cycle jumps is covered in Section 4.3.3. The input data file is stored in a Fatigue and Corrosion Data file (.FCD).

4.2.2 Simulation Section

After the preparation phase is complete, CorrFLP prepares the ABAQUSTM input file (.INP) and exports it to the ABAQUSTM solver. CorrFLP runs each analysis step and finally extracts its results from the ABAQUSTM results database file. The extracted analysis results are then processed by CorrFLP which starts predicting the damage caused by this loading cycle to all the elements in the mesh using the user-chosen fatigue damage model (from a library of built-in strain-based damage models, as explained in Chapter 2). CorrFLP consequently changes the material properties of the damaged elements, prepares the model for the next loading cycle, exports it to ABAQUSTM which runs this cycle, and in turn returns it back to CorrFLP and so on until the process is interrupted by the user, or reached its pre-defined duration limit, or the studied component fails. The communication process between CorrFLP and ABAQUSTM is schematically explained in Figure 4.2.

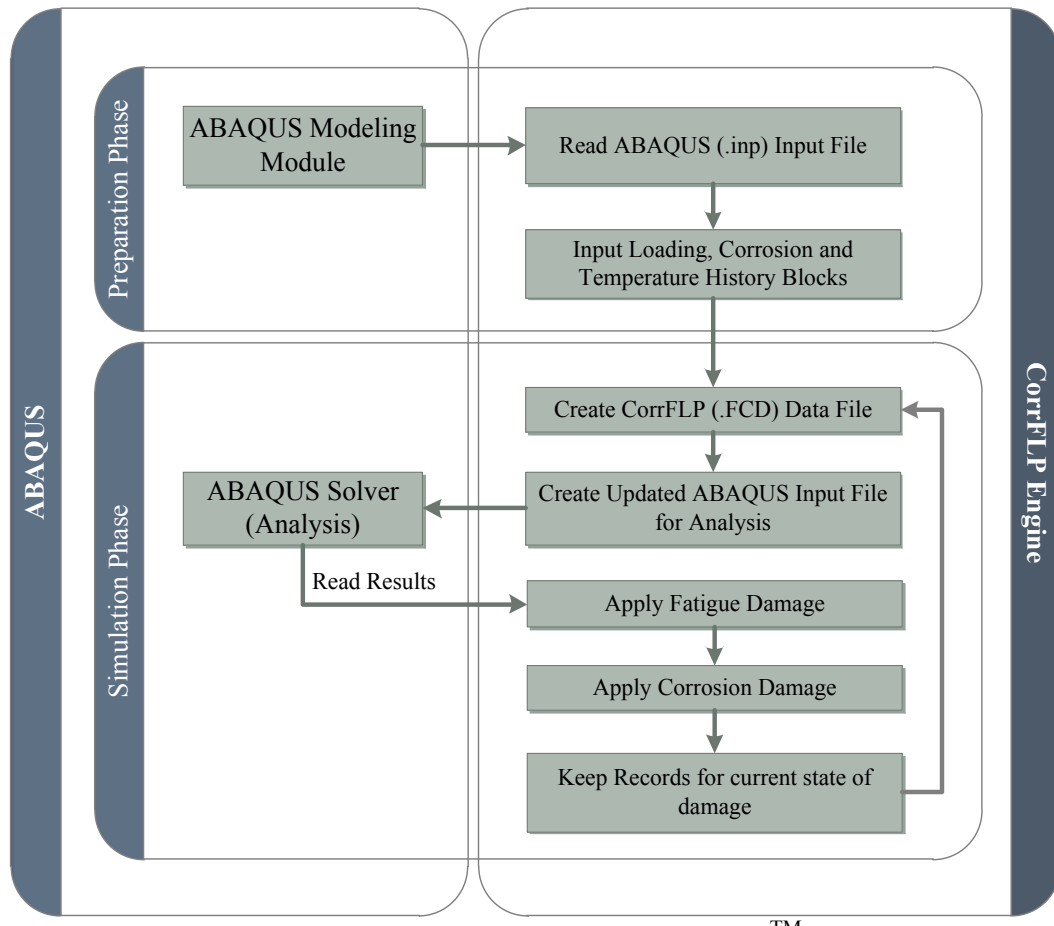


Figure 4.2 Schematic drawing for the CorrFLP and ABAQUSTM communication process

4.2.3 CorrFLP's User Interface

CorrFLP is designed to have a user friendly interface which is totally independent of the ABAQUSTM interface; in that it is not necessary to have the ABAQUSTM user interface open while using CorrFLP. CorrFLP can display the models along with all results within its interface. CorrFLP provides a detailed log window for all processes working in the background during the analysis.

Figure 4.3 shows a screenshot of CorrFLP's user interface during an analysis showing the real-time logging of the calculations being done in the background.

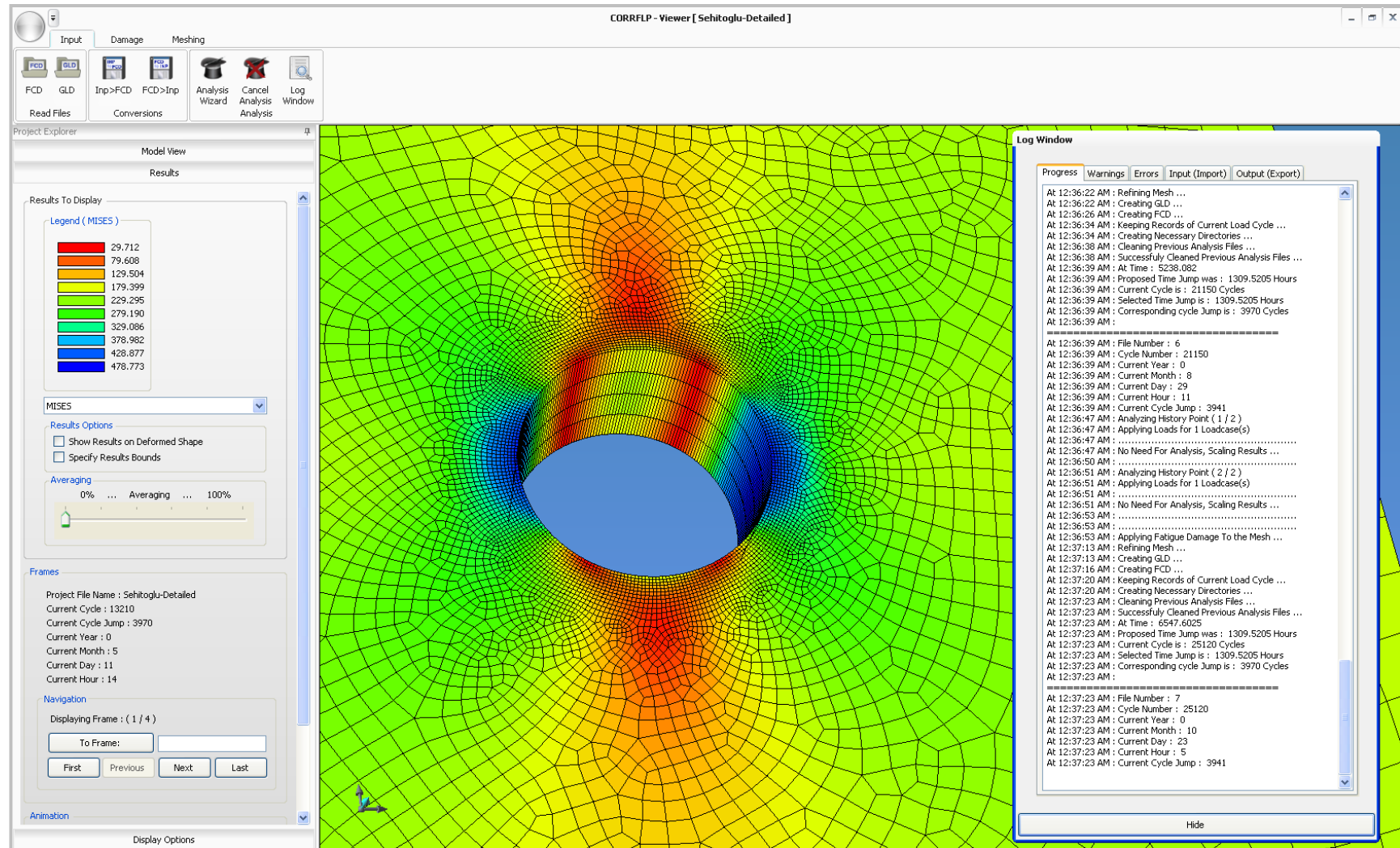


Figure 4.3 CorrFLP's user interface snapshot

4.2.4 Material Editor

As previously mentioned, CorrFLP acts as an add-on to FEM packages, thus it adds extra fatigue features to the regular FE input. CorrFLP accepts the input of many fatigue cyclic properties such as the cyclic and hysteresis fatigue curve constants. CorrFLP has a big library of fatigue properties for many materials (over 70 different steel and Aluminum types) gathered from available published literature. . A list of these materials is provided in Appendix B. If the user does not have any fatigue data available, CorrFLP can derive fatigue properties from elastic and plastic material properties using the “Uniform Material method” of Baumel et al. (1990). Figure 4.4 shows the material editor interface. The cyclic properties provided in the material editor are used to construct the static stress strain curve that is used in the FE analysis. The material editor can be used to input material properties required for crack propagation analysis too.

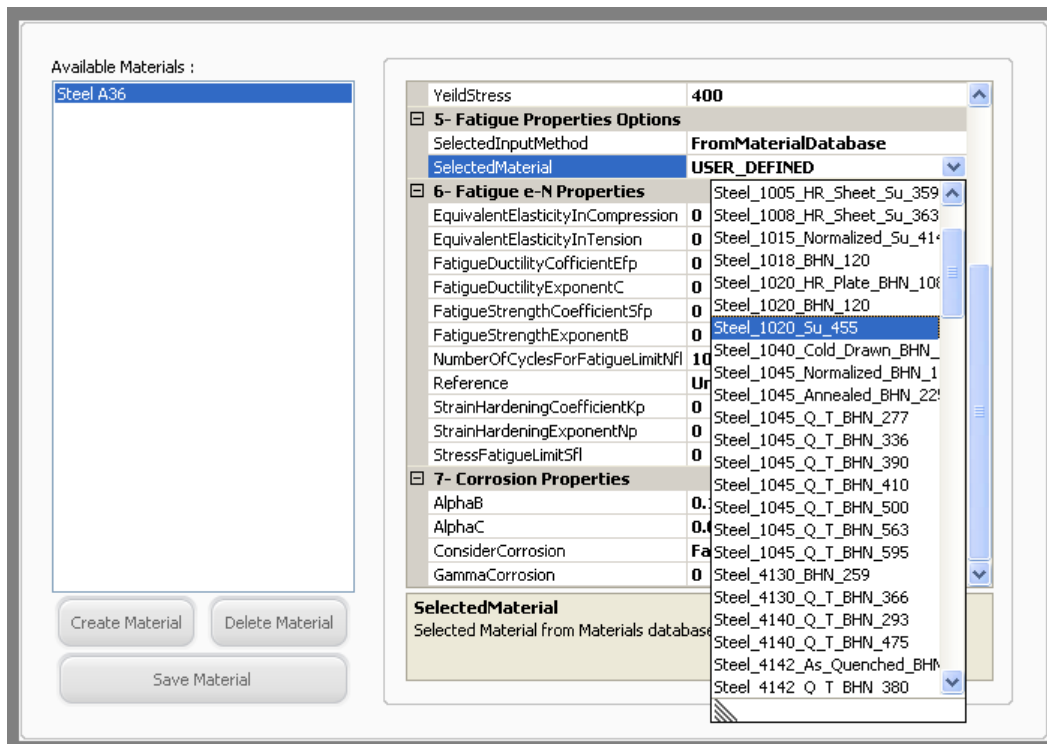
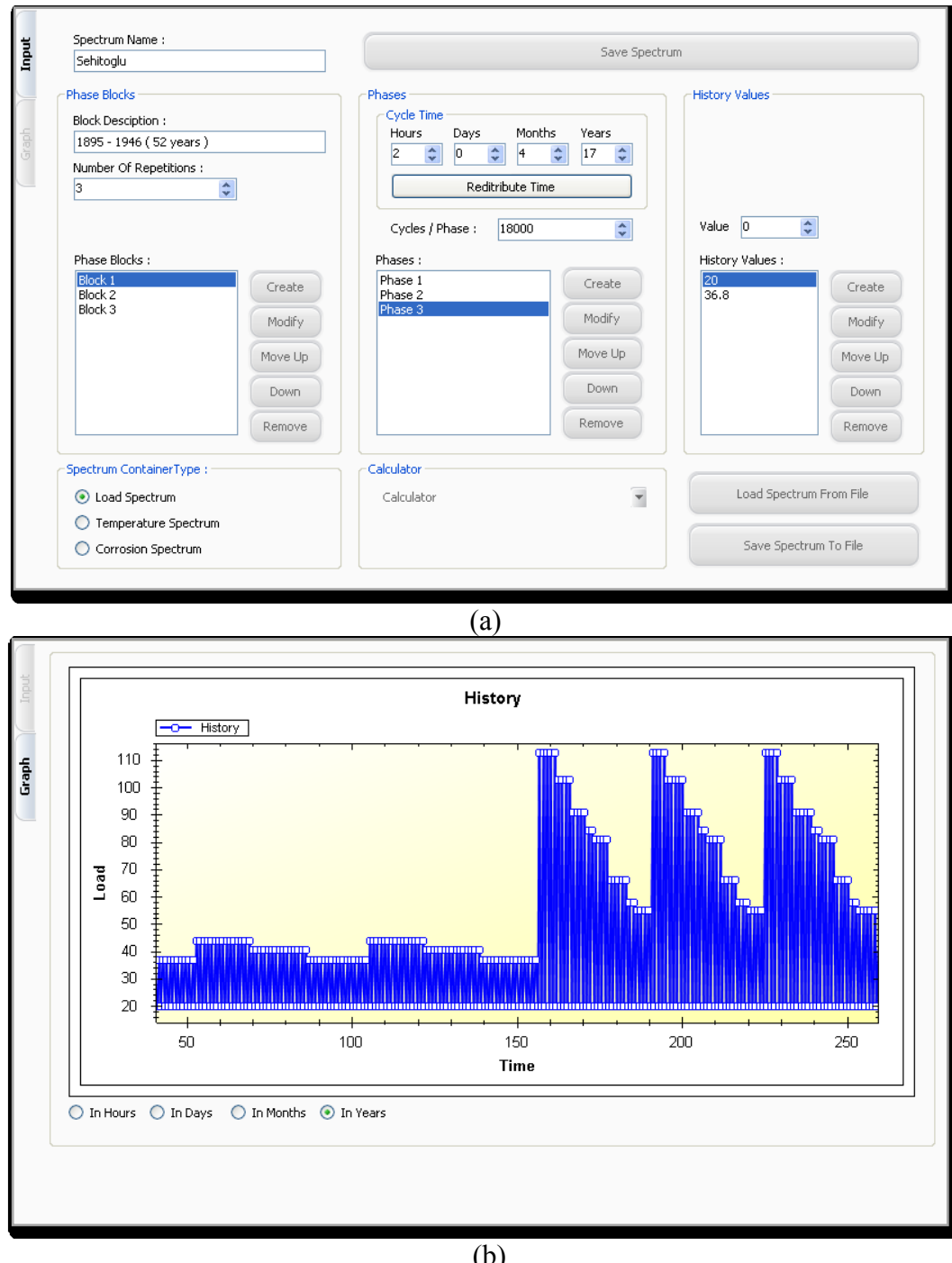


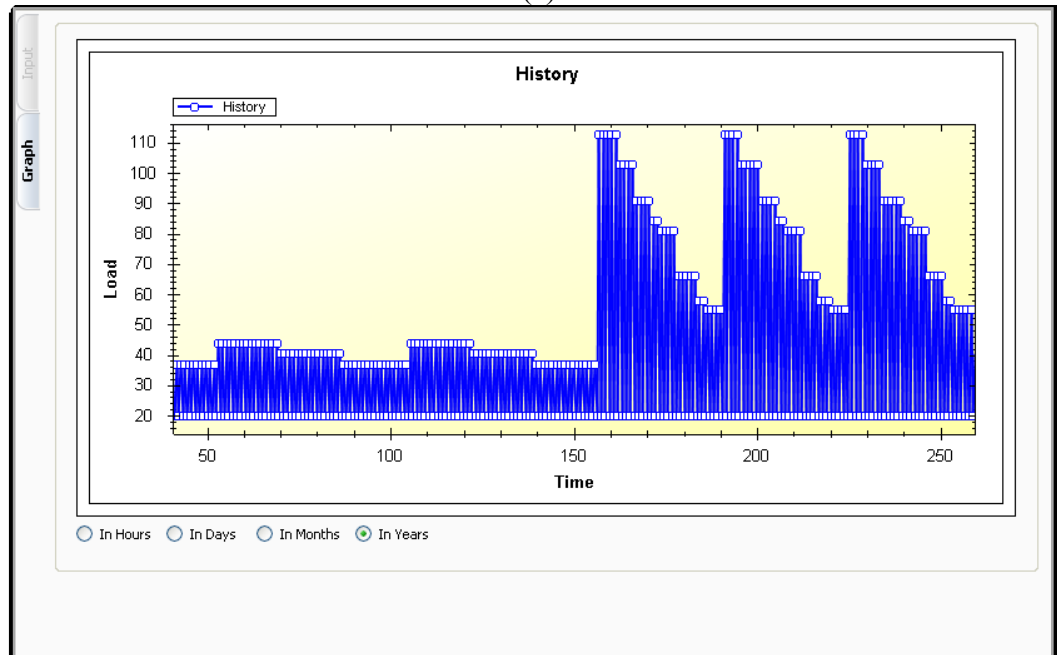
Figure 4.4 CorrFLP’s material editor (showing the list of built-in materials library)

4.2.5 Spectrum Editor

The spectrum editor enables the user to input load spectra, corrosion rate spectra and temperature spectra. Figure 4.5 shows the spectrum editor interface.



(a)



(b)

Figure 4.5 CorrFLP's spectrum editor (a) Input window, and (b) History graph window

4.3 Analysis Section

4.3.1 CorrFLP's Object Oriented Structure

CorrFLP was programmed using an extendible object oriented structure and having a rich 2D and 3D finite element library of elements. When the ABAQUS™ finite element model is imported into CorrFLP along with the results, CorrFLP updates its originally generated mesh with that updated information. The previous mesh elements automatically communicate together to modify their sizes and orientations in space. The mesh can be automatically refined without affecting the boundaries such that the finite elements optimally capture the stress gradients at locations of stress concentration. Next sub-sections will illustrate the object oriented hierarchy of the classes (objects) within the “Main Mesh Object”.

4.3.2 Main Mesh Object

CorrFLP has one “Main Mesh Object” that stores all data. It has a structure made up of several managerial objects (programming classes) that monitor the input and output of the program and make decisions based on their (each managerial object) specialization. Figure 4.6 shows the main structure of the “Main Mesh Object” and its most important manager objects. The following sub-sections give detailed description for each manager object.



Figure 4.6 Schematic drawing for the mesh managers in CorrFLP

4.3.2.1 Fatigue Management Object

The “Fatigue Management Object” is responsible for communicating with the material class object of each element to extract its fatigue cyclic properties and its current damage state in order to pursue the fatigue damage calculations. The “Fatigue Management Object” calculates the expected endurances at each integration point. Moreover, it calculates the stress intensity factors at the stress raiser locations for crack propagation analysis. It can also specify the expected locations for crack initiation to monitor the crack initiation length.

4.3.2.2 Corrosion Management Object

The “Corrosion Management Object” is responsible for applying uniform corrosion (reduction in shell element thickness) on the mesh based on values gathered from the input corrosion spectrum. It is also responsible for providing corrosion data modifications corresponding to the current temperature and the material properties. The user specifies the expected corrosion type (i.e. galvanic corrosion, crevice corrosion, fretting corrosion, etc.) such that the “Corrosion Management Object” defines the appropriate corrosion rates. As the analysis proceeds, the “Corrosion Management Object” assigns corrosion states to each external surface of the studied component individually based on its real level of exposure.

4.3.2.3 Temperature Management Object

The “Temperature Management Object” is responsible for applying uniform temperature on the mesh based on values gathered from the input temperature spectrum. The “Temperature Management Object” can also assign individual surface temperatures for each external surface of the studied component individually based on its real temperature. It can also modify the material’s stress strain curves based on the specified normal temperature.

4.3.2.4 Interaction Management Object

The “Interaction Management Object” is responsible for synchronizing results and data obtained from the fatigue, corrosion and temperature managers and applies user’s selected interaction rules to couple the effects of corrosion and temperature with fatigue. This feature is added for applying any coupling effects between the input factors in future based on the advancements in the body of knowledge available.

4.3.2.5 Refinement Management Object

The “Refinement Management Object” is responsible for all mesh geometrical editing processes. It is capable of subdividing elements, splitting or resizing elements without affecting the connectivity of the elements. The “Refinement Management Object” communicates with the “Fatigue Management Object” to get the locations of stress concentrations and crack initiation. For crack propagation analysis, the “Refinement Management Object” is capable of modeling the crack tip and inserting the appropriate singular crack-tip elements. Although crack propagation analysis is beyond the scope of this thesis, this feature is implemented for future extensions. The “Refinement Management Object” communicates with the “Corrosion Management Object” to geometrically apply thickness reduction or element removal based on the specified corrosion rate for each element. For example, in order to simulate corrosion for a given corrosion thickness loss history, the 2D elements change their thicknesses with time, while the 3D solid elements adaptively move their faces inwards to simulate the effect of loss of thickness over time. This happens by having all elements communicate together to know the outer faces, and decide which faces will be moved. More details on this technique will be demonstrated in Chapter 5.

4.3.2.6 Element Damage Management Object

The “Element Damage Management Object” is responsible for storing all damage and damage rates information for each integration point in the element. The rules for strain based damage models are covered in Chapter 2. The “Element Damage Management Object” manages the averaging of damage per element. Also, it detects the stress gradient per element and communicates with the “Refinement Management Object” to refine the element to capture this gradient.

4.3.2.7 Spectrum Management Object

The “Spectrum Management Object” is responsible for managing all input time-history spectra (load spectra, corrosion rates spectra and temperature spectra). It gathers data from all spectra at the current simulation time and then applies the appropriate values corresponding to the current time. The “Spectrum Management Object” interacts with the “Fatigue Management Object” to get a reasonable value for the cycle jumps (as will be discussed in section 4.3.3).

4.3.2.8 Input/Output Management Object

The “Input Output Management Object” is responsible for importing data files from different finite element software packages into CorrFLP. It is also responsible for exporting CorrFLP data files to other finite element software input file formats. This manager is responsible for generating animation frames for the gradual damage happening to the studied model. Figure 4.7 shows the file formats supported by CorrFLP.

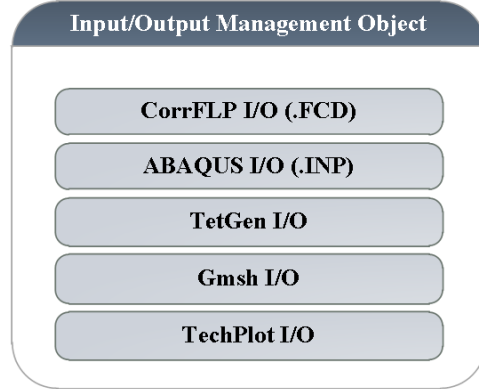


Figure 4.7 Supported formats for the Input Output Management Object

4.3.2.9 FE Components Object

The “FE Components Management Object” acts as a container for all CorrFLP’s finite element objects such as Elements, Nodes, Sections, and Surfaces, etc. It is responsible for adding, modifying or removing those components and synchronizing them. Figure 4.8 shows the components managed by the “FE Components Management Object”.

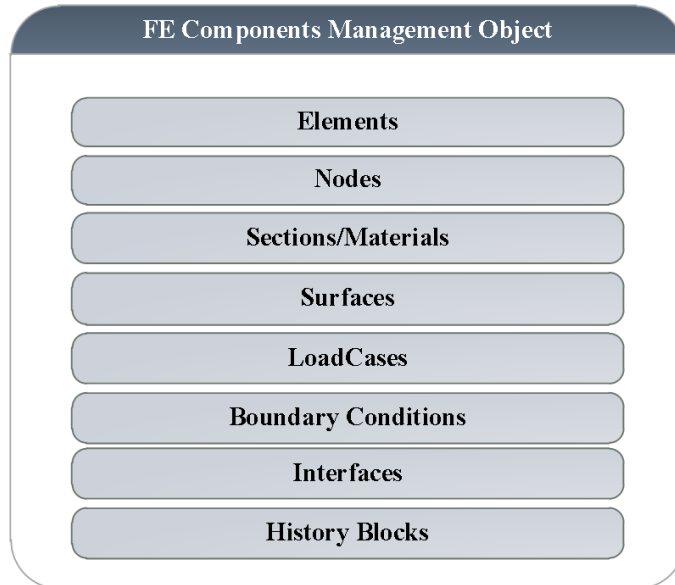


Figure 4.8 Components managed by the FE Components Management Object

4.3.2.10 FE Containers Object

The “FE Containers Management Object” acts as a container for container-types. Container-types are groups that contain several objects. For example, an “Element Set” is a container-type that refers to a group of “Elements”. Another example for container-types is a “Part” which physically represents a component. A “Part” could include many elements, nodes, surfaces, sections, etc. An “Assembly” is a collection of “Parts” that make up the whole component. The program uses the same terms and conventions used in most finite element packages. Figure 4.9 shows the containers managed by the “FE Containers Management Object”.

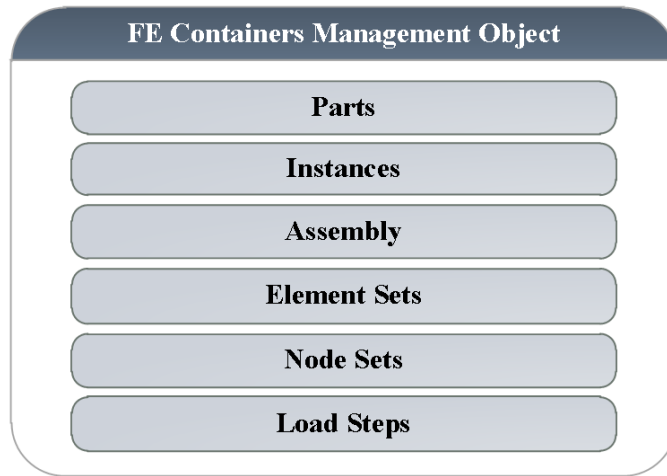


Figure 4.9 Containers managed by the FE Containers Management Object

4.3.2.11 Searching Management Object

The “Searching Management Object” is responsible for tracking and searching all components in the smart mesh. It could fetch any component in the mesh based on various searching criteria. For example, the “Searching Management Object” can fetch an “Element Set” of “Elements” that lie within a certain radius in the vicinity of a certain

point in space. Moreover, the “Searching Management Object” can fetch “Elements” that are damaged beyond a certain level.

4.3.2.12 Statistics Management Object

The “Statistics Management Object” is responsible for statistically populating the damaged elements and the proposed cycle jumps at each integration point. This manager helps other managers of the smart mesh in taking decisions.

4.3.2.13 Mesh Info Management Object

The “Mesh info Management Object” is responsible for storing all project information such as project name, current cycle number, current cycle jump, current time, etc.

4.3.3 Cycle Jumps

A loading cycle has two peak amplitudes; one in tension and one in compression, with respect to a certain mean stress. To simulate a cycle with minimal computation effort, one needs to perform at least two analyses; one for tension loading and another for compression. One way for having a time efficient analysis is to jump or skip some cycles by considering a “super-cycle” that is equivalent to a certain amount of cycles and having its same effect. The concept of cycle jumps was adopted by many researchers using different cycle jump criteria, for further details, refer to Paepegem et al. (2001) and Cojocaru (2006).

4.3.3.1 The cycle jump concept

CorrFLP automatically chooses the size of the “cycle jump” depending on the expected life of the component based on how much its mesh is damaged and within the limits specified by the user. Figure 4.10 illustrates the concept of cycle jump. The cycle jump technique adopted in CorrFLP is the same one used by Paepegem et al. (2001). Since each fatigue loading cycle represents a physical amount of time, then the cycle jump for all elements of the mesh must be the same, but it has to be carefully chosen such that it captures the flow of damage in the critically stressed parts of the mesh without sacrificing the sensitivity of the analysis. Mesh zones having relatively low stress levels and low damage rates would be rather safe to jump relatively larger cycle jumps without leading to errors in the damage distribution. On the other hand, other zones with high stress levels and high stress gradients or having high rates of damage flow, must have small cycle jumps that are small enough to capture the stress redistribution to the neighbouring zones and consequently accurately model the flow of damage in the mesh elements.

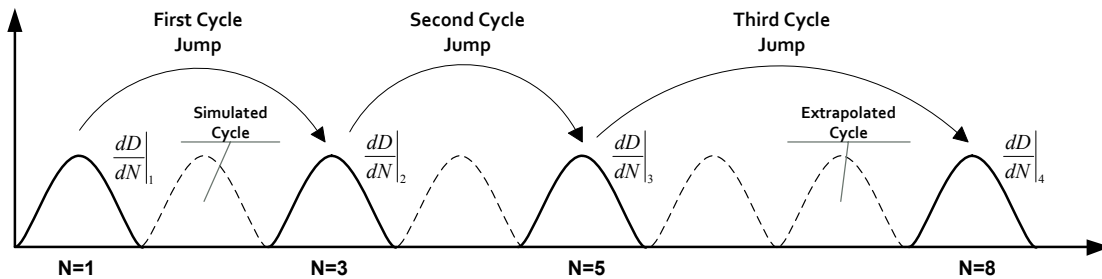


Figure 4.10 The super cycle and cycle jump concept Paepegem et al. (2001)

4.3.3.2 Calculation of Local Cycle jump

CorrFLP automatically calculates the proposed cycle jump for each element in the mesh at each of its Gauss points based on its current damage state and the previous rate of damage. Damage can then be extrapolated based on the chosen cycle jump at each Gauss point using the simple Euler explicit integration formula:

$$D_{N+\Delta N} = D_N + \frac{dD}{dN} \Big|_N \Delta N_{Local} \quad (4-1)$$

Where D_N and $D_{N+\Delta N}$ are the damage states before and after the cycle jump; respectively. $\frac{dD}{dN} \Big|_N$ is the previous rate of damage at the studied integration point. In order to accurately capture the damage flow, the extrapolated damage $D_{N+\Delta N}$ can be limited by a certain increment; for example $D_N + \Delta D$ where ΔD is the damage tolerance that can be specified by the user. Based on this damage tolerance, a maximum local value (at each Gauss point) for the cycle jump ΔN_{Local} can be determined. Figure 4.11 illustrates the concept of limiting the number of cycles based on a certain limited extrapolated damage.

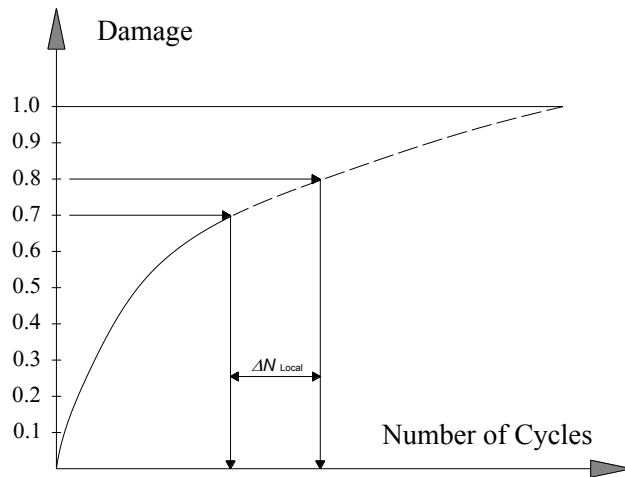


Figure 4.11 Damage extrapolation and corresponding cycle jump

4.3.3.3 Choice of the Global Cycle jump

The global cycle jump ΔN_{Global} for all mesh elements must be the same. The simplest way for choosing ΔN_{Global} is by taking the minimum ΔN_{Local} . Although this approach would be the most accurate method, but it is not recommended as it will increase the processing time. Alternatively, ΔN_{Global} could also be taken as the number of cycles ΔN_{Time} corresponding to a certain time interval specified by the user. The approach adopted in CorrFLP would be by taking ΔN_{Global} as a percentage of the cumulative relative frequency distribution of ΔN_{Local} without exceeding ΔN_{Time} . Figure 4.12(a) shows the relative frequency distribution of the local cycle jumps ΔN_{Local} calculated at each element's Gauss points. Figure 4.12(b) shows the cumulative relative frequency distribution of the local cycle jumps ΔN_{Local} showing the choice of ΔN_{Global} as a chosen percentage of the cumulative relative frequency, this percentage is recommended by (Paepegem et al., 2001) to be less than 15%. The “Statistics Object” is responsible for all these calculations.

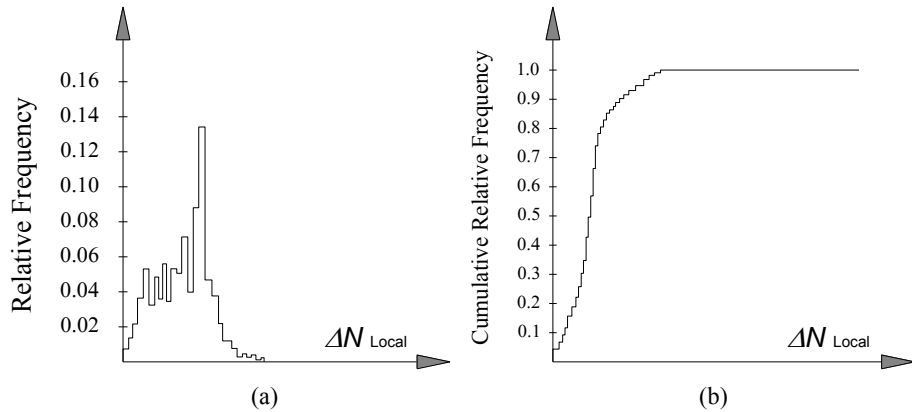


Figure 4.12 Choice of global cycle jump based on frequency distribution (Paepegem et al., 2001)

4.3.4 CorrFLP's Fatigue calculations:

4.3.4.1 Fatigue Life Prediction

Fatigue analysis in CorrFLP is based on the strain-based method. CorrFLP implements all the endurance prediction rules listed in section 2.4.2. It also implements the Rainflow counting algorithm for simplifying complex loading histories. Cycle counting in CorrFLP takes into account the material memory effects by following the material's hysteresis backbone curve as discussed in section 2.4.2. After each analysis step, the material input for the next super-cycle is affected by the current damage state of each element, for instance, Young's modulus would be degraded to $E_o(1 - D)$ where E_o is the initial value for Young's modulus and D is the damage, which varies from 1 to 0 (1 for completely damaged, 0 for undamaged virgin material).

CorrFLP predicts the estimated number of cycles for crack initiation using the theory of critical distances mentioned in section 2.4.5. Any element with high damage rates and high stress gradients is further meshed (as a parent element) into smaller elements (children elements) that are automatically chosen within 0.01mm to 0.05mm or can be specified by the user to capture stress gradients at the critical distance inside the material below the mesh outer surface. The sub-meshing process of parent elements into children elements can take various techniques based on the type of element used and the existing meshing, a sample sub-meshing technique is shown in Figure 4.13.

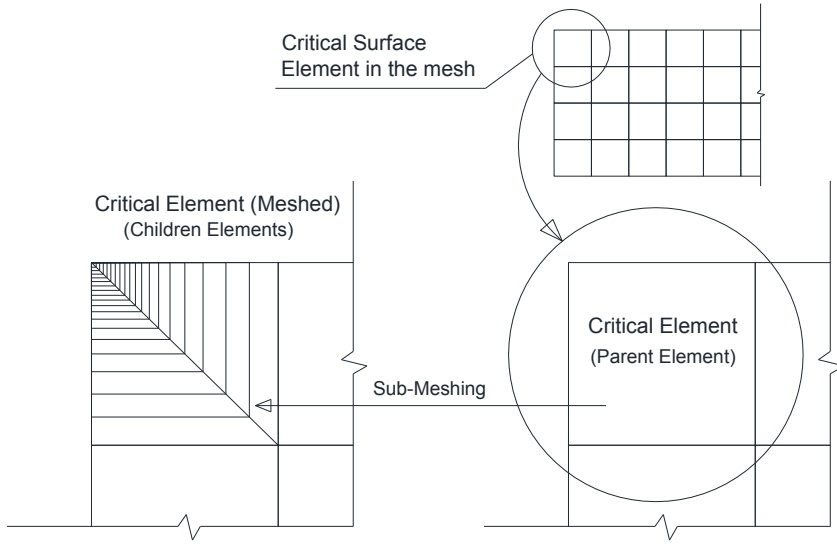


Figure 4.13 Sub-meshing of critical (parent) elements into fine (children) elements

Decisions are taken by the parent elements based on the total stress and strain gradients within their children elements. Volumetric calculations within the parent element are performed to calculate several factors such as the stress intensity factor range ΔK_I . If the amount of damaged children elements passed the critical distance “ L ” that can be calculated from (2-10), the number of cycles predicted N_P is stored as an average estimate for the fatigue crack initiation life. ΔK_{th} can be specified by the user based on values published in literature. For a wide variety of values of ΔK_{th} for different materials, the reader can refer to rich resource for fatigue thresholds in the compendium of fatigue thresholds written by Taylor (1985). In air environment, the fatigue threshold ΔK_{th} in various steels tested at a stress ratio of $R=0.1$ is equal to about $6.162 \text{ MPa}\sqrt{\text{m}}$. The critical stress range $\Delta\sigma_o$ is equal to the fatigue limit the number of cycles elapsed (Taylor, 2008). In order to cover some of the uncertainties involved in the calculations

and the error in the provided material fatigue properties. A $\pm 15\%$ in the calculated critical length is proposed to give two fatigue life estimates for a specimen. The range of $\pm 15\%$ was arbitrarily chosen, and it proved to result in very good predictions of fatigue life, as will be shown later. Hence, CorrFLP provides an upper and lower bound for the estimated crack initiation life corresponding to $0.85L$ and $1.15L$. Where $N_{P,Lower}$ and $N_{P,Upper}$ are the estimated crack initiation lives corresponding to the damage propagating along critical distances of $0.85L$ and $1.15L$; respectively. This range is a preliminary estimate proposed in this research and can be modified by the user. Figure 4.14 shows the propagation of damage in the (children) elements of a critical surface element.

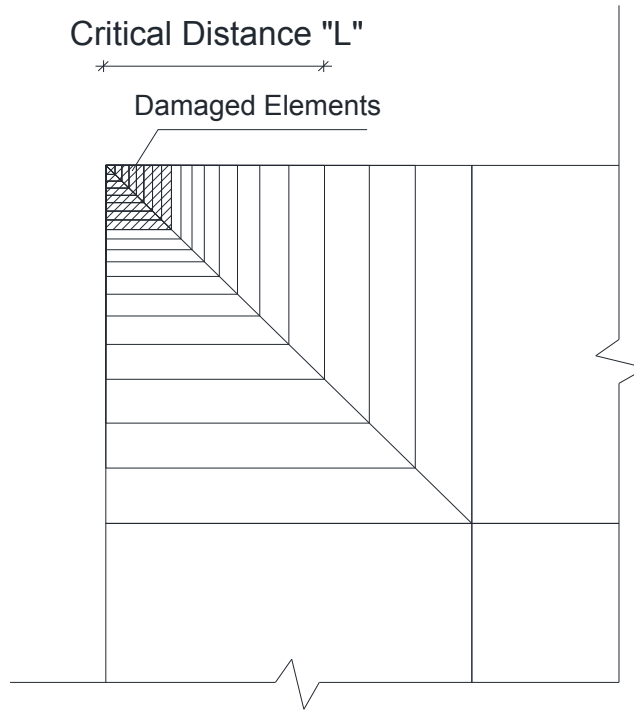


Figure 4.14 Propagation of Damage in (children) elements

4.3.4.2 Analysis Procedure

The main analysis procedure is schematically described in Figure 4.15 in the form of a flowchart showing the function of each manager in the process.

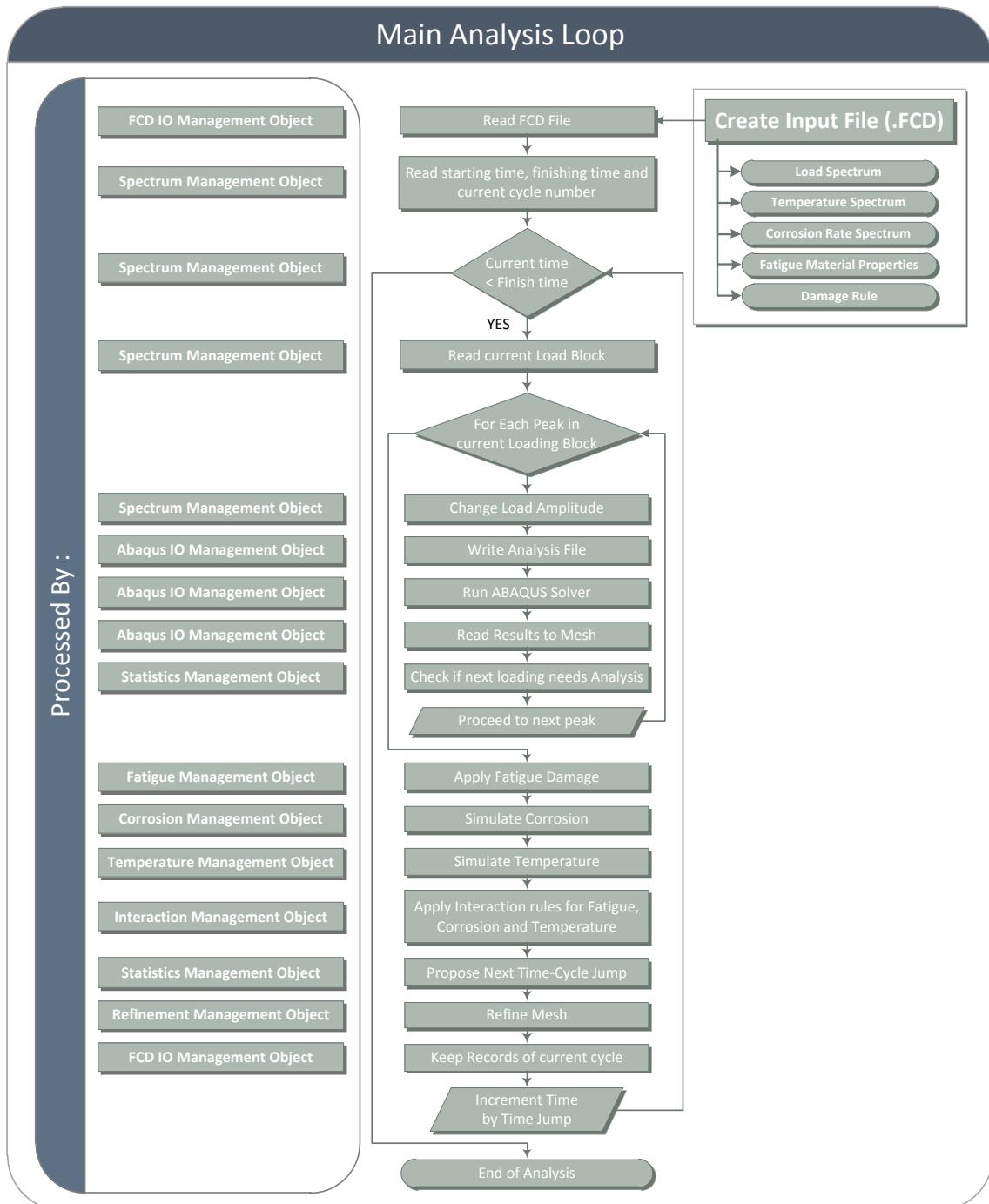


Figure 4.15 Schematic flow chart for the analysis process showing the “Management Object” responsible for each task

4.4 Post-Processing Phase

The program displays the mesh at studied time intervals by:

1. Plotting damage contours at each analysis step for each element in the mesh.
2. Plotting contours of the expected remaining life for each element.
3. Plotting contours of principal stresses and strains and their ranges for each element at any time interval.
4. Plotting contours for stress concentration factors (with respect to a remote load in an elastic analysis).
5. Animating the change in mesh with time displaying the input change at each cycle, the time elapsed and the remaining life of the whole component.
6. Generating detailed reports on crack initiation locations and damage values and rates at the integration points of each element.

4.5 Verification with experimental results

Using CorrFLP and the analytical techniques and procedures described earlier in this chapter, fatigue analyses of several details from literature are carried out to predict their fatigue lives. The following subsections present a description of the test setup, results, description of the finite element models and analysis details.

4.5.1 Case Study 1: Plate with a circular hole

4.5.1.1 Test Description

In this case study, CorrFLP is verified using the experimental work reported by Sehitoglu (1983). The researcher performed fatigue tests on hot rolled ASTM A36 steel plates with a circular hole subjected to uniform tension. This detail is chosen because the test data and details are well listed. Moreover, both the stress concentration factor and the stress intensity factor for this detail are well established in literature.

4.5.1.2 Specimen Dimensions and Material Properties

The test specimens consisted of 280 x 50 x 5.7 mm with a 7.6 mm diameter hole at its centre. The effective part of the plate is its middle 100 mm part; as there are about 90 mm of grip lengths at each end as illustrated in Figure 4.16. The specimens were tested under load control conditions.

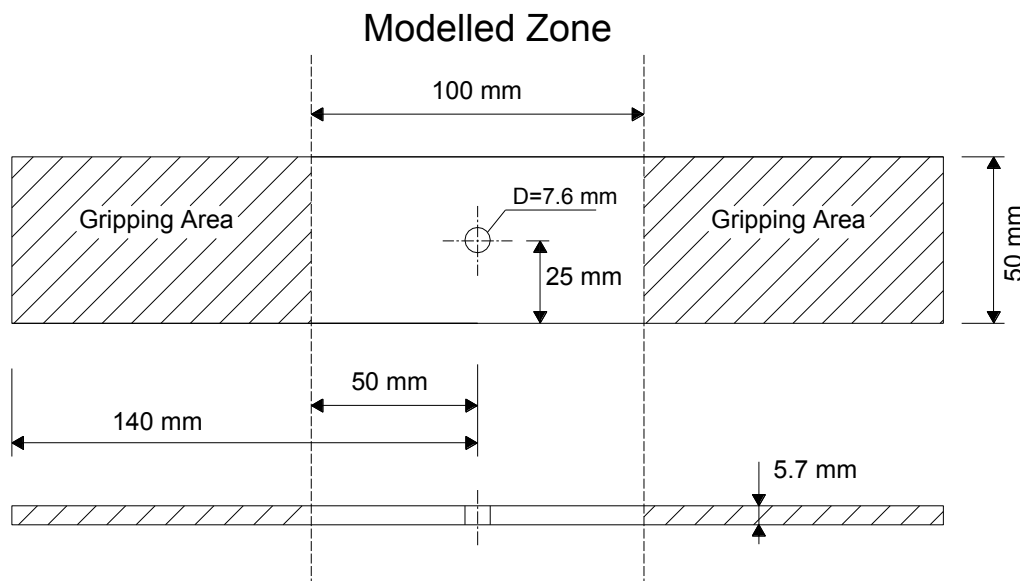


Figure 4.16 Test specimens from Sehitoglu (1983)

A fully reversed cyclic loading was applied. The cyclic stress vs. strain and fatigue properties of the tested material have been reported by Sehitoglu (1983); $E = 200,000$ MPa, $K' = 1336$ MPa, $n' = 0.226$, $\sigma'_f = 1118$ MPa, $b = -0.11$, $\varepsilon'_f = 0.242$ and $c = -0.48$. Therefore, based on the cyclic parameters provided by Sehitoglu (1983), the cyclic isotropic hardening material model can be expressed by:

$$\frac{\Delta\varepsilon}{2} = \frac{\Delta\sigma/2}{200000} + \left(\frac{\Delta\sigma/2}{1336} \right)^{1/0.226} \quad (4-2)$$

where $\Delta\varepsilon$ and $\Delta\sigma$ are the strain range and stress range, respectively.

4.5.1.3 Finite Element Model

A 3D finite element model has been modeled. The reduced integration solid continuum element C3DR from the ABAQUS FE library was used. The stress strain curve is defined as a series of stress and strain pairs based on equation (4-2). Figure 4.17 shows the finite element model showing the loading, boundary conditions and meshing.

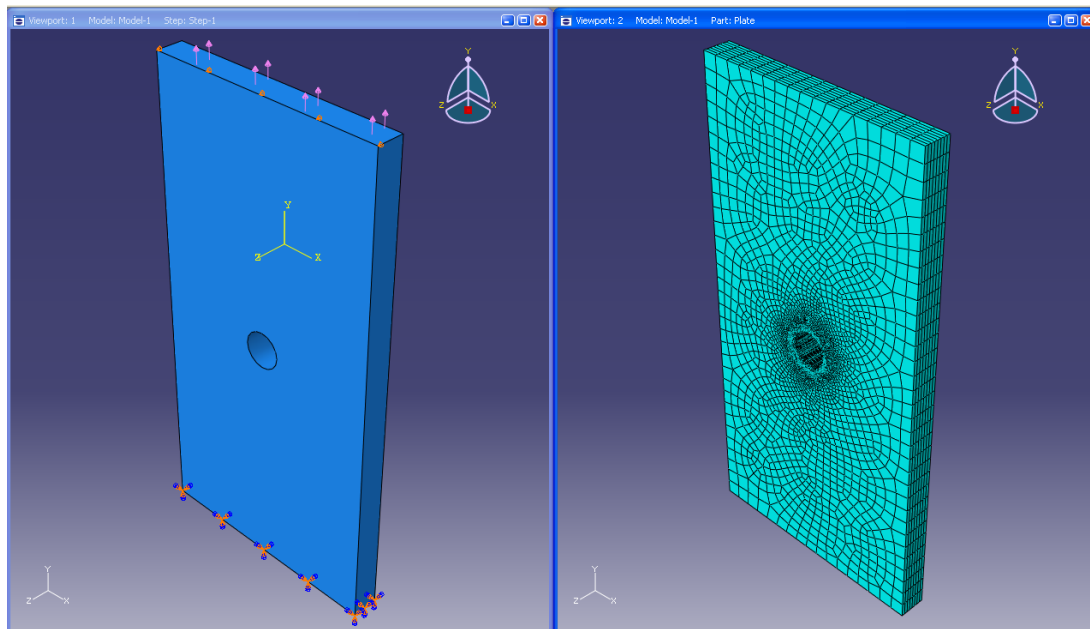


Figure 4.17 The finite element model (Loading on the left, meshing on the right) using CorrFLP

Static nonlinear finite element analyses of the specimens were carried out at several load levels. Each load level represents certain nominal stress amplitude on the net area, which varied from 118 MPa to 271 MPa.

4.5.1.4 Fatigue Life Prediction

Several analyses have been performed for each stress level using different strain-life prediction models such as the Smith-Watson-Topper (SWT) method, the Brown-Miller and the regular strain endurance method. Figure 4.18 shows a snapshot of the damage contours at crack initiation. Crack initiation life is determined as the micro-cracks propagate to a certain critical length. The critical length crack initiation length in CorrFLP was taken as an average of 0.077mm to cover the range of 0.066mm to 0.088mm reported by Sehitoglu (1983) so that the reported crack initiation lives could be accurately compared.

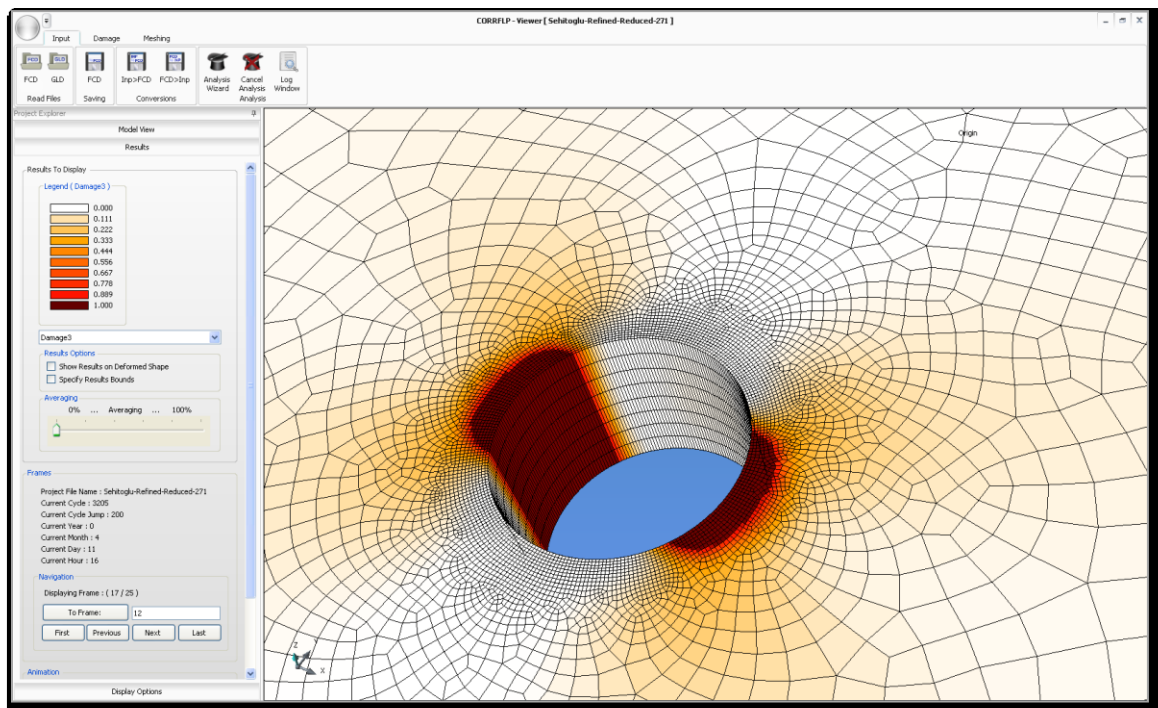


Figure 4.18 Damage during the crack initiation life using CorrFLP

As can be seen in Figure 4.19, there is a very good agreement between the crack initiation lives reported by Sehitoglu (1983) and the results obtained by CorrFLP using different strain-life prediction approaches. This very good correlation can be attributed to the simplicity of the model (simple plate with a hole) and the accuracy of the meshing. The reduced integration elements C3DR were used as the fully integrated elements can produce high gradients at locations of stress concentration which numerically gives unrealistic fatigue life predictions. Moreover, this element is less computationally expensive too. The results obtained by the SWT method were usually better than the other approaches; this observation is in agreement with many other experimental observations for metals (Drapper, 2008).

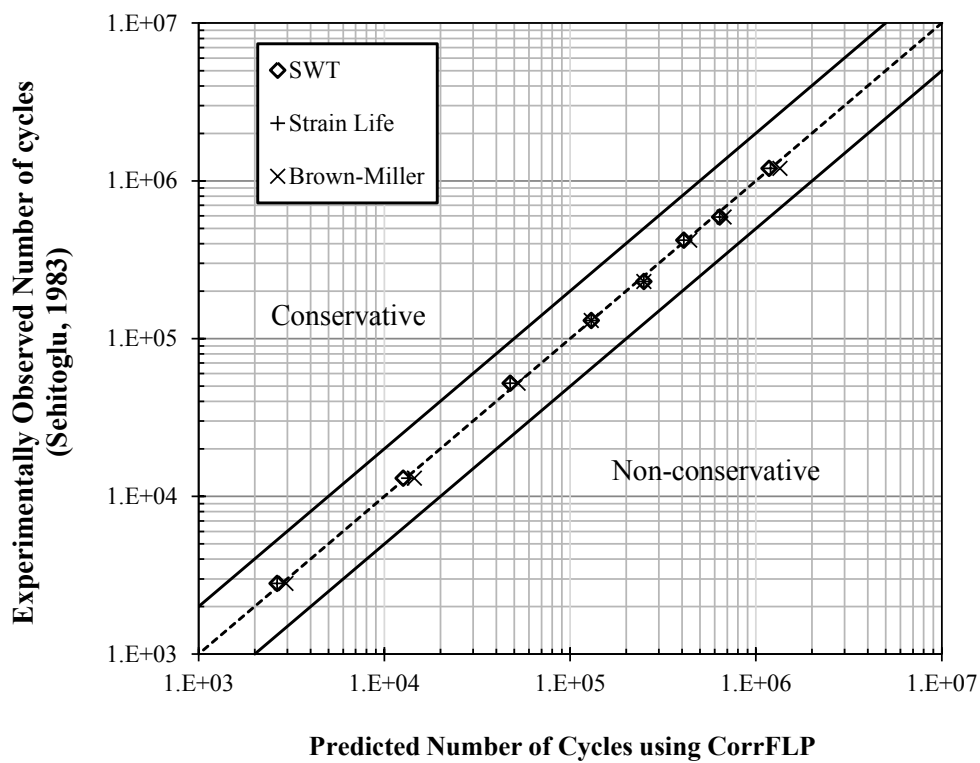


Figure 4.19 Predicted lives using CorrFLP vs. experimentally observed by Sehitoglu (1983) using three different criteria

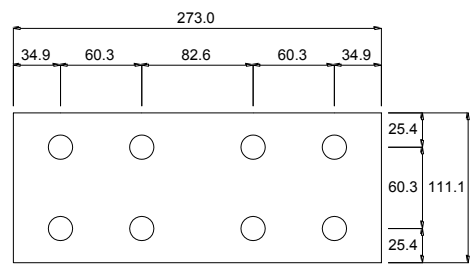
4.5.2 Case Study 2: Bolted plates with staggered circular holes

4.5.2.1 Test description and geometry

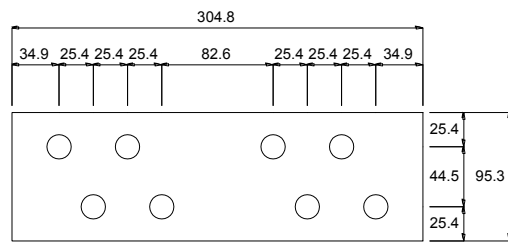
In this case study, CorrFLP is verified using the experimental work done by Josi et al. (1999). The researchers performed fatigue tests on hot rolled CSA G40.21 300W steel double splice plates with circular holes in order to investigate the effect of bolt hole stagger on fatigue resistance of bearing-type connections. The four series correspond to different hole staggers, s , namely (S0) having $s = 0$ mm, (S1) having $s = 25.4$ mm, (S2) having $s = 50.8$ mm and (S3) having $s = 76.2$ mm. The holes configurations and the dimensions of the specimens are shown in Figure 4.20. The plate width = 95 mm. The thickness of the main plates is taken as 25 mm, while the splice plates were chosen to have a thickness of 9.5 mm to be the critical elements in the testing specimens. The 20 mm diameter bolt holes were match drilled for 19 mm bolts, which were installed to a snug tight condition.

4.5.2.2 Materials and Properties

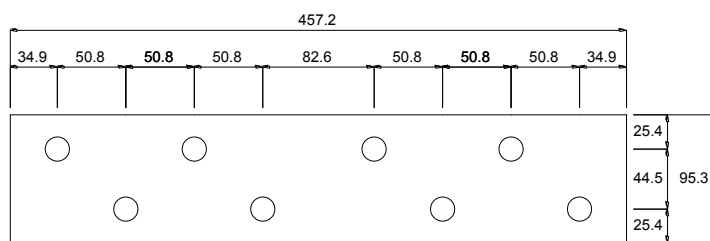
Three tension coupons were tested from the splice plate materials (Josi et al., 1999). It was reported that the average elastic modulus is 212000 MPa; static yield strength is 420 MPa. The cyclic fatigue properties were not reported, thus the material properties presented by Sehitoglu (1983) for A36 steel are used for the finite element analysis and the fatigue life predictions.



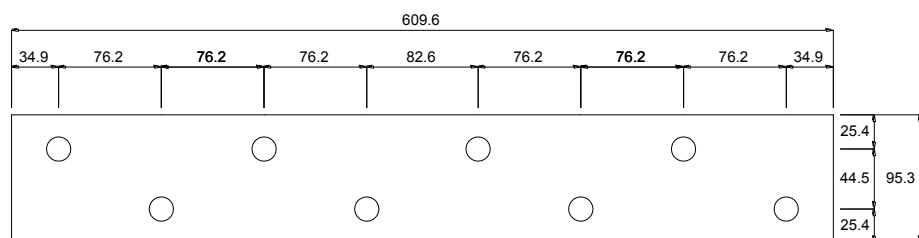
S0-Series (No stagger)



S1-Series (1 in. stagger)



S2-Series (2 in. stagger)



S3-Series (3 in. stagger)

Figure 4.20 Test specimens of Josi et al. (1999)

4.5.2.3 Finite Element Model

The plates were modeled using solid C3DR reduced integration elements. Only one half was modeled due to symmetry. The bolts were assumed to be rigid relative to the plates as the failure in all tests was in the plates, thus they were modeled as analytical surfaces (a feature in ABAQUSTM that will be discussed in the next section.) to reduce the calculations. Figure 4.21 shows the boundary conditions, loading and meshing of the FE model for (S0) series. The top of the bolt heads are modelled rounded for simplicity; this would not have an effect of the fatigue life prediction of the tested specimens.

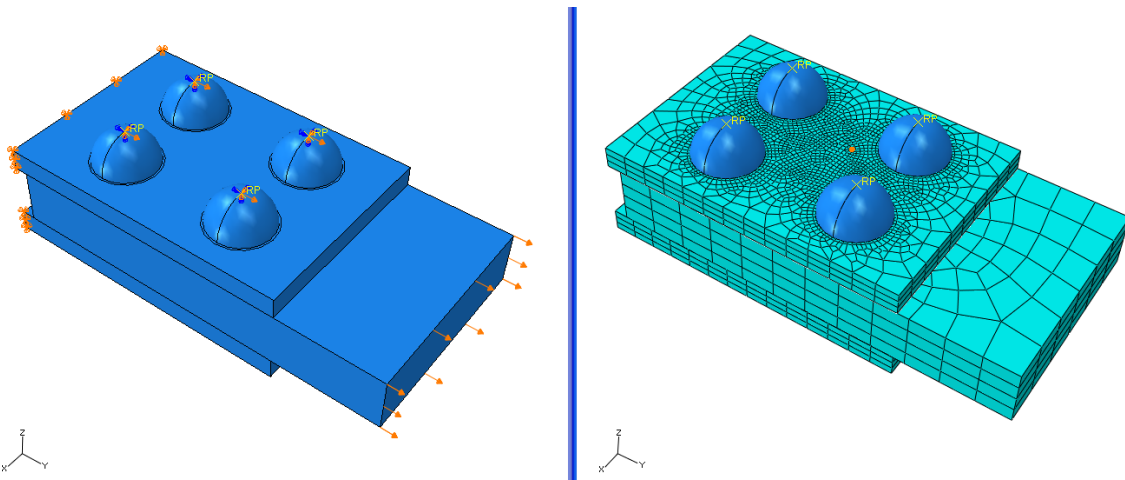


Figure 4.21 The Finite Element model for series (S0) from Josi et al. (1999) (Meshing on the left and boundary conditions on the right) using CorrFLP

4.5.2.4 Interaction surfaces

The analytical surfaces in ABAQUSTM can be used to model the bearing of bolts on the plates by specifying appropriate interaction surfaces. To accurately model the interaction of the bolt or rivet head with the plates, several interaction surfaces have to be defined in the model for each bolt. The interaction surfaces will detect the bearing of any surface on another and will smoothly transfer the loads accordingly. The formulation of

the interaction surfaces was assumed to be frictionless as the bolts usually become loose with time and they do not provide significant pretensioning that can clamp the plates together and transmit forces by friction. The surface-to-surface contact discretization with small sliding formulation is chosen as it gives more accurate results. At each iteration step in the analysis the constraints between the contacting surfaces have to be enforced using one of several methods provided by the solver. The augmented Lagrange method was chosen as it uses augmentation iterations to improve the accuracy of the approximation. The way the solver works is by finding a converged solution with the penalty method. If a slave node (on one surface) penetrates the master surface by more than a specified penetration tolerance (usually one-tenth of a percent of the characteristic interface length), the contact pressure is “augmented” and another series of iterations is executed until convergence is once again achieved. ABAQUSTM solver continues to augment the contact pressure and find the corresponding converged solution until the actual penetration is less than the penetration tolerance.

The default penalty stiffness for the augmented Lagrange method is 1000 times the representative underlying element stiffness. Lagrange multipliers are used for the augmented Lagrange method if the penalty stiffness exceeds 1000 times the representative underlying element stiffness computed by ABAQUSTM; otherwise, no Lagrange multipliers are used. Therefore, Lagrange multipliers are not used for the augmented Lagrange method with the default penalty stiffness.

Figure 4.22 illustrates the locations of the required interaction surfaces to accurately simulate the interaction between the bolts and the plates. It is assumed that there is no clamping force in the bolts such that the bolt is only bearing on the plates

without holding them tightly together. In bearing type connections where clamping forces can be neglected, it can be assumed that the same modelling technique can be applied for riveted and bolted connections.

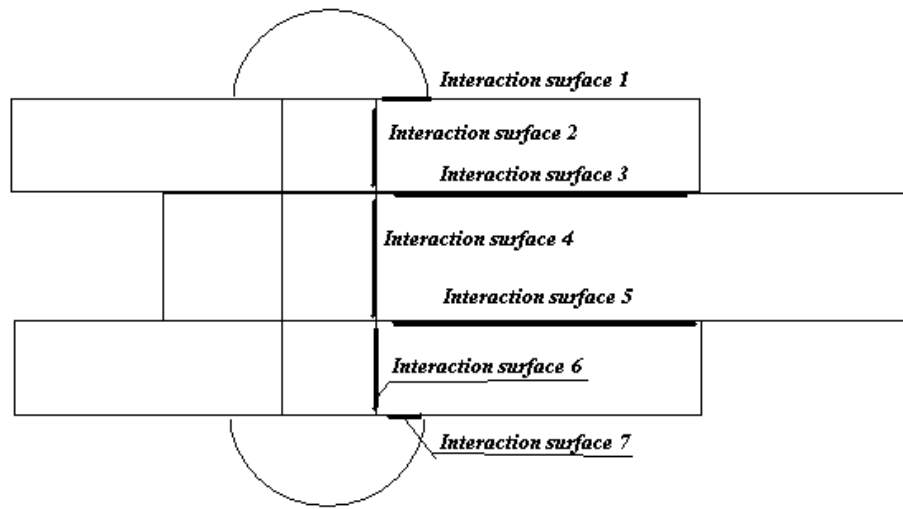


Figure 4.22 Locations of interaction surfaces in the Finite element model

4.5.2.5 Fatigue Life Prediction

Since the specimens were not tested under a fully reversed condition, finite element analysis was conducted at both the maximum load and the load amplitude used in the tests to get the exact stress range and mean stresses as the experiment. Several analyses have been performed for each stress level studied by Josi et al. (1999) using the SWT strain-life prediction model. Figure 4.23 shows section cut through one line of bolts in the analyzed model to show the relative movement between the plates and the stress concentration at the edges of the bolt holes near the bolt head. Figure 4.24 shows section cut through one line of bolts in the analyzed model to show the distribution of damage in the specimen calculated by CorrFLP.

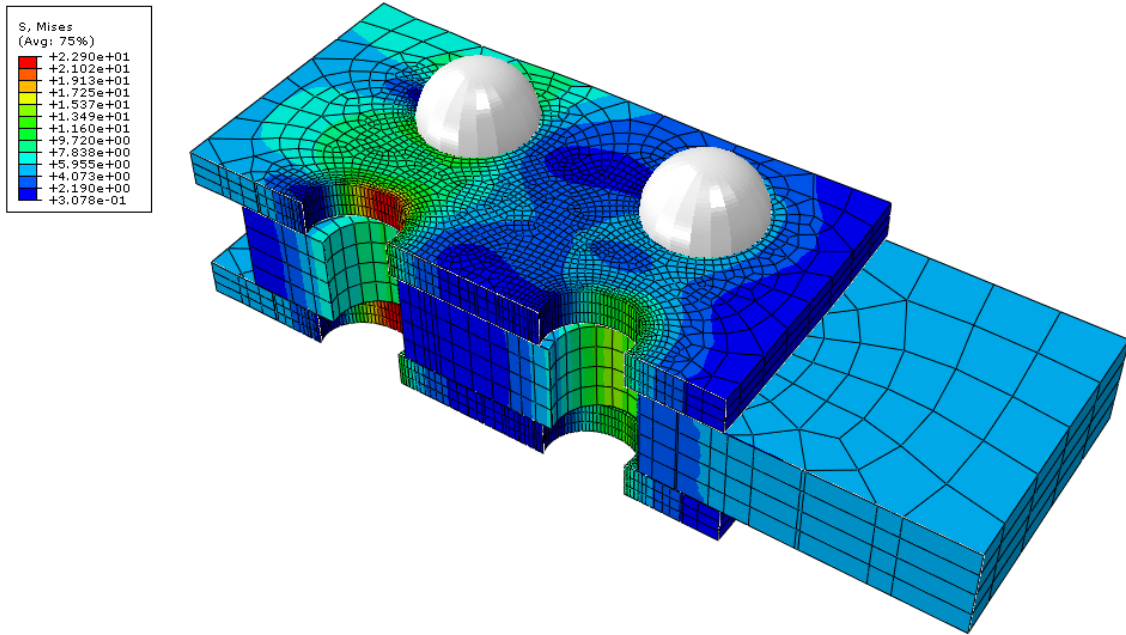


Figure 4.23 Section cut in the CorrFLP FE model showing the stress distribution and the relative sliding between interaction surfaces (Scaled deformed shape for illustration)

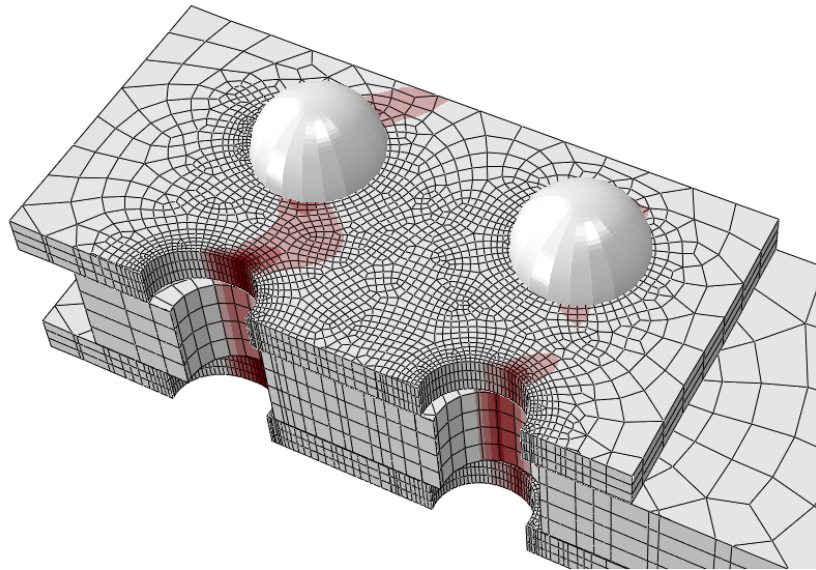


Figure 4.24 Damage during the crack initiation life using CorrFLP surfaces (Scaled deformed shape for illustration)

The results obtained by Josi et al. (1999) have a noticeable scatter within the three different replicas of the each specimen; this is quite common in fatigue tests as the number of cycles to failure could vary in an order of a magnitude, or even two, in some cases. As the crack initiation lengths were not reported, so CorrFLP's default method discussed in section 4.3.4.1 was implemented giving a range for the expected crack initiation life. Table 4.1 shows the results obtained by Josi (1999) versus the range of expected lives from CorrFLP. Figure 4.25 shows a plot of the results in Table 4.1 such that the minimum expected result from CorrFLP is compared to the minimum observation obtained from the experimental work and vice versa.

Josi (1999)			CorrFLP	
Specimen	Load Range	Observed Number Of Cycles	$N_{P,Lower}$	$N_{P,Upper}$
S0 a	190	2167000		
S0 b1	190	5720000	1500000	2100000
S0 b2	190	767000		
S0 c1	240	355000		
S0 c2	240	620000	400000	460000
S0 d	240	578000		
S1 a1	200	255000		
S1 a2	200	303000	225000	350000
S1 b	200	1558000		
S1 c1	160	2827000		
S1 c2	160	2900000	2750000	5000000
S1 d	160	8520000		
S2 a1	200	1062000		
S2 a2	200	307000	300000	450000
S2 b	200	649000		
S2 c1	160	3801000		
S2 c2	160	1497000	1500000	2500000
S2 d	160	2650000		
S3 a1	200	675000		
S3 a2	200	695000	450000	600000
S3 b	200	515000		
S3 c1	130	3562000		
S3 c2	130	13673000	3300000	6000000
S3 d	130	Runout		

Table 4.1 Observed Results from Josi et al. (1999) vs. minimum and maximum expected cycles to crack initiation from CorrFLP

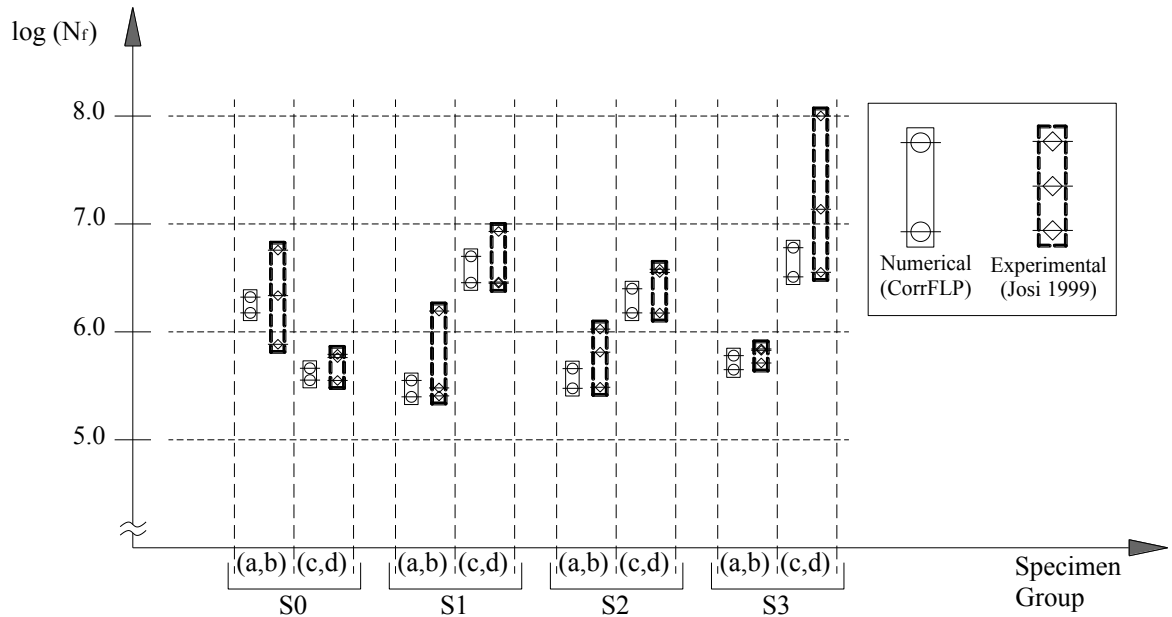


Figure 4.25 Predicted lives using CorrFLP vs. experimentally observed by Josi et al. (1999) using three different criteria

4.5.2.6 Discussion of results

It had been reported that most of the shear splices showed single cracks at the time of failure which was always the case in CorrFLP simulations due to the stress concentrations near the holes. The fatigue life of the test specimens varied from 3×10^5 to 13×10^6 cycles depending on the geometry and the applied load level of the bolted connection. This considerable scatter in the experimental results in a relatively simple connection can be attributed to several factors; such as the amount of clamping forces in the bolts that can help in increasing the fatigue life of the specimen. The determination of the exact clamping force is one of the main problems of the fatigue assessment of the existing bolted connections because it depends on how the bolt was initially hammered and its pretensioning loosens with time. The modeled specimens in CorrFLP had no

clamping forces assumed to get the most conservative condition. Moreover, the existence of any micro-cracks or defects can cause premature failure in the specimens. The results had a wide scatter that shows the probabilistic nature of fatigue problems.

It is worth mentioning that Josi et al. (1999) reported that the regression analysis of their test results indicates that the slope of the fatigue curve for the bearing-type shear splices tested has a slope, m , equal to 7. This is significantly different from the slope defined in the modern codes for other fatigue (welded) details that all have a slope of $m=3$. This conclusion should not be generalized on all bolted connections, but it points out that categorizing all bolted details under a single fatigue category is not accurate in most of the design codes and needs future investigation. This emphasises on the importance of carrying out further experimental and/or numerical simulations on bolted structural details to correctly classify them.

4.5.3 Case Study 3: Built-up beams

4.5.3.1 Introduction

In order to calibrate and verify the fatigue life prediction of CorrFLP for more complex assemblies such as built-up riveted girders, another case study will be simulated and verified against some of the experimental work conducted by the NCHRP (National Cooperative Highway Research Program, NCHRP (1988). The NCHRP has published several reports to determine the fatigue categories and behaviour of several steel details. These reports helped shaping the current design standards for fatigue.

4.5.3.2 Experimental Tests

Fourteen full-scale riveted girders, all removed from riveted steel bridges, were tested by Fisher et al. (1988) in the NCHRP report 302 to evaluate their fatigue and fracture resistance. The test girders were obtained from three different sources Girders 1 to 8 were obtained from the Santa Fe Railroad. Girders 9 to 12 were supplied from an Ocean County, New Jersey, highway bridge that was dismantled. Girders 13 and 14 were removed from the Minsi Trail Bridge in Bethlehem, Pennsylvania, at the time it was dismantled. Except for Ocean County girders, which were heavily corroded, the other girders were generally in good condition. The stress ranges of the cycles applied before dismantling the girders were mostly below fatigue limit as it has been reported by Fisher et al. (1988) that no fatigue cracks were detected in any of the test girders before the laboratory tests. Thus it could be said that the loading history prior to laboratory testing can be ignored. Figure 4.26 and Figure 4.27 show the geometry and profiles of the test girders.

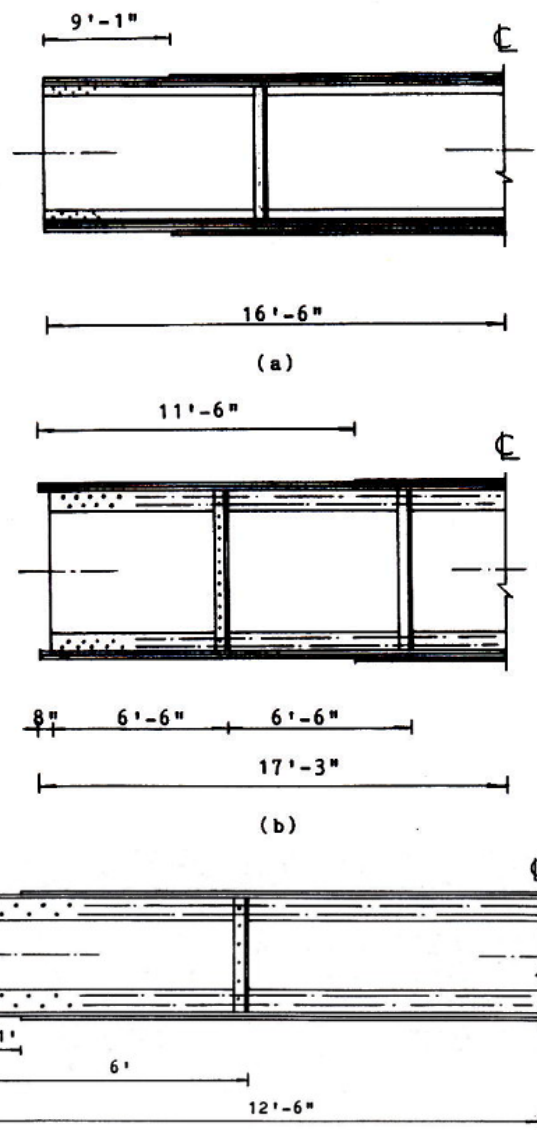


Figure 4.26 Riveted Girders tested by Fisher et al. (1988)

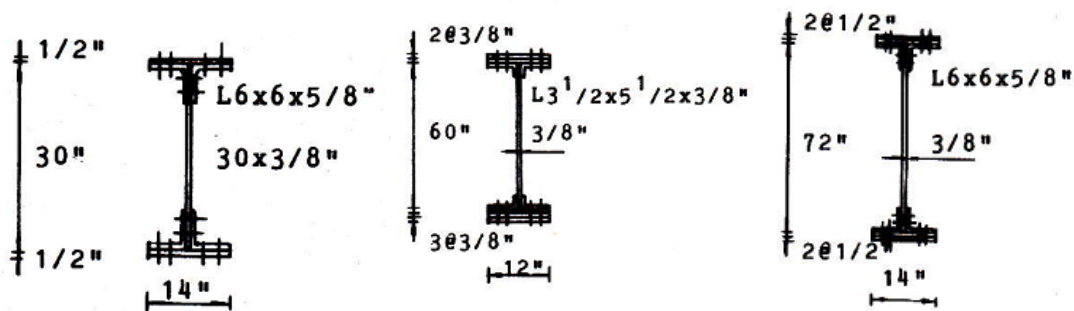


Figure 4.27 Cross-Section of tested girders Fisher et al. (1988)

Only three out of the fourteen bridges will be selected and used for this verification; only the tests conducted in the room temperature without any severe corrosion will be used for verification. Therefore, Minsi trail bridge girders and the Ocean Country girders will be excluded from this study. Unfortunately, no corrosion rates or any data on the corrosivity of the environment were reported for the Ocean country bridges which were the only bridges that were severely corroded. Table 4.2 lists the tested specimens, their sources and the minimum, maximum flexural stresses applied during testing.

Table 4.2 Selected Specimens in this study from NCHRP Report 302 (1988)

Source Bridge	Specimen ID (Current Study)	Specimen ID (NCHRP report 302)	Minimum Stress (MPa)	Maximum Stress (MPa)	Stress Range (MPa)
Santa Fe	SF-1	1	14	117	103
Santa Fe	SF-2	2	14	117	103
Santa Fe	SF-3	4	14	97	83

4.5.3.3 Materials

Tensile tests were conducted for each of the different types of girders. The results show that all of the test girders were fabricated from mild steel with yield strength between 200 MPa and 290 MPa. Table 4.3 lists the static material properties of the girder parts. No fatigue properties for the strain based method have been reported as the tests were targeting the stress based method.

Table 4.3 Material properties of NCHRP report 302 (1988)

Source Bridge	Yield Stress (MPa)		Ultimate Stress (MPa)	
	Angles and Webs	Cover Plates	Angles and Webs	Cover Plates
Santa Fe	198	218	371	399

4.5.3.4 Experimental Test Procedure

The girders were tested under four-point bending. Two 490-kN Amsler jacks were used to load each test girder. A 1.52 m constant moment length between the jacks permitted a significant length of beam to be subjected to the same stress range. In order to provide lateral stability of the girder compression flange, two lateral bracing bars were attached to the compression flanges. Two lateral bracing bars were connected to the bottom flange to simulate the restraint of the bracing system in the bridges and to minimize the lateral movement of the tension flange. Cyclic loading was applied so that the bending stresses at the outer fibres of the lower cover plates would conform with the values listed in Table 4.2.

4.5.3.5 Finite Element Model

The girders were modeled in ABAQUS to be simulated for fatigue analysis in CorrFLP. All the girders where modelled using the C3DR reduced integration elements. Surface interaction between rivet surface and the attached plates are modelled using the same techniques discussed in section 4.5.2.4. To reduce the computational time of the model, only one quarter of the beam cross section is modeled. It had been reported that all failures were in the zone of constant moment, thus a small segment of the beam length at the constant moment zone will be considered as shown in Figure 4.28. A denser mesh is provided around the holes susceptible to crack initiation, to accurately monitor the damage propagation.

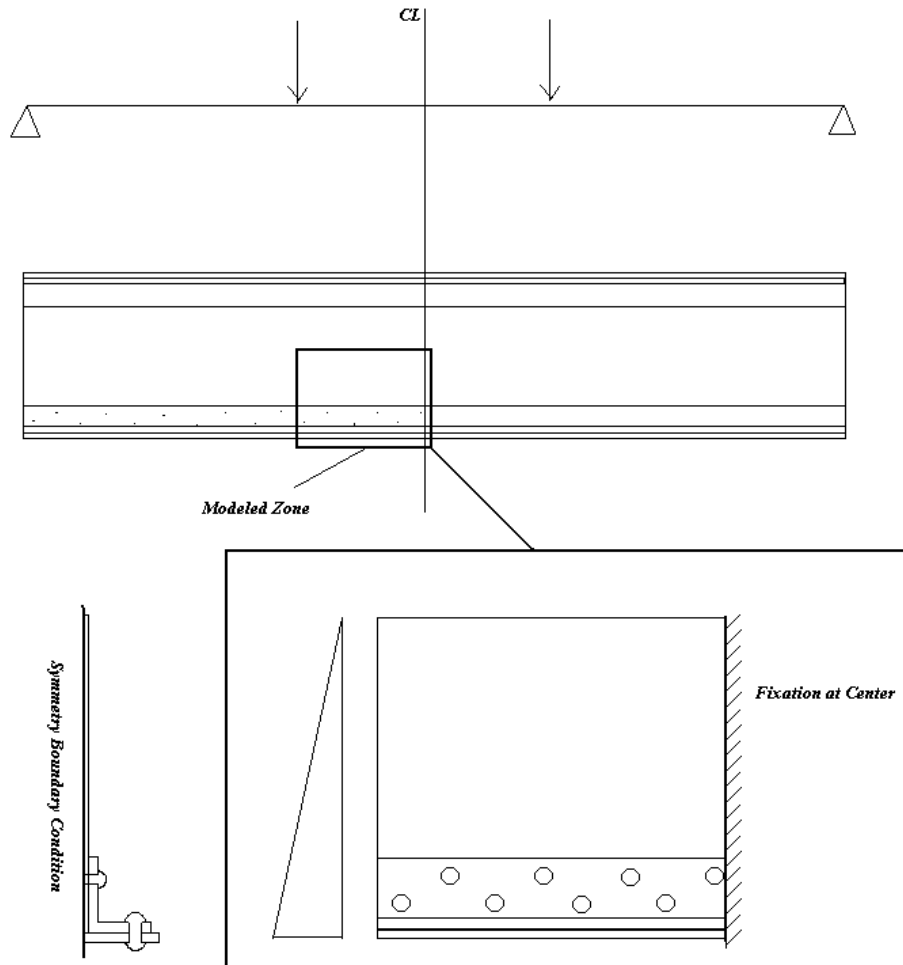


Figure 4.28 Extraction of modeled part in CorrFLP analysis

4.5.3.6 Boundary Conditions and Loading

Symmetry boundary conditions are applied along the center plane of the web. A fixation boundary condition is applied to the surfaces along the girder center line. All rivets where restrained from rotation about their axis. A gradient stress is applied such that the stress at the girder horizontal centerline (at zero strain) and the stress at the extreme fibres is taken from the values listed in Table 4.2. Figure 4.29 shows the loading, boundary conditions and meshing of the model representing Santa Fe girders.

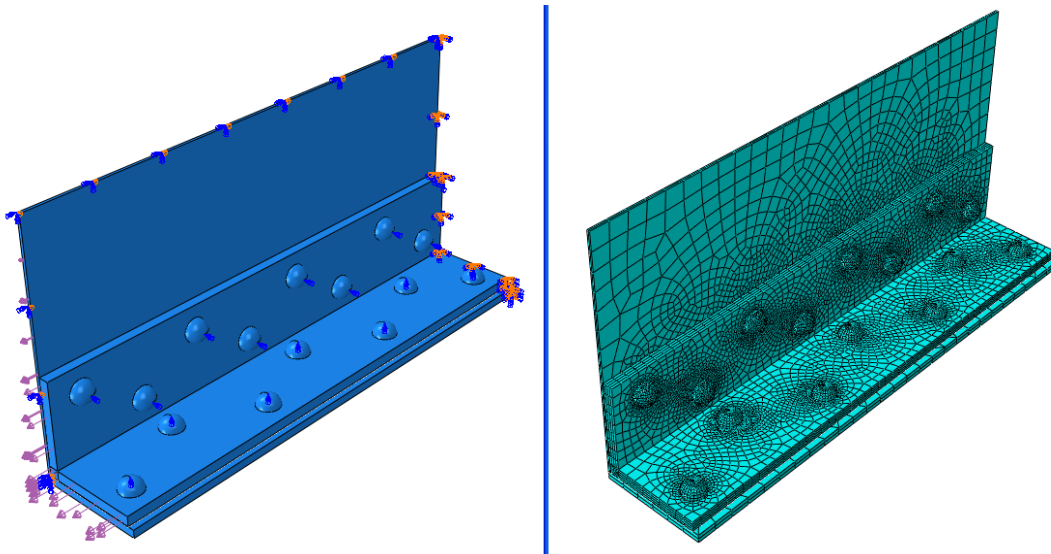


Figure 4.29 Finite Element Model for Santa Fe Girders (Loading and boundary conditions on the left, meshing on the right)

4.5.3.7 Modeling material properties

The materials were considered as elastic perfectly plastic. Modulus of elasticity was taken as 200,000 MPa. As no fatigue strain based properties were reported, cyclic fatigue properties were assumed using the Unified Material Method mentioned in section 2.4.2.6. Since the static properties $E = 200,000 \text{ MPa}$, $\sigma_u = 400 \text{ MPa}$ for Santa Fe and Ocean Country Girders are same, thus the calculated cyclic stress strain and fatigue properties for both girders are; $K' = 660 \text{ MPa}$, $n' = 0.15$, $\sigma_f' = 600 \text{ MPa}$, $b = -0.087$, $\varepsilon_f' = 0.59$ and $c = -0.58$.

4.5.3.8 Fatigue Life Prediction

The same procedure discussed in section 4.3.4.1 was adopted. Table 4.4 lists the number of cycles to detection of fatigue cracks reported by Fisher et al. (1988) versus the minimum and maximum estimated number of cycles to crack initiation obtained from

CorrFLP. Figure 4.30 plots the number of cycles to detection of fatigue cracks reported by Fisher et al. (1988) versus each of the minimum and maximum estimated number of cycles to crack initiation obtained from CorrFLP.

Table 4.4 Fatigue Crack initiation lives for Santa Fe Girders from the NCHRP report 302 (1988) and from CorrFLP simulation

Specimen	NCHRP report 302		CorrFLP	
	Stress Range	Cycles to Detection of fatigue cracks	$N_{P,Lower}$	$N_{P,Upper}$
SF-1	103	588000	500000	750000
SF-2	103	1094000	500000	750000
SF-3	83	2630000	1900000	2800000

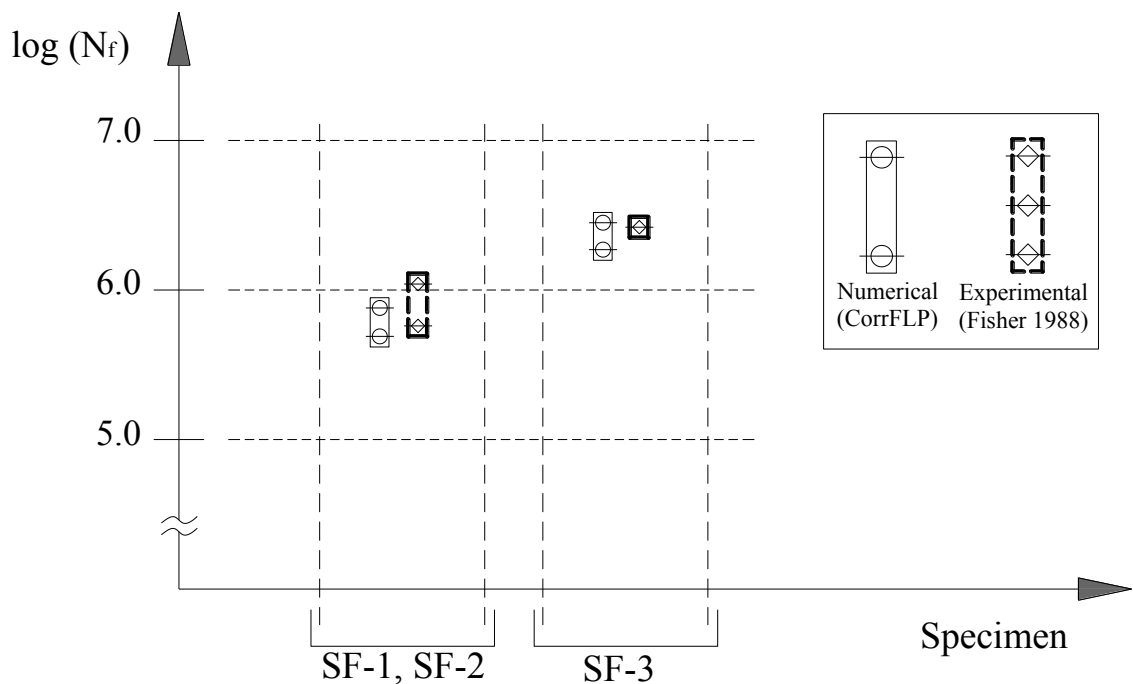


Figure 4.30 Plot for Fatigue crack initiation lives for Santa Fe Girders from the NCHRP report 302 (1988) vs. those from CorrFLP simulation

All of the cracks in Santa Fe girders were reported to initiate from the rivet holes. This was clear from the analysis of damage propagation patterns obtained from CorrFLP. Moreover, there is a very good correlation between the life estimations obtained from CorrFLP and the observed number of cycles reported by Fisher et al. (1988). Figure 4.31 shows, as an example, the crack initiation and propagation patterns reported by Fisher et al. (1988) versus the crack initiation patterns obtained from CorrFLP.

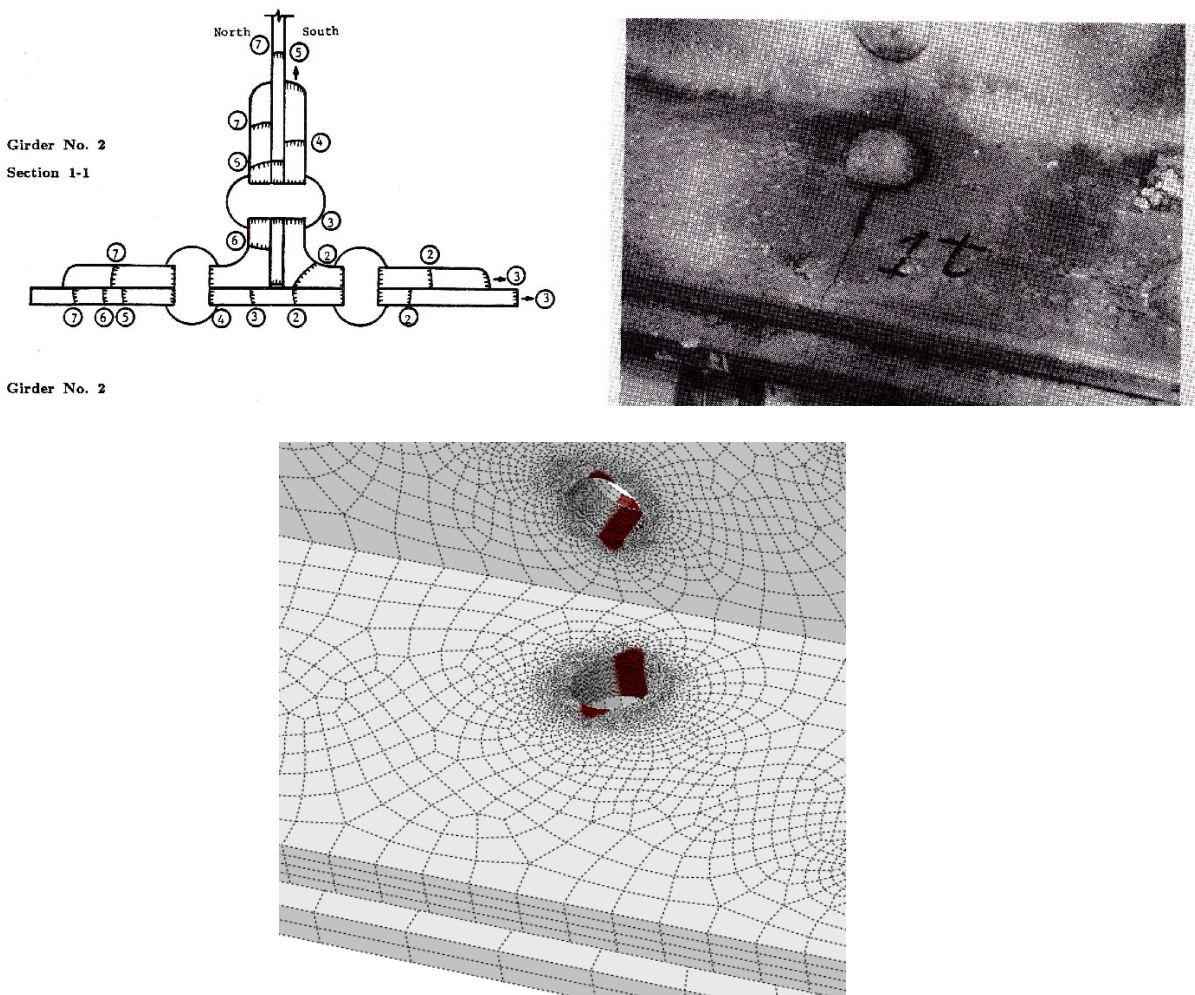


Figure 4.31 Reported crack initiation and propagation (Fisher et al., 1988) vs. CorrFLP damage initiation for specimen SF-2

4.5.3.9 Summary

The built-up riveted girders used in this verification example are widely used in many existing bridges. It is very important to be able to simulate them with an acceptable level of confidence. Results obtained from Santa Fe Girders are of very good agreement with the experimental results obtained. Thus, the modeling technique using the FEM adopted in this validation example is convenient and can be extended to any built-up girder configuration. It is important to note that this technique is sensitive to the boundary conditions and the interactions applied, thus it is important to calibrate the model using experimental tests or field measurements ensure that the finite element model is representative of the real girders. Moreover, the fatigue crack initiation lives predicted using CorrFLP are usually on the conservative side, due to the assumptions of neglecting the friction between plates and neglecting the clamping forces in the rivets. In fatigue simulations, it is common that results within an order of magnitude or two are considered to be acceptable. Thus, the level of accuracy of the results obtained by CorrFLP, which were usually within one order of magnitude, can be considered as a good agreement with the experimental results. Moreover, it is worth noting that the fatigue lives estimated by CorrFLP are usually on the safe side.

4.6 Discussion

Three case studies were conducted to verify the accuracy of CorrFLP. The first is a plate with a hole to be used as a benchmark test for CorrFLP. The numerical predictions showed very good agreement with experimental results; this gives confidence in the numerical tool in performing fatigue analysis for simple models. The study was then

extended to bearing-type shear splice plates connected together using bolts subjected to shear. The model is more complicated and involves interactions between surfaces. The analysis was performed ignoring the effect of clamping forces to give the most critical (conservative) fatigue life estimate. Numerical predictions from this study had a good agreement with the experimental results. This is a good indicator of the capability of the developed program to test more complex plate assemblies in fatigue. A third case study was conducted on built-up steel riveted girders which are commonly used in existing old bridges. The fatigue life predictions from CorrFLP were of good agreement with the experimental results. This gives a high level of confidence in the results obtained by the developed tool. Next chapter will discuss the procedure for extending this tool to simulate the fatigue behaviour of corroding elements.

CHAPTER 5

EFFECT OF CORROSION ON FATIGUE LIFE

5.1 Introduction

Corrosion is a process of degradation of a metal by an electrochemical reaction with its environment. This means a loss of electrons of metals reacting with water and oxygen. The weakening of iron due to oxidation of the iron atoms is a well-known example of electrochemical corrosion which is commonly known as rust (Trethewey et al., 1988). Much of the corrosion damage in structures within the last 40 years might have been caused by a change in the chemical composition of the air due to increased industrial activity (Boden, 1989). Atmospheric deterioration is influenced by the following natural factors: moisture, temperature (mean value and variations), sunlight, air movement (wind speed and direction), sea salt, and fog. Some experiments in literature (Vernon, 1935) indicate that corrosion at relative humidity below 50% is minimal. As the relative humidity increases from 60% to 80% or even greater, the protective oxidized layer on the metal surface breaks down and allows corrosion. Moisture in the form of rain may, however, reduce atmospheric corrosion by washing away dangerous pollutants.

As previously discussed in Chapter 2, there is not so much experimental data for fatigue tests on corroded structural components. Moreover, there are almost no tests available for full scale specimens that are cyclically loaded along with the environmental effect of corrosion being simulated simultaneously. This shows the importance of the numerical tool developed in this thesis to simulate the simultaneous effects of corrosion along with cyclic loading.

5.2 Implementing the effect of corrosion

There are two proposed approaches for simulating the effect of corrosion; the first one is by geometrically simulating the thickness loss and pitting. The other approach is to model the deterioration in material properties due to corrosion by implementing a newly proposed strain-life fatigue model that simulates the degrading effect of corrosion on the fatigue life. The next subsections will cover the aforementioned approaches.

5.2.1 Geometrical representation of corrosion

CorrFLP can simulate the thickness loss due to corrosion; moreover, it can approximately simulate the effect of pitting corrosion by applying a stress concentration factor based on the pit dimensions. CorrFLP's "Corrosion Management Object" is responsible for communicating with the "Spectrum Management Object" to know the current time and current corrosion rate and thus selects the appropriate corrosion thickness loss (penetration). The "Corrosion Management Object" also communicates with the "Main Mesh Object" and locates the points of high stress concentration, to be points of initiation of stress corrosion, given any model that could be developed for it in future. The user can also specify any node in the finite element model and identify it as an expected location of pitting corrosion initiation. The user can specify the initial pit aspect ratio to model an existing corrosion pit. CorrFLP can calculate the stress concentration factor for the stresses at this node using the numerical method provided by Cerit et al. (2009) as shown in Figure 5.1. This feature is included for future work, as the topic of pitting corrosion is so complicated and is out of the scope of this research.

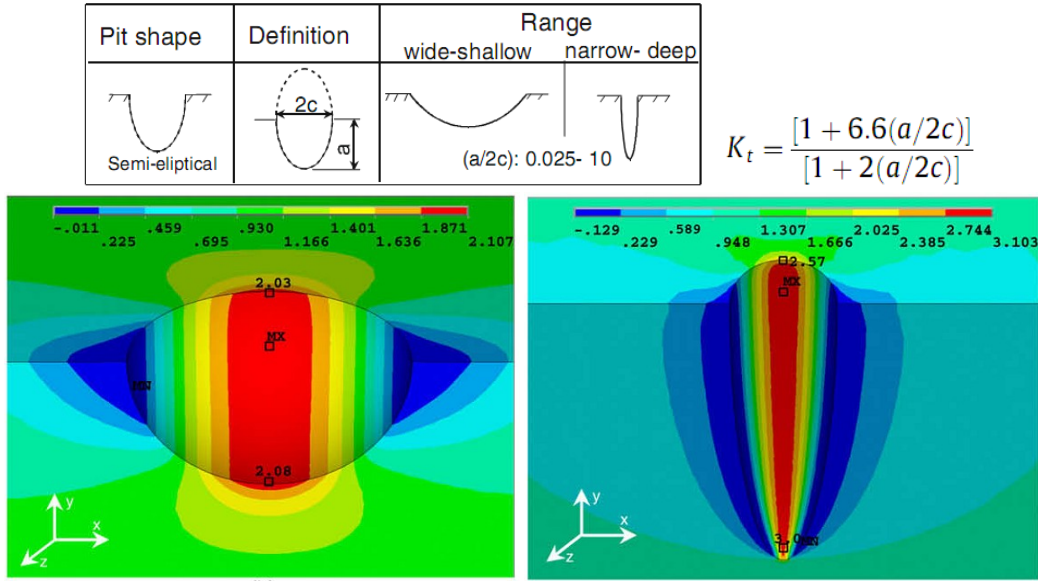


Figure 5.1 Stress concentration factor due to pitting corrosion depending on pit shape (Cerit et al., 2009)

CorrFLP can also incorporate many available corrosion damage functions to account for different atmospheric conditions and different concentrations of sulphur dioxide and oxidants (when this data is available for the user). Geometrical simulation of the corrosion thickness loss is done by communication between the “Corrosion Management Object” and the “Refinement Management Object” where the latter geometrically moves the external surfaces or faces of the corroding elements by the amounts decided by the “Corrosion Management Object”. The amount of corrosion penetration Δt_p applied to any surface can be calculated by multiplying the corrosion rate at the current time $\Delta t_p(t)$ by the time corresponding the cycle jumps applied as shown in equation (5-1).

$$\Delta t_p = \Delta t_p(t) \times \text{time jump} \quad (5-1)$$

Each surface can have a different corrosion rate history attached to it to realistically simulate the non-uniform corrosion rates of different surfaces in some structural assemblies. Figure 5.2 shows how specific surfaces can be selected and assigned a specific corrosion rate on a sample FE half-model of a built-up I-beam. Figure 5.3 shows how CorrFLP simulates the corrosion thickness loss in the FE model shown in Figure 5.2.

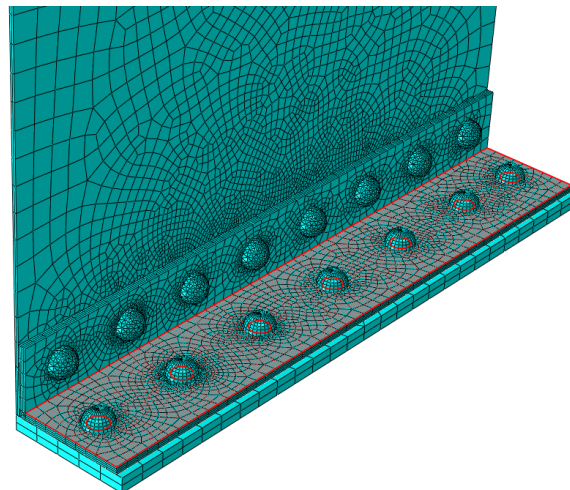


Figure 5.2 Assigning corrosion rate factors for mesh surfaces in CorrFLP

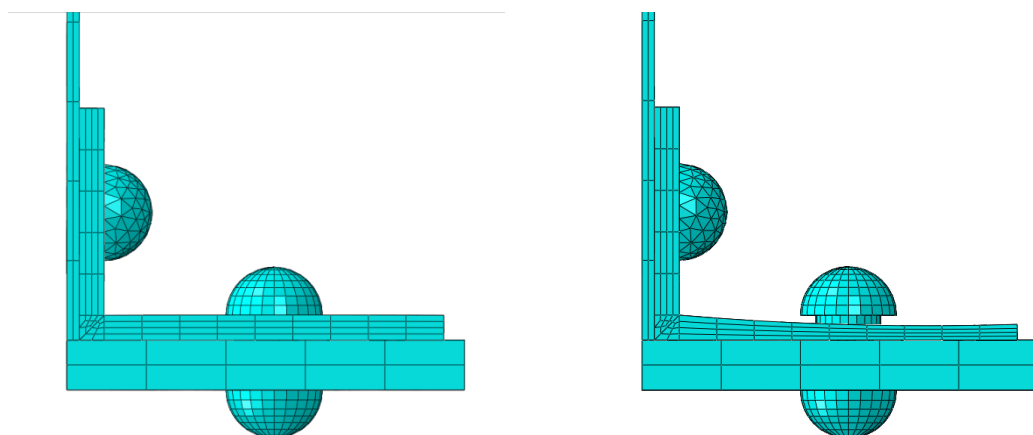


Figure 5.3 Simulation of corrosion thickness loss on selected critical surfaces
(Left: No Corrosion, Right: Corrosion (not shown to-scale))

The user can assign different corrosion histories and different rates to different surfaces on the model to simulate the real conditions. For example, while modeling a built-up I-beam, there are several zones of corrosion severity, these zones could be specified by the user. A useful resource (Kulicki et al., 1990) for the various locations susceptible to have more corrosion damage can be used as a guideline for the user. CorrFLP also provides several environmental corrosion damage functions provided by Boden (1989).

5.2.2 Proposed corrosion fatigue strain-life model

It is very important to note that due to the complexity of the corrosion-fatigue phenomenon and due to the very long time its experiments take, there are very limited experimental data, especially in the field of civil engineering on structural steels.

In this research, several approaches for modeling the corrosion-fatigue were investigated. One of the approaches was to use a modified corrosion-fatigue stress intensity threshold ΔK_{th} for the studied material and use it for determining the critical length L for the studied specimen in a corrosive environment. This approach is difficult and unpractical as many researchers such as Novak (1983) and Taylor (1985) reported that they could not get a clear value for ΔK_{th} in corrosive environments. Moreover, the fatigue limit is not usually clear in corrosive environments.

Since the critical distance “ L ” depends on both the ΔK_{th} and the fatigue limit which are not clear in corrosive environments, thus this approach will not be useful until further detailed research is done in this particular point. Alternatively, the hot-spot method –regularly used in fatigue prediction software– will be used in the developed

numerical tool with a newly proposed strain-life model. This method uses the maximum strain values at the surfaces of the elements.

Before proposing the model, a brief introduction to some of the strain-life approach basics should be done. As it is already known, the endurance of any material to cyclic loading can be determined using any of the strain-life methods mentioned in section 2.4.2 by using an elastic part and a plastic part. The elastic part is usually defined by the fatigue strength exponent, b , also known as Basquin's exponent which is a material property. The plastic part is defined by the fatigue ductility coefficient, c , which is a material property known as Coffin-Manson exponent. Combining both the elastic and plastic parts from the total endurance life as shown in Figure 5.4.

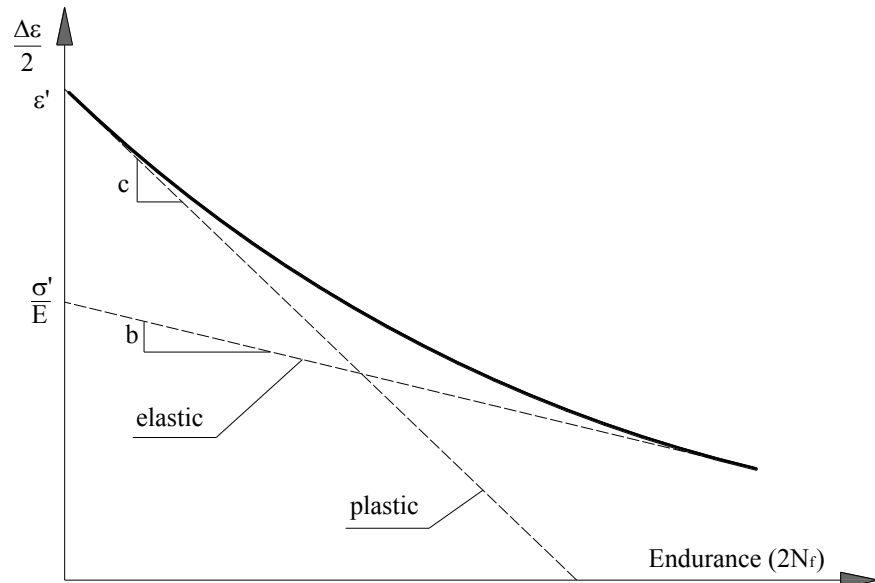


Figure 5.4 Relationship between total strain amplitude and endurance in a non-corrosive environment

In this research, it is proposed to experimentally obtain modified values for b and c for a certain corrosive environment and they will be denoted as b' and c' respectively.

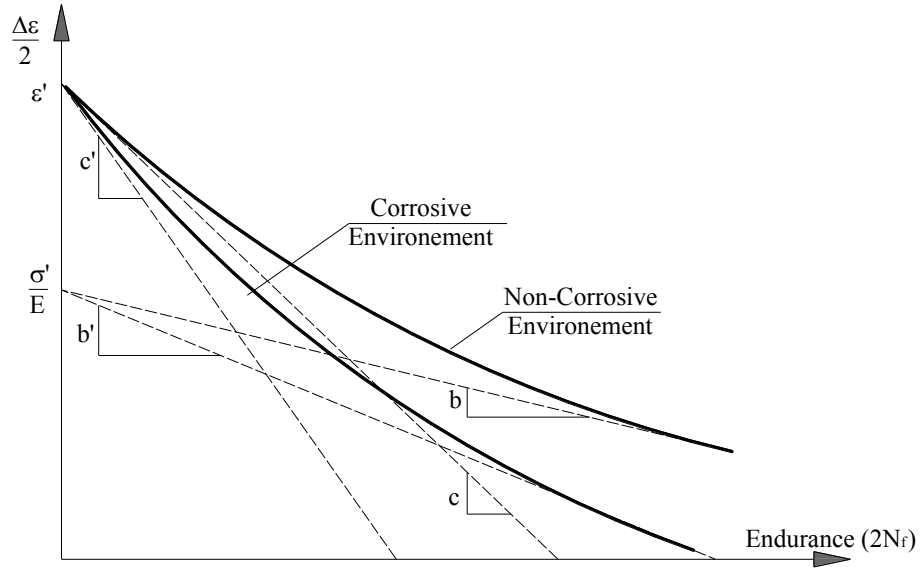


Figure 5.5 Relationship between total strain amplitude and endurance in a highly corrosive environment

Four new factors will be proposed, namely α_b , α_c , γ_{corr} , γ_σ . The factor α_b will be the ratio of b' / b where b' is measured in a standard NaCL 3.5% highly corrosive environment. Similarly, α_c will be the ratio of c' / c where c' is to be measured in a standard NaCL 3.5% highly corrosive environment as a way of standardizing the procedure. The factor γ_{corr} will be the environmental corrosivity intensity factor varying from 0 to 1, where 0 corresponds to a totally non-corrosive environment and 1 corresponds to a highly corrosive environment equivalent to the NaCL 3.5% solution simulation environment usually used in accelerated corrosion tests. The factor γ_σ will be introduced as a correction factor for the mean stress effects. Once we have our experimental data plotted, b' and c' corresponding to $\gamma_{corr} = 1$ can be easily calculated,

then both α_b and α_c can be obtained and saved as material constants for a harsh environment corresponding to $\gamma_{corr} = 1$.

For any other corrosive environment corresponding to $\gamma_{corr} = 0 \rightarrow 1$, both b' and c' can be easily calculated using the following equations:

$$b' = b (1 + \gamma_{corr} \gamma_\sigma \alpha_b) \quad (5-2)$$

$$c' = c (1 + \gamma_{corr} \gamma_\sigma \alpha_c) \quad (5-3)$$

From surveying the literature and from the results obtained in the case studies conducted in the previous chapter, it has been observed that the SWT model mentioned in section 2.4.2.3 predicts the fatigue endurance of metals with a relatively high accuracy as it takes into account the mean stress effects. In this research, a proposed modification is introduced to the SWT strain-life method to accommodate for the different environment systems will be by replacing b by b' and replacing c by c' . Thus the modified SWT model format becomes:

$$\frac{\Delta \varepsilon}{2} \sigma_{max} = \frac{(\sigma_f')^2}{E} (2N_f)^{2b'} + \sigma_f' \varepsilon_f' (2N_f)^{b'+c'} \quad (5-4)$$

Where the factors b' and c' incorporate the factor γ_{corr} , which varies from 0 to 1 depending on the corrosivity of the environment. The factor γ_σ is a correction factor that depends on the maximum applied stress σ_{max} .

The assumptions made in this proposed strain based corrosion model are logically acceptable and the constants proposed for each material can be derived from experimental data. Yet, it would be difficult to accurately verify the exact values for both α_b and α_c for a certain material (in the current time) as there is very limited corrosion fatigue data in literature. Thus, there would be a need for testing enough structural materials in order to have a comprehensive database of their proposed environmental properties. The proposed environmental corrosivity intensity factor γ_{corr} could be correlated to the categories provided by the ISO-9223 (1992) and the ISO-9224 (1992) as shown in Table 5.1.

5.2.3 Calibration of the proposed model

In this research, a relation is proposed to correlate the environmental corrosivity intensity factor γ_{corr} with the average annual penetration in ($\mu\text{m}/\text{year}$). This relationship was deduced by calibrating with the work done by Albrecht et al. (1994) which will be further discussed in the next section. Equation (5-5) shows the proposed relation between the logarithm of the penetration versus the proposed corrosion factor γ_{corr} .

$$\gamma_{corr} = 0.0761 \log(p_a)^2 + 0.2109 \log(p_a) + 0.221 \quad (5-5)$$

where p_a is the average annual penetration in ($\mu\text{m}/\text{year}$). Figure 5.6 shows the plot used to deduce the proposed equation.

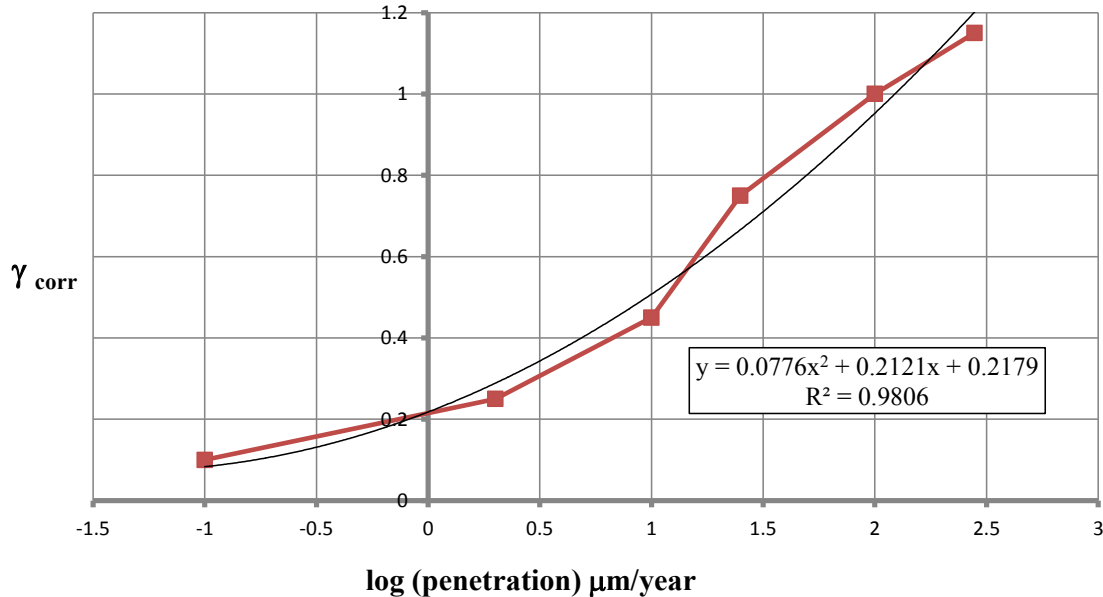


Figure 5.6 Plot for the proposed relation between the log of the penetration versus the proposed corrosion factor γ_{corr} .

Table 5.1 Correlation between and the ISO-9224 categories

	ISO-9224 category (r_a = average corrosion rate)	γ_{corr}
Very low corrosivity	C1 ($r_a \leq 0.1 \mu\text{m}/\text{year}$)	0 → 0.09
Low corrosivity	C2 ($0.1 \leq r_a \leq 2 \mu\text{m}/\text{year}$)	0.09 → 0.29
Medium corrosivity	C3 ($2 \leq r_a \leq 8 \mu\text{m}/\text{year}$)	0.29 → 0.47
High corrosivity	C4 ($8 \leq r_a \leq 15 \mu\text{m}/\text{year}$)	0.47 → 0.57
Very High corrosivity	C5 ($15 \leq r_a \leq 80 \mu\text{m}/\text{year}$)	0.57 → 0.9

Due to the limited experimental corrosion fatigue life data available for plain specimens made of structural steel presented in the form of strain-life data points, it is necessary to be able to convert any available S-N data points for a corrosive environment and to convert them to strain-life data points. In this research, the author was able to obtain stress-life (S-N) corrosion fatigue life data for plain coupons of weathering steel (which is usually used in bridges) tested by Kunihiro et al. (1972). Kunihiro et al. (1972)

tested plain specimens fabricated from SMA weathering steel commonly used in Japan, which is also similar to the A588 weathering steel commonly used in North America (Albrecht, 1983). All specimens were 19 by 50 by 459 mm. Figure 5.7 shows a typical set of Kunihiro's data showing the 0 years (unweathered) coupons versus the 2 years weathered coupons.

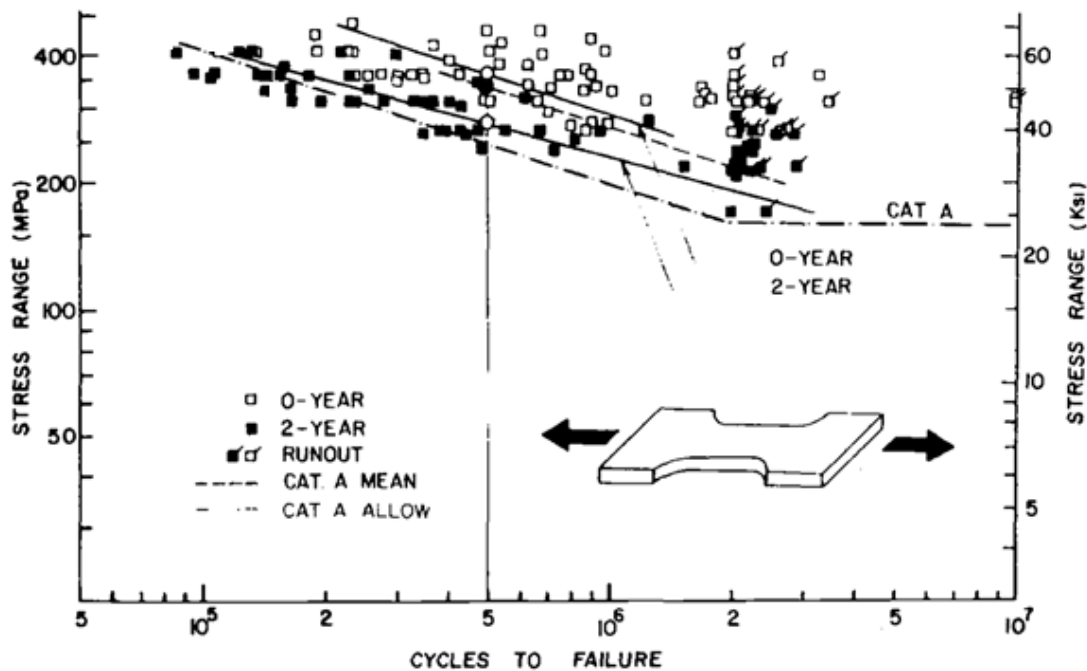


Figure 5.7 Fatigue strength of two year weathered plain rolled SMA steel specimens (Kunihiro et al., 1972)

The data was then digitized and transformed into strain-endurance life data points by using the cyclic fatigue properties of this steel which are $K' = 1400$ MPa, $n' = 0.15$ using equation (5-6). The S-N data was adjusted by using an average notch factor of 1.3 reported by Kunihiro et al. (1972).

$$\frac{\Delta\varepsilon}{2} = \frac{\Delta\sigma/2}{200000} + \left(\frac{\Delta\sigma/2}{1400} \right)^{1/0.15} \quad (5-6)$$

The properties of SMA weathering steel is of an average of 580 MPa tensile strength, 355 MPa yield point and $E = 200\,000$ MPa. Using the universal material method of Baumel et al. (1990) we obtain $K' = 1400$ MPa, $n' = 0.15$, $\sigma_f' = 870$ MPa, $b = -0.09$, $\varepsilon_f' = 0.59$ and $c = -0.58$. By processing the data, we can obtain e-N data points for the steel as shown in Figure 5.8. The curve fitted with no corrosion had a best fit with the fatigue exponents $b = -0.11$ and $c = -0.59$ which are very reasonable values for steels. The curve fitted with 2-year corrosion had a best fit using $b' = -0.13$ and $c' = -0.61$. Thus, the proposed corrosion material constants to be $\alpha_b = 0.182$ and $\alpha_c = 0.034$ for this material.

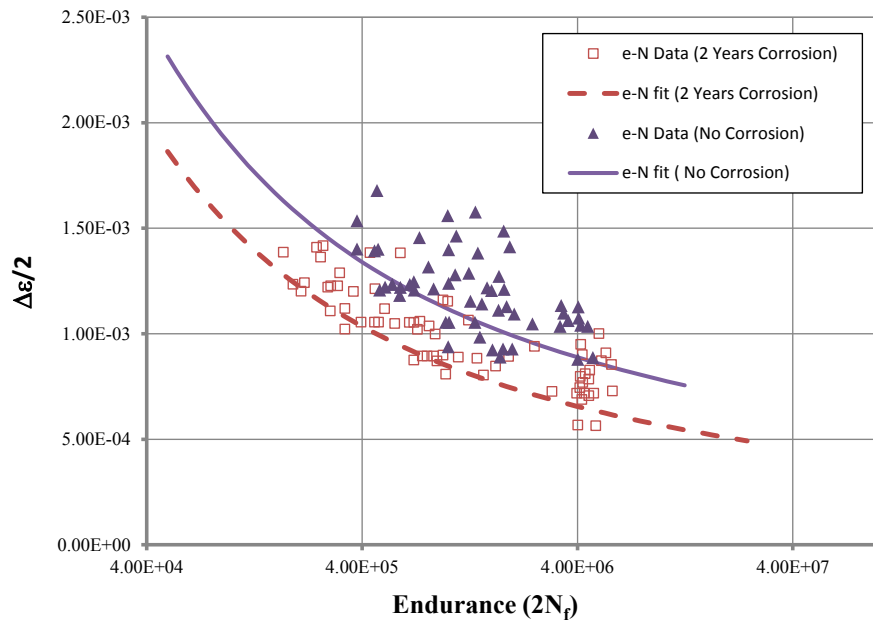


Figure 5.8 Kunihiro et al. (1972) data points converted into strain-life data points and fitted

Kunihiro et al. (1972) tests were performed in an open exposed environment, the severity of this environment was not reported, thus it was not possible to correlate the proposed environmental corrosivity factor γ_{corr} to environment. In this case, the properties of SMA steel can be reported for a regular service environment as the product

$\gamma_{corr} \gamma_\sigma \alpha_b = 0.182$ and the product $\gamma_{corr} \gamma_\sigma \alpha_c = 0.034$. If the environmental data is available, γ_{corr} can be interpolated based on the average penetration per side as an indicator of the corrosivity of the environment. Figure 5.9 shows the corrosion penetration of several types of steel as reported by Albrecht (1983). Further research is recommended to further correlate different environments to the proposed factor γ_{corr} .

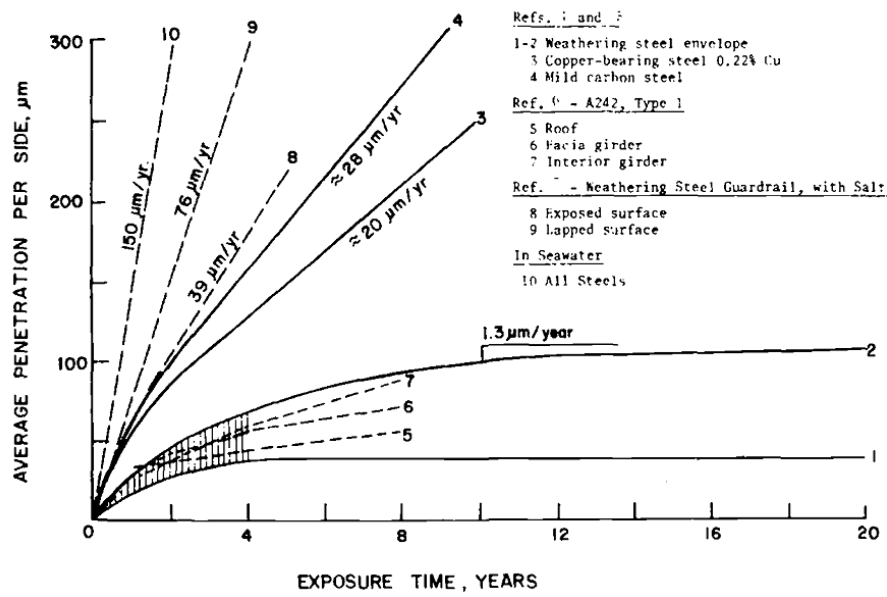


Figure 5.9 Corrosion of weathering steel compared with copper-bearing and mild steels
(Albrecht, 1983)

5.2.4 Implementation in CorrFLP

The proposed technique is adopted in CorrFLP, where the user should be able to provide the material-environment properties α_b and α_c of the tested material. Based on the environmental data available about the surrounding environment, the user can specify the level of corrosivity using the factor γ_{corr} . The fatigue life prediction cannot be performed the same way as described in section 4.3.4.1 due to the inaccuracy of the

fatigue threshold in corrosive environments. Thus, the theory of critical distances cannot be applied. In this study, the hot-spot approach will be used (which uses the values of strain on the surface of the specimen). In order to model the probabilistic nature of fatigue, a range of values of γ_{corr} corresponding to $\gamma_{corr} \pm 0.05$ will be used to give a predicted life range. Moreover, the user can also provide several corrosion thickness loss histories and apply them to different surfaces on the studied element to accurately simulate the real conditions.

5.3 CorrFLP (Corrosion Module) Verification

5.3.1 Introduction

In order to calibrate and verify the fatigue life prediction of CorrFLP in corrosive environments, a real case study will be simulated and verified against published test results. The chosen experimental investigation was done by Albrecht et al. (1994) to investigate the fatigue behaviour of 25 corroded rolled beams made of A588 steel. The beams were weathered under two conditions. One set was boldly exposed to the environment for 62 months and stress cycling in a moist freshwater environment. The other set was exposed for 67 months under a metal deck that simulated the shelter provided by highway bridge decks and was lightly sprayed with a salt solution during the winter months to simulate the use of de-icing salts for snow removal. A spreader beam distributed the load to two points spaced 914 mm (3 ft) apart as shown in Figure 5.10. The loading frequency was 0.75 Hz. The period of $1/0.75 = 1.33$ s corresponds to the time needed for a truck to cross a 30 m long highway bridge at a speed of 80 km/h (50 mph).

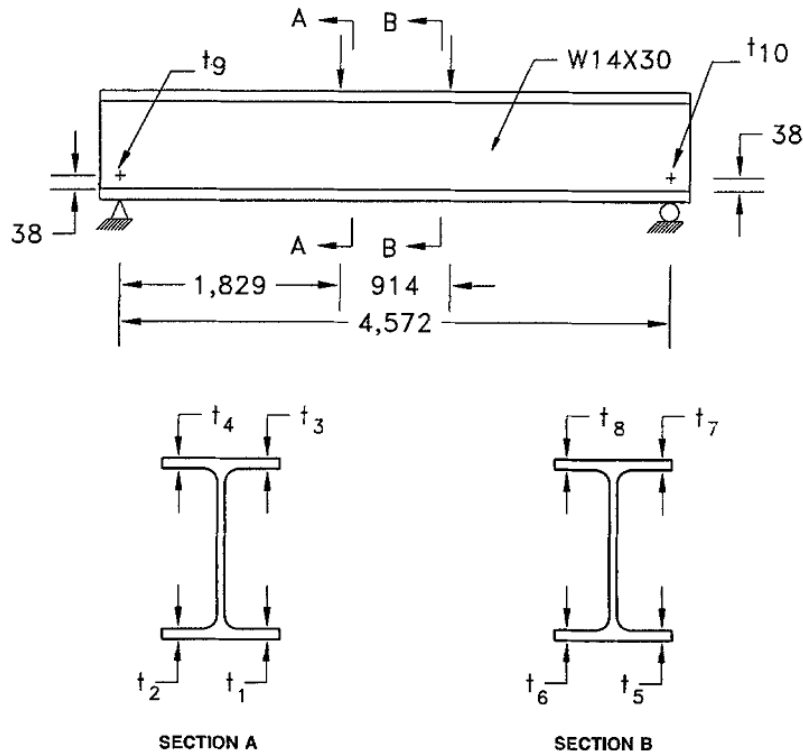


Figure 5.10 Configurations of tested beams (Albrecht et al., 1994)

The corrosion rates were monitored and reported by Albrecht et al. (1994) as shown in Figure 5.11. These values were used to generate suitable corrosion rate histories for each face (surface) of the finite element model representing the studied beam.

Beam (1)	Weathering time (month) (2)	MEAN CORROSION PENETRATION (μm) ^a					MEAN CORROSION RATE ($\mu\text{m}/\text{yr}$) ^a				
		Bottom flange p_b (3)	Top flange p_t (4)	Web		Bottom flange r_b (7)	Top flange r_t (8)	Web		Exposed ^b r_w (9)	Sheltered ^c r_w (10)
				Exposed ^b p_w (5)	Sheltered ^c p_w (6)			Exposed ^b r_w (9)	Sheltered ^c r_w (10)		
(a) Boldly Exposed Beams											
B1, B2, B8-B10	63	64	62	55	—	12	12	5.4	—		
B3-B6	59	49	28	47	—	10	5.8	10	—		
B11, B12, B15	66	85	55	51	—	16	10	9.1	—		
Mean	62.5	64	50	52	—	12	9.4	9.9	—		
(b) Sheltered Beams											
B1S-B7S	65	1,170	307	244	1,280	226	56	46	244		
B8S-B9S	66	1,560	414	198	1,570	284	76	36	284		
B10S-B13S	71	1,680	312	526	1,940	284	53	89	328		
B14S-B15S	70	1,560	236	419	1,350	267	41	71	231		
Mean	67.4	1,430	363	335	1,500	254	56	58	269		

^aValues of corrosion penetration and rate are per exposed surface.

^bBeam end exposed to rain-washing.

^cBeam end sheltered from rain-washing.

Figure 5.11 Test matrix and corrosion rates table adapted from Albrecht et al. (1994)

5.3.2 Material

The beams were made of A588 grade B weathering steel ("A588 Standard" 1992) with average 577 MPa tensile strength, 408 MPa yield point (regularly 345 MPa) and $E = 200\ 000$ MPa. Using the universal material method Baumel, et al. (1990) we obtain $K' = 1400$ MPa, $n' = 0.15$, $\sigma'_f = 870$ MPa, $b = -0.09$, $\varepsilon'_f = 0.59$ and $c = -0.58$. Since it was reported by Albrecht (1983) that the properties of SMA steel are similar to those of A588 steel, the proposed environmental constants will be taken for the boldly exposed specimens as concluded in section 5.2.2 as $\gamma_{corr} \gamma_\sigma \alpha_b = 0.182$ and $\gamma_{corr} \gamma_\sigma \alpha_c = 0.034$. By comparing the values of corrosion penetration rates reported by Albrecht et al. (1994) and the values listed in Table 5.1, the factor $\gamma_{corr} = 0.45$ was selected as an average for the specimens boldly tested in air. Also, the factor $\gamma_{corr} = 0.75$ was selected as an average value for the specimens tested in moist freshwater environment. For the sheltered specimens tested in moist saltwater environment, which is a very harsh environment, the values from the ISO-9224 were extrapolated and the factor $\gamma_{corr} = 1.1$ was used as an average value to represent this environment. As the critical length theory will not be used while including the effect of corrosion, the approach of using percentages of the critical length "L" to get an estimated range for the expected fatigue life cannot be applied. In order to get a realistic estimated range for the expected life for each specimen, the expected lives corresponding to $\gamma_{corr} \pm 0.05$ will be used.

5.3.3 Finite Element Model

A 3D finite element model has been modeled. The reduced integration solid continuum element C3DR from the ABAQUS FE library was used. Quarter of the beam is modelled using the symmetry about the section centerline and the beam centerline. One half of each concentrated load is applied to the top of the flange. Figure 5.12 shows the finite element model showing the loading, boundary conditions and meshing.

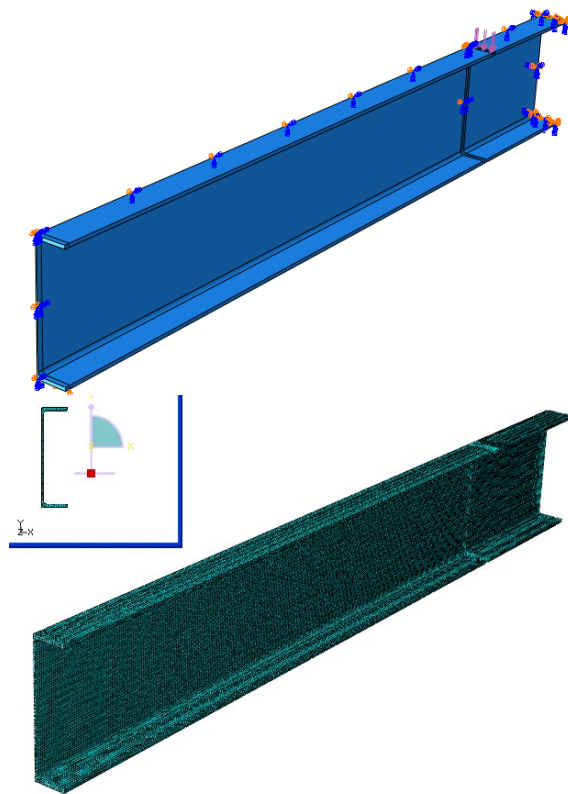


Figure 5.12 Finite element model for the girder (loading and boundary conditions in the top, meshing and cross-section in the bottom)

Twenty four beams were modeled; the loading was based on stress ranges for the unweathered sections. Fatigue calculations were based on the final weathered sections. Corrosion rates for each part of the specimens were reported by Albrecht et al. (1994) and all the geometric and loading input values are listed in Table 5.2.

Table 5.2 Input data for the finite element model

Beam	Non-Weathered Section					Weathered Section			Weathering Time (Months)	Corrosion Rate Bottom Flange (mm/year)	Corrosion Penetration Bottom (mm)	Corrosion Rate Top Flange (mm/year)	Corrosion Penetration Top (mm)	Corrosion Rate Web (mm/year)	Corrosion Penetration Web (mm)	Number of Cycles to Failure	
	Stress Range (MPa)	Minimum Stress (MPa)	Maximum Stress (MPa)	Pmin (Newton)	Pmax (Newton)	Maximum Strain Range	Stress Range (MPa)	Max Stress (MPa)									
Group 1: Boldly Exposed Beams Tested in Air																	
B3	248	7	255	2633.13	95921.27	0.001240	250.40	257.47	0.001252	59.00	0.0100	0.0492	0.0058	0.0285	0.0100	0.0492	1750000
B4	248	7	255	2633.13	95921.27	0.001240	250.41	257.47	0.001252	59.00	0.0100	0.0492	0.0058	0.0285	0.0100	0.0492	4042600
B5	248	7	255	2633.13	95921.27	0.001240	250.41	257.47	0.001252	59.00	0.0100	0.0492	0.0058	0.0285	0.0100	0.0492	4424600
B6	248	7	255	2633.13	95921.27	0.001240	250.41	257.47	0.001252	59.00	0.0100	0.0492	0.0058	0.0285	0.0100	0.0492	1734200
Group 2: Boldly Exposed Beams tested in moist saltwater environment																	
B11	165	7	172	2633.13	64699.84	0.000825	167.71	174.83	0.000839	66.00	0.0170	0.0935	0.0110	0.0605	0.0091	0.0501	1595500
B12	165	7	172	2633.13	64699.84	0.000825	167.71	174.83	0.000839	66.00	0.0170	0.0935	0.0110	0.0605	0.0091	0.0501	1576600
B8	214	7	221	2633.13	83131.77	0.001070	216.40	223.48	0.001082	63.00	0.0120	0.0630	0.0120	0.0630	0.0054	0.0284	1036000
B10	214	7	221	2633.13	83131.77	0.001070	216.40	223.48	0.001082	63.00	0.0120	0.0630	0.0120	0.0630	0.0054	0.0284	940500
B1	276	7	283	2633.13	106453.80	0.001380	279.09	286.17	0.001396	63.00	0.0120	0.0630	0.0120	0.0630	0.0054	0.0284	386400
B2	276	7	283	2633.13	106453.80	0.001380	279.09	286.17	0.001396	63.00	0.0120	0.0630	0.0120	0.0630	0.0054	0.0284	456700
B9	276	7	283	2633.13	106453.80	0.001380	279.09	286.17	0.001396	63.00	0.0120	0.0630	0.0120	0.0630	0.0054	0.0284	435600
Group 3: Sheltered Beams tested in moist saltwater environment																	
B15S	47	7	54	2633.13	20312.74	0.000235	66.56	76.48	0.000333	70.00	0.2670	1.5575	0.0410	0.2392	0.2310	1.3475	6943200
B7S	69	7	76	2633.13	28588.30	0.000345	91.43	100.70	0.000457	65.00	0.2260	1.2242	0.0560	0.3033	0.2440	1.3217	4952100
B8S	69	7	76	2633.13	28588.30	0.000345	99.99	110.13	0.000500	66.00	0.2840	1.5620	0.0760	0.4180	0.2840	1.5620	1884600
B9S	69	7	76	2633.13	28588.30	0.000345	99.99	110.13	0.000500	66.00	0.2840	1.5620	0.0760	0.4180	0.2840	1.5620	1551300
B10S	110	7	117	2633.13	44010.93	0.000550	169.20	179.97	0.000846	71.00	0.2840	1.6803	0.0530	0.3136	0.3280	1.9407	468900
B11S	110	7	117	2633.13	44010.93	0.000550	169.20	179.97	0.000846	71.00	0.2840	1.6803	0.0530	0.3136	0.3280	1.9407	497400
B13S	110	7	117	2633.13	44010.93	0.000550	169.20	179.97	0.000846	71.00	0.2840	1.6803	0.0530	0.3136	0.3280	1.9407	420000
B5S	147	7	154	2633.13	57928.92	0.000735	194.78	204.06	0.000974	65.00	0.2260	1.2242	0.0560	0.3033	0.2440	1.3217	132900
B4S	152	7	159	2633.13	59809.73	0.000760	201.41	210.68	0.001007	65.00	0.2260	1.2242	0.0560	0.3033	0.2440	1.3217	201800
B6S	152	7	159	2633.13	59809.73	0.000760	201.41	210.68	0.001007	65.00	0.2260	1.2242	0.0560	0.3033	0.2440	1.3217	105500
B1S	208	7	215	2633.13	80874.79	0.001040	275.61	284.89	0.001378	65.00	0.2260	1.2242	0.0560	0.3033	0.2440	1.3217	154400
B2S	214	7	221	2633.13	83131.77	0.001070	283.56	292.84	0.001418	65.00	0.2260	1.2242	0.0560	0.3033	0.2440	1.3217	112400
B3S	214	7	221	2633.13	83131.77	0.001070	283.56	292.84	0.001418	65.00	0.2260	1.2242	0.0560	0.3033	0.2440	1.3217	16200

5.3.4 Fatigue Life Prediction

In order to include the mean stress effects and relate it to the material properties, values of $\gamma_{corr} \gamma_\sigma$ were plotted against the values of the maximum stress normalized to the ultimate stress σ_{max} / σ_u as shown in Figure 5.13.

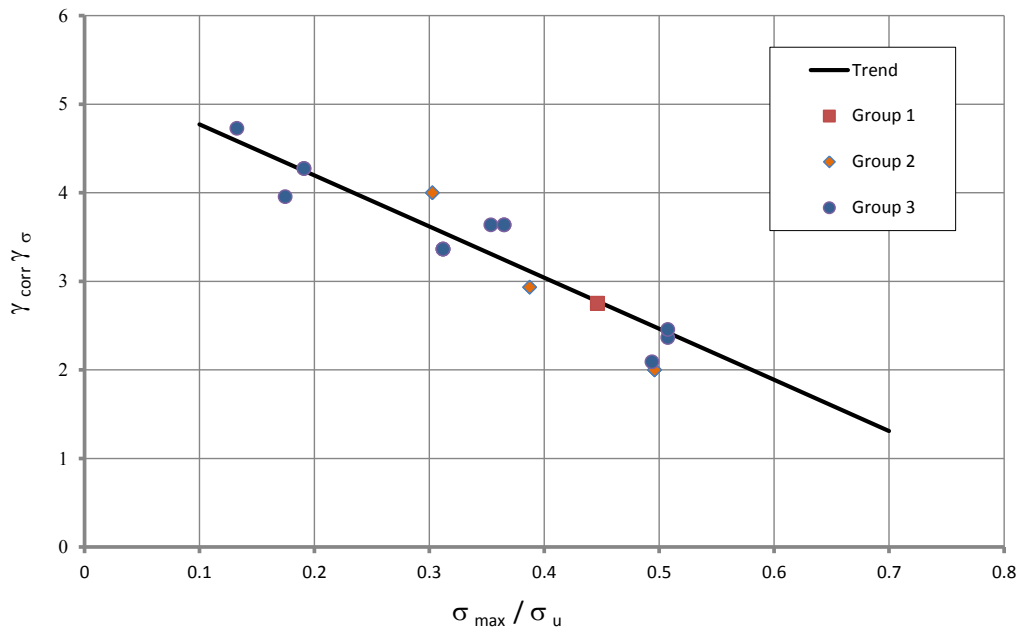


Figure 5.13 Plot of $\gamma_{corr} \gamma_\sigma$ values versus σ_{max} / σ_u .

By curve fitting, an equation (5-7) was derived as follows:

$$\gamma_{corr} \gamma_\sigma = 5.77 \left(\frac{\sigma_{max}}{\sigma_u} \right) + 5.35 \quad (5-7)$$

By having the values of γ_{corr} defined for each environment, values of $\gamma_{corr} \gamma_\sigma$ are derived and thus the fatigue life for each specimen based on the modified SWT model proposed in equation (5-4) can be determined. Values of all factors and predicted lives are listed in Table 5.3.

Table 5.3 Derived Corrosion factors and estimated number of cycles to failure

Beam	Non-Weathered Section				Weathered Section		Number of Cycles to Failure	Estimated number of cycles (SWT)	Estimated number of cycles (Lower Bound)	Estimated number of cycles (Upper Bound)	$\gamma_{corr} \gamma_\sigma$	$\gamma_{corr} \gamma_\sigma$	γ_σ	σ_{max} / σ_u	γ_{corr} (Min)	γ_{corr} (Max)	
	Stress Range (MPa)	Minimum Stress (MPa)	Maximum Stress (MPa)	Maximum Strain Range	Max Stress (MPa)	Strain Range											
Boldly exposed Beams Tested in Air																	
B3	248	7	255	0.001240	257.47	0.001252	1750000	19000000	1350000	2350000	1.11	1.39	2.775	0.45	0.4	0.5	
B4	248	7	255	0.001240	257.47	0.001252	4042600	19000000	1350000	2350000	1.11	1.39	2.775	0.45	0.4	0.5	
B5	248	7	255	0.001240	257.47	0.001252	4424600	19000000	1350000	2350000	1.11	1.39	2.775	0.45	0.4	0.5	
B6	248	7	255	0.001240	257.47	0.001252	1734200	19000000	1350000	2350000	1.11	1.39	2.775	0.45	0.4	0.5	
Boldly exposed Beams tested in moist saltwater environment																	
B11	165	7	172	0.000825	174.68	0.000838	1595500	82000000	1700000	3300000	2.52	2.88	3.603	0.30	0.7	0.8	
B12	165	7	172	0.000825	174.68	0.000838	1576600	82000000	1700000	3300000	2.52	2.88	3.603	0.30	0.7	0.8	
B8	214	7	221	0.001070	223.48	0.001082	1036000	58000000	650000	1000000	2.18	2.49	3.115	0.39	0.7	0.8	
B10	214	7	221	0.001070	223.48	0.001082	9405000	58000000	650000	1000000	2.18	2.49	3.115	0.39	0.7	0.8	
B1	276	7	283	0.001380	286.17	0.001396	386400	6300000	250000	370000	1.74	1.99	2.488	0.50	0.7	0.8	
B2	276	7	283	0.001380	286.17	0.001396	456700	6300000	250000	370000	1.74	1.99	2.488	0.50	0.7	0.8	
B9	276	7	283	0.001380	286.17	0.001396	435600	6300000	250000	370000	1.74	1.99	2.488	0.50	0.7	0.8	
Sheltered beams tested in moist saltwater environment																	
B15S	47	7	54	0.000235	76.48	0.000333	6943200	53000000	9300000	19000000	4.81	5.27	4.59	0.13	1.05	1.15	
B7S	69	7	76	0.000345	100.70	0.000457	4952100	254000000	2650000	5000000	4.56	4.99	4.34	0.17	1.05	1.15	
B8S	69	7	76	0.000345	110.13	0.000500	1884600	230000000	1800000	3300000	4.46	4.89	4.25	0.19	1.05	1.15	
B9S	69	7	76	0.000345	110.13	0.000500	1551300	230000000	1800000	3300000	4.46	4.89	4.25	0.19	1.05	1.15	
B10S	110	7	117	0.000550	179.97	0.000846	468900	77500000	305000	480000	3.73	4.08	3.55	0.31	1.05	1.15	
B11S	110	7	117	0.000550	179.97	0.000846	497400	77500000	305000	480000	3.73	4.08	3.55	0.31	1.05	1.15	
B13S	110	7	117	0.000550	179.97	0.000846	420000	77500000	305000	480000	3.73	4.08	3.55	0.31	1.05	1.15	
B5S	147	7	154	0.000735	204.06	0.000974	132900	115500000	200000	300000	3.47	3.81	3.31	0.35	1.05	1.15	
B4S	152	7	159	0.000760	210.68	0.001007	201800	93000000	190000	270000	3.41	3.73	3.24	0.37	1.05	1.15	
B6S	152	7	159	0.000760	210.68	0.001007	105500	93000000	190000	270000	3.41	3.73	3.24	0.37	1.05	1.15	
B1S	208	7	215	0.001040	284.89	0.001378	154400	6800000	90000	120000	2.63	2.88	2.50	0.49	1.05	1.15	
B2S	214	7	221	0.001070	292.84	0.001418	112400	5150000	90000	110000	2.54	2.78	2.42	0.51	1.05	1.15	
B3S	214	7	221	0.001070	292.84	0.001418	16200	5150000	90000	110000	2.54	2.78	2.42	0.51	1.05	1.15	

Table 5.3 lists the predicted number of cycles predicted by the original SWT model without considering corrosion. The introduction of the factor γ_σ was useful in calibrating the model as it was clear that the results were stress level dependant. By trial and error, the curve fitting in Figure 5.13 was adjusted to be upper bound to most of the sample points in order to give conservative fatigue life for most of the test specimens. As the ratio σ_{max} / σ_u gets less, the sensitivity of the factor $\gamma_{corr} \gamma_\sigma$ gets higher. Several trends were tested, the simple linear trend proposed in equation (5-7) was chosen. Having more experimental data points would help in further calibration of this proposed equation.

5.3.5 Discussion of results

The results obtained for the expected life for each specimen are presented as a range corresponding to $\gamma_{corr} \pm 0.05$ for each testing environment. The range of ± 0.05 was arbitrarily chosen, and it proved to result in very good predictions of fatigue life, as will be shown later. The ranges of values of the predicted number of cycles to failure are plotted versus the experimentally determined values from Albrecht et al. (1994) in Figure 5.14. Despite the valuable reported data and results regarding the tested twenty four beams that were used to calibrate the numerical model, it is worth mentioning that the experimental data is a bit scattered with different loadings and environmental conditions and that there is still a need for more available data points to further calibrate the model.

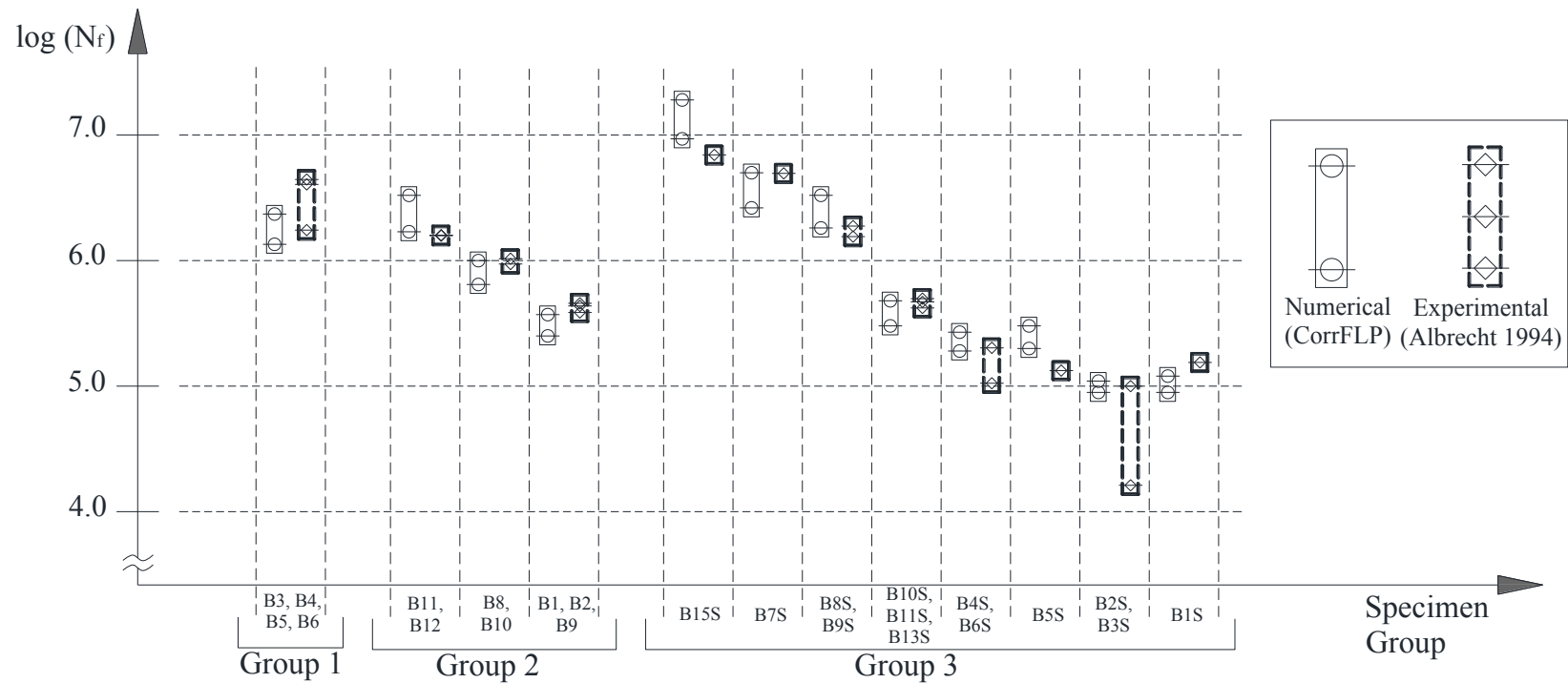


Figure 5.14 Predicted lives using CorrFLP vs. experimentally observed by Albrecht et al. (1994)

5.3.5.1 Discussion of group 1 results

Beams in this group have the same values for stress ranges and maximum applied stresses. There is already a considerable scatter in the results of the identical tested beams in Group 1, with a standard deviation of about 1.45 million cycles which is 70% of the minimum experimentally obtained results and 28% of the maximum experimental result. Numerical simulations of the predicted fatigue life of this group could be visually compared by the range bars plotted in Figure 5.14. From Figure 5.14 it can be seen that the upper bound predicted value is close to the mean of the experimental bar, whereas the lower bound expected value is less than (i.e. conservative than) the minimum experimental result by 22%. From the previous observations, it could be concluded that the predicted fatigue lives using the proposed model (in term of ranges) are in good agreement with the available experimental results and tend to be on the conservative side.

5.3.5.2 Discussion of group 2 results

Beams in this group have different values for stress ranges and maximum applied stresses. Beams B8 and B10 had the closest mean predicted fatigue life as compared to the mean experimental value, where the difference between the means of the predicted and the experimental values was about 12%. The maximum predicted life is almost the same as the mean of the experimental result, while the minimum predicted life was 31% less than the minimum experimental result. Beams B1, B2 and B9 had the most conservative life predictions as all the numerical results lied below the experimental with a difference of 4% between the maximum expected result and the minimum experimental value obtained. Beams B11 and B12 had the most non-conservative life predictions as all

the predicted results lied above the experimental with a difference of 8% between the minimum predicted result and the maximum experimental value obtained.

5.3.5.3 Discussion of group 3 results

Beams in this group have a very wide spectrum of different values for stress ranges and maximum applied stresses. All the predicted lives in this group were on the conservative side except for beams B15S and B5S. This highlights the need for more experimental tests in order to further calibrate the proposed $\gamma_{corr} \gamma_\sigma$ function. Specimens B2S and B3S are important to mention as they have a relatively high stress range and the highest ratio of σ_{max} / σ_u being equal to 0.51. There is a very big scatter in the experimental results between these two identical specimens which indicates that specimen B3S might have experienced premature failure. This is highly probable, especially given that the predicted analytical range of fatigue life is so close to that of B2S. In general, it could be concluded that the numerical predictions of fatigue life using the proposed model correlates very well with the measured experimental fatigue life of the twenty four tested beams.

5.3.5.4 Conclusions

As can be seen from Figure 5.14 and from the previous observations and taking into consideration the complexity of the corrosion-fatigue phenomenon, there is a relatively good agreement between the results obtained using the proposed model and the values reported. The proposed model generally gives conservative results. Moreover, there is a big scatter in the results of some of the experimental specimens, this shows the efficiency of providing the results in ranges rather than providing a single definite value.

It can be noticed from the numerical results that the predicted range of fatigue cycles increases as the stress level decreases, and vice versa. The effect of the maximum applied stress was found to be of significant importance in this study and was taken into account by the factor $\gamma_{corr} \gamma_\sigma$ which is a function in the ratio σ_{max} / σ_u . The relation between the ratio σ_{max} / σ_u and the factor $\gamma_{corr} \gamma_\sigma$ was found to be inversely proportional with a linear trend. Further experimental work is needed to calibrate the proposed function and to check if the observed behaviour would be the same for other types of steel.

Moreover, by comparing to experimental results available which are already in a corroded state (reduced sections), it can be said that it is not sufficient to model corrosion just by geometrically reducing the section, as this would not provide a numerically accurate estimation for the fatigue life as is clear from the predicted fatigue life predictions using the original SWT model listed in Table 5.3. Hence, it is important to implement the newly proposed strain-life model to account for the effect of corrosion and the effect of maximum applied stress.

5.3.6 Standardizing a procedure for determining new material constants

More future experimental data is needed to further calibrate the proposed model. For this purpose, the author proposes a standardized experimental methodology for obtaining the proposed corrosion constants for any material.

1. Perform several strain-controlled axially loaded fatigue endurance tests on standard specimens according to the ASTM E606 - 04e1 Standard Practice for Strain-Controlled Fatigue Testing in a 3.5% NaCL solution which will be assumed to correspond to $\gamma_{corr} = 1$.
2. By curve fitting the obtained results with a confidence level of 95% (as a lower bound), values for b' and c' can be graphically obtained.
3. Having the target values of b' and c' , and using the value of γ_σ from equation (5-7), the values of α_b , α_c can be obtained and used as material constants.

By having these factors for each material, the fatigue life of different materials in corrosive environment can be predicted using the proposed modified SWT model.

5.3.7 Summary

A new strain-life model has been proposed as a modification to the Smith Watson Topper model. The new model takes into account the effect of the corrosivity of the environment. The newly proposed model uses several proposed constants that depend on the material and the corrosivity of the environment. The proposed model is validated with available experimental work. The results obtained for the expected life for each specimen are presented as a range corresponding to $\gamma_{corr} \pm 0.05$ for each testing environment to

give a range for the expected fatigue life instead of providing one value for the expected life. Results obtained from the newly proposed model were of good agreement with the experimental work available. The results tend to be more conservative than the experimental values for most of the specimens. A standardized method to obtain the proposed material parameters has been proposed. It is worthy to mention that all the available experimental work for corrosion in literature is done on already corroded members. Thus, the derived material properties represent the most severe case which is conservative for design purposes.

5.4 Guidelines for developing corrosion-fatigue design charts

5.4.1 Introduction

One of the benefits of CorrFLP is the ability to perform a real-time simulation for a certain detail using real loads along with environmental effects such as corrosion. CorrFLP uses the strain-based fatigue analysis which is more accurate than the stress based method commonly used in developing the S-N curves in several codes of practice. By performing the analysis on a given detail, the expected fatigue life can be predicted under any realistic loading history (not limited to constant amplitude loading). This could facilitate the generation of series of S-N curves for several structural details for design purpose. By simulating several stress ranges, corresponding number of cycles to failure can be determined and plotted to create an S-N curve for a given detail. In this section, several S-N curves for different structural details will be created under different corrosive environments.

This section is not intended to provide any quantitative measures for the fatigue life of the demonstrated details, as the results are material and detail dependant. Moreover, in order to be able to confidently assign a fatigue category to a certain detail, several parameters still have to be varied experimentally, which is beyond the scope of this study. This section provides qualitative guidelines on how to use the developed numerical tool to generate detail-specific S-N corrosion-fatigue curves. Appendix C provides details on how the S-N curves can be statistically constructed.

5.4.2 Method for generating environmental S-N curves for various riveted details

In the following sections, several S-N curves for three commonly used structural steel riveted details will be qualitatively constructed for different levels of corrosive environments. This section is intended to demonstrate the capabilities of such a tool for classifying any connection using the finite element method existing in different corrosive environments. It provides systematic procedures for carrying out parametric study that can be conducted for several commonly used details that would lead to the development of environmentally dependant S-N curves to be implemented in code provisions. Different corrosion rates for different metals could be obtained from Albrecht et al. (1989). Charts can be generated for a wide spectrum of values for the factor γ_{corr} . The designer can interpolate to get other intermediate values. Figure 5.15 shows a qualitative example of the expected S-N curves to be generated for a sample riveted detail in different environmental corrosivity values corresponding to values for the factor $\gamma_{corr} = 0.0, 0.5$ and 1.0 .

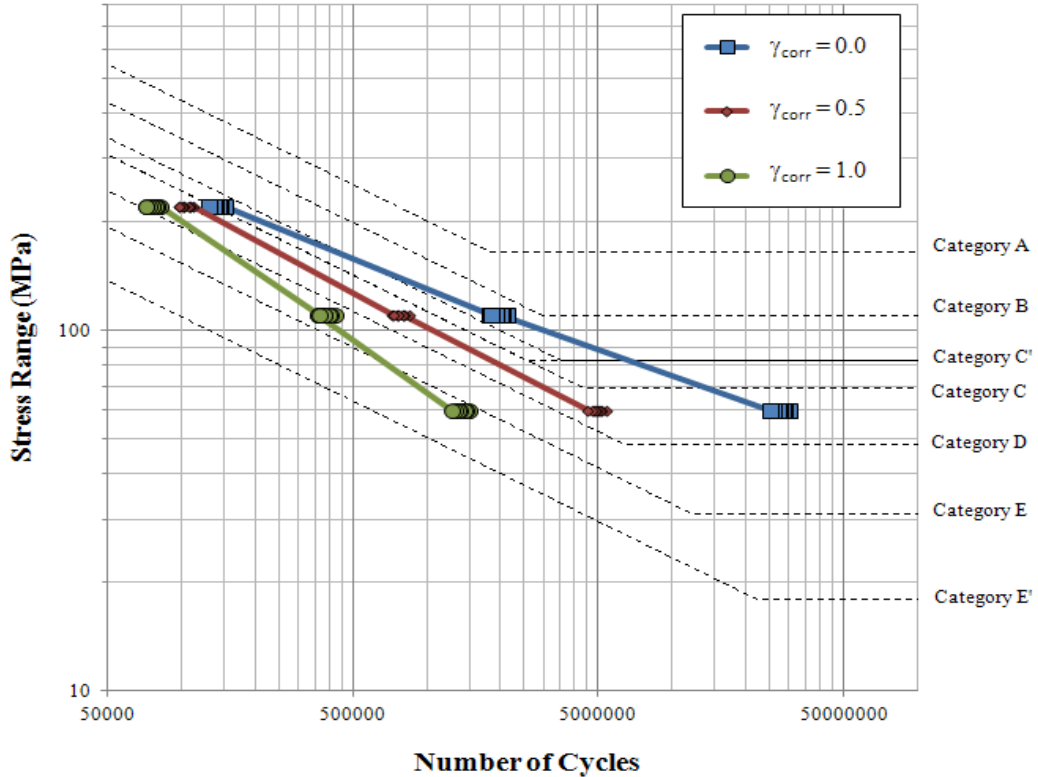


Figure 5.15 Sample S-N curves for a studied detail for several corrosion rates

5.4.3 Splice Plates

In this section, the connection studied in section 4.5.2 will be used. This detail is chosen because it is commonly used as splices in the flanges of bridge girders and in truss bridge members. The same FE model used in section 4.5.2 can be used here. Three rivet diameters can be chosen; for example 16mm, 20mm, and 25mm to represent different bearing ratios (ratio of bearing stress in the bolt to the average tensile stress in the plate). Three thicknesses for the outer plates (more critical) can be used; for example 12mm, 16mm and 20mm. Figure 5.16 shows a schematic drawing for the parametric FE model. It is important to note that this model is not a generalization for all configurations of similar connections, but acts as an example to show the methodology that can be adopted to generate ensemble of S-N curves for a given detail.

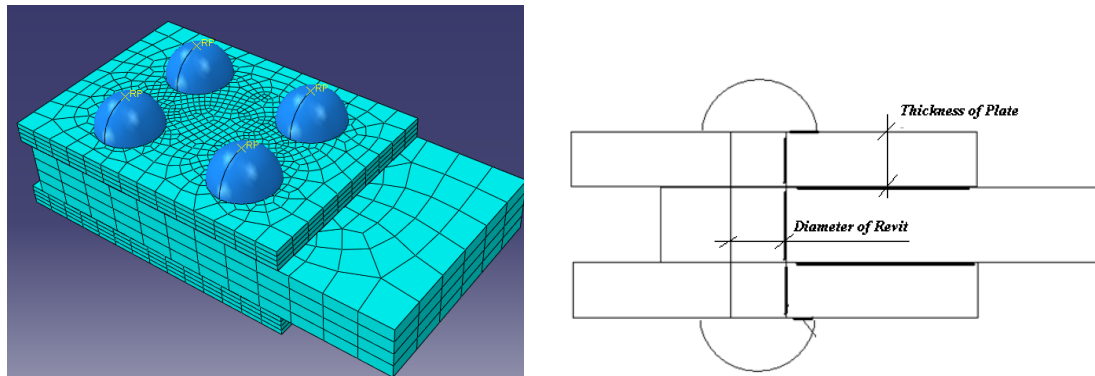


Figure 5.16 The finite element model for “Splice Plate” series

The stress applied loads are chosen so that the stress ranges calculated at the net section (passing through the rivets) could have the values ranging from 0.2 of the yield stress to 0.8 of the yield stress. The stress ratio R (ratio of low stress to high stress) can be included as a factor, but it will drastically increase the required test samples, thus the stress ratio R is recommended to be 0.2, which is a practical value used as a lower bound for many fatigue tests. Figure 5.17 shows a schematic drawing illustrating the dimensional variables chosen for this study. The study can be repeated for several types of commonly used steels as their behaviour in corrosive environment could be significantly different.

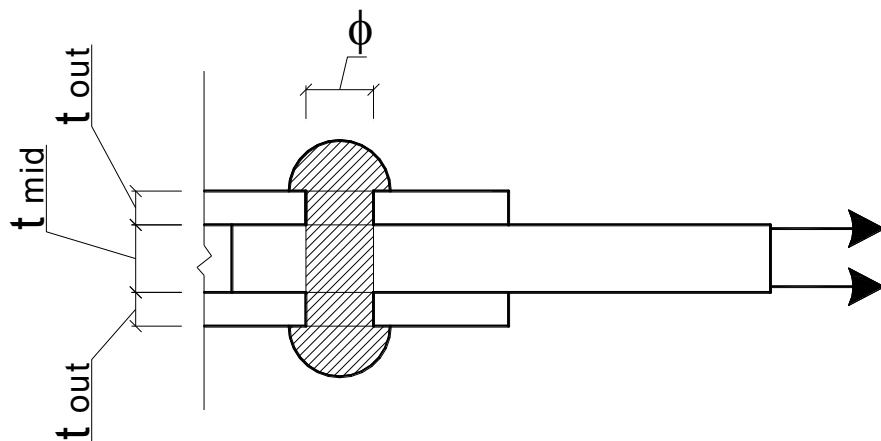


Figure 5.17 Schematic drawing for the test variables

5.4.4 Angles connected to Gusset Plates

This detail is chosen because it is commonly used in the flanges of bridge girders and as splices in truss members. Three rivet diameters can be used; for example 16mm, 20mm, and 25mm to represent different bearing ratios (ratio of bearing stress in the bolt to the average tensile stress in the plate). Three thicknesses for the outer plates (more critical) can be used; 12mm, 16mm and 20mm. Figure 5.18 shows a schematic for the parametric FE model.

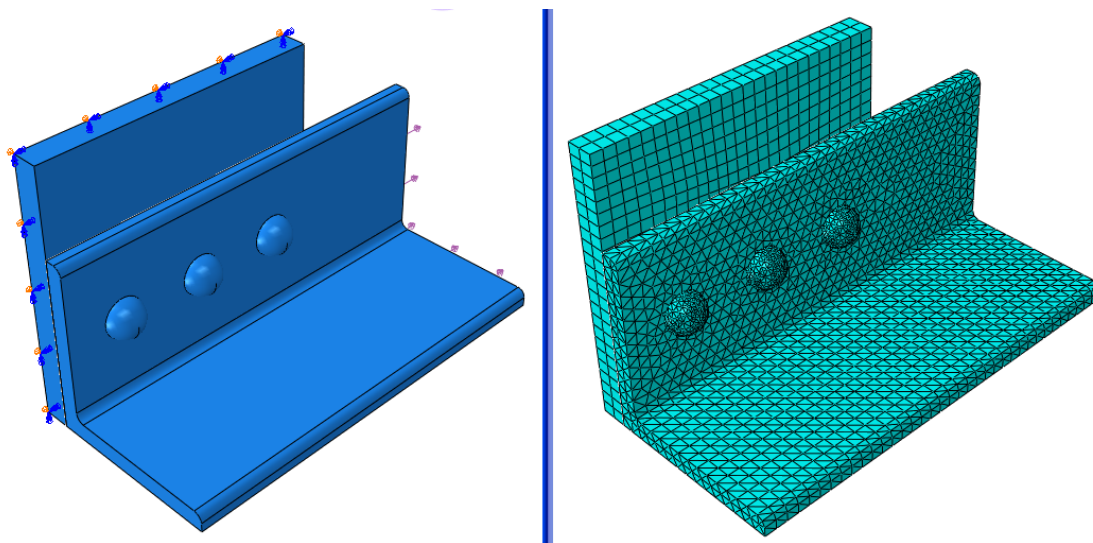


Figure 5.18 The finite element model for the “Angles connected to Gusset Plates” series

Figure 5.19 shows a schematic drawing illustrating the dimensional variables chosen for this study. The stress applied loads are chosen so that the stress ranges calculated at the net section (passing through the rivets) could have the values ranging from 0.2 of the yield stress to 0.8 of the yield stress. The stress ratio R (ratio of low stress to high stress) can be included as a factor, but it will drastically increase the required test samples, thus the stress ratio R is recommended to be 0.2, which is a practical value used as a lower bound in many fatigue tests.

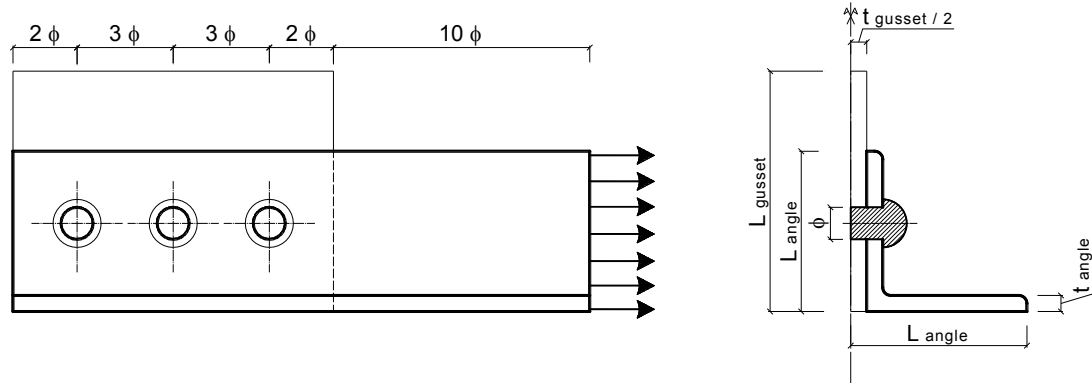


Figure 5.19 Schematic drawing for the test variables

5.4.5 Angles in built-up Plate Girders

In this section, the connection studied in section 4.5.3 is used for the generation of S-N curves. The same FE modeling technique used in section 4.5.3 can be used here. Figure 5.20 shows a schematic for the parametric FE model.

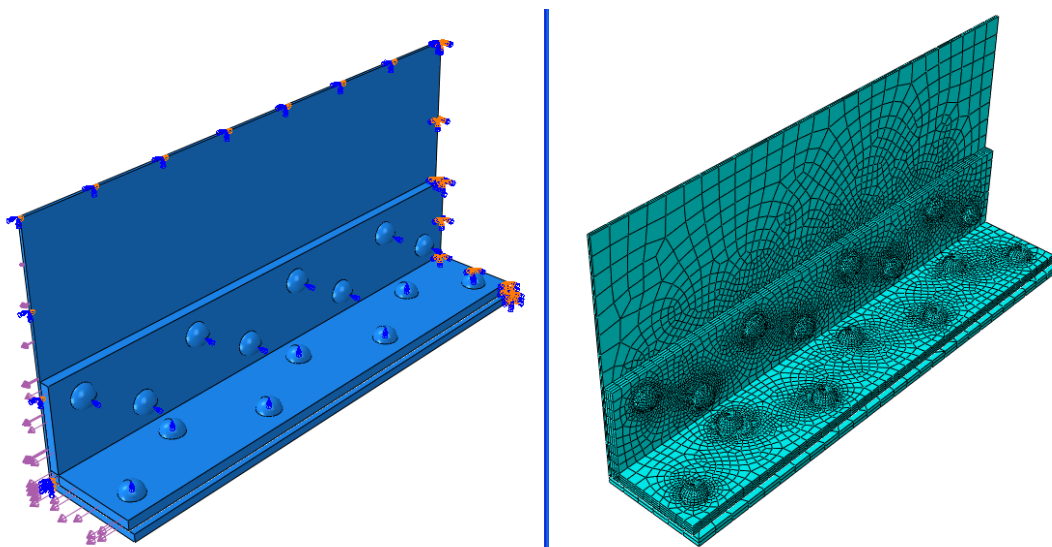


Figure 5.20 The finite element model for the “Built-up Beam” series

Figure 5.21 shows a schematic drawing illustrating the dimensional variables chosen for this study. The stress applied loads are chosen so that the stress ranges calculated at the net section (passing through the rivets) could have the values ranging from 0.2 of the yield stress to 0.8 of the yield stress. The stress ratio R (ratio of low stress to high stress) can be included as a factor, but it will drastically increase the required test samples, thus the stress ratio R is recommended to be 0.2, which is a practical value used as a lower bound for many fatigue tests. Practical values for the stress gradient ratio (S_{\min}/S_{\max}) range from 0.7 to 0.9 depending on the overall height of the girder, thus an average stress gradient ratio equal to 0.8 can be used. The plotted values of stresses should be the flexural stresses calculated on the net section passing through the rivets.

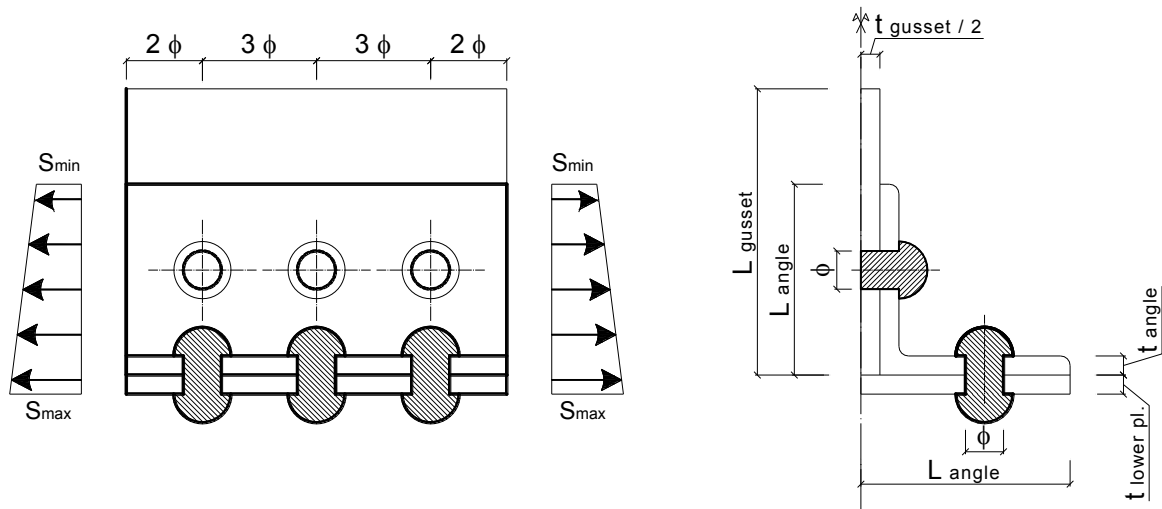


Figure 5.21 Schematic drawing for the test variables

5.5 Future work

The proposed strain-life model is based on the hypothesis that the corrosion affects both the elastic and plastic behaviour of the material, and that the proposed material properties α_b and α_c are constant. Further research should be done on monitoring and quantifying this behaviour for different materials. The author recommends future work for accurately correlating the environmental corrosivity intensity factor γ_{corr} could be correlated to the categories provided by the ISO-9223 (1992) and the ISO-9224 (1992) to standardize this factor. The author recommends following the proposed qualitative guidelines in order to create corrosion fatigue design charts for several riveted connection details.

CHAPTER 6

CONTRIBUTIONS, CONCLUSIONS AND RECOMMENDATIONS

6.1 Summary and Contributions of this research

The main objective of this study is to overcome the current limitations in numerical modeling tools used for predicting the fatigue life of structural steel components by developing a tool that takes into account the effect of corrosion, which is an influential parameter on the fatigue life of railway or highway steel bridges. In general, structural engineers could use either the stress-life approach or the strain-life approach for the fatigue life prediction. This study contributes to both approaches.

As for the stress-life approach, a new damage accumulation model called the VTLC (for Virtual Target Life Curves) is proposed in Chapter 3. This model can take into account the effect of the overloads and can be calibrated to the material mechanical characteristics using a proposed material constant. The proposed method is validated using experimental work results from literature (which includes results of over 700 steel wire specimens). A case study on assessing the fatigue life of a bridge member was conducted to demonstrate the practical application of the proposed method.

Regarding the strain-life approach, a numerical tool is developed in Chapter 4 to predict the fatigue life of any riveted or bolted component. The numerical tool (CorrFLP) utilizes the finite element method and can be used as an add-on to many well-known commercial FEM packages to add fatigue features to them. CorrFLP uses most of the classical strain-life models in literature and can predict the fatigue life using the hot-spot

approach. To model the probabilistic nature of fatigue, a new approach is introduced to make use of the theory of critical distances in order to obtain a range for the predicted fatigue life instead of obtaining a single deterministic value as per the approach of other current available tools. Three case studies were modeled to calibrate the numerical tool and to validate the proposed method.

As an extension to the work done for fatigue life prediction, a new strain-life model based on the SWT (Smith-Watson-Topper method of uniaxial fatigue damage calculation) model that includes the effect of corrosion on the fatigue life prediction is proposed in Chapter 5. The newly proposed model uses several proposed constants that depend on the material and the corrosivity of the environment. The proposed model was validated with available experimental work. As it is common to have a scatter in the results of some of the fatigue tested specimens, it is only practical to provide the results of the analytical simulations in ranges (as has been introduced in this thesis) rather than providing a single definite value for the predicted fatigue life time. A standardized method to obtain the proposed material parameters is also provided.

One of the practical benefits of this study is the possibility of generating environmentally dependant S-N curves that could be adopted by design codes concerned with the fatigue assessment of riveted steel railway and highway bridges. The last section of Chapter 5 provides a systematic methodology for developing such charts following a more comprehensive prospective parametric study.

6.2 Features of the developed numerical tool:

6.2.1 CorrFLP Applications:

CorrFLP was developed to serve several purposes and overcome many common limitations in available fatigue simulation programs. The numerical tool has several usages:

1. Fatigue life prediction of new structural elements to be designed; that is by simulating the expected loading, corrosion and temperature histories along with applying appropriate damage models.
2. Fatigue life prediction of existing structural elements including the effect of corrosion under the current loading.
3. Evaluation and rating of structural elements using different future loading scenarios. This will be achieved by creating a model simulating the past loading history including the accumulated effect of corrosion, the model can be simulated from this state using different loading scenarios and predict the fatigue life for each one.
4. Development of S-N curves for a given detail by running several analyses at different stress range levels including the environmental effects.

6.2.2 CorrFLP Advantages:

1. Quickly simulates models with complex loading patterns that cannot be easily simulated experimentally.
2. Includes the effects of corrosion which is difficult, time consuming and expensive to prepare experimentally.

3. Has the smart meshing feature to capture high stress gradients.
4. Acts as an add-on that integrates with different finite element packages.
5. Can be extended to implement the combined effect of temperature and fatigue (not in the scope of this study).

6.2.3 CorrFLP Current Limitations:

Although the numerical approaches, in general, are appealing -as they are time and cost effective compared to experimental work- they have several limitations that need to be considered. The following are the current limitations of CorrFLP:

1. Similar to other numerical tools, use of the finite element method for fatigue life prediction, requires a good knowledge of finite element modeling. The accuracy of the output highly depends on the accuracy of the finite element model, the input loads and boundary conditions.
2. Does not support creep and thermal fatigue (not in the scope of this study).
3. Does not support fretting fatigue (not in the scope of this study).
4. Does not support energy methods in fatigue life prediction.
5. Does not support crack propagation analysis (not in the scope of this study).
6. Damage models are not general to all materials or even all kinds of steels, so they need to be chosen based on references. The program gives some guidelines for the user, but it is recommended to have a strong background about the used material fatigue properties.
7. Some of the damage models in literature need the user to know some parameters that have to be calibrated with experimental work.

6.3 Significance of this Research

In this research, a numerical tool that predicts the fatigue life of deteriorating corroded steel members or connections using the finite element method is developed and coded. The advantage of the developed numerical tool is its effectiveness in the evaluation of existing structural details and predicting their fatigue lives, simulating the effect of corrosion and the possibility of applying the actual complex loading history.

This tool is a significant addition to the scientific resources in the area of fatigue; where researchers will be able to use it to examine the influence of different reported fatigue damage models on various structural details and investigate the interaction with other factors such as corrosivity of the environment and the temperature (which is not within the scope of this research). Moreover, the researcher can add user-defined rules for fatigue-corrosion-temperature interaction and assess their applicability. The author implemented several strain-life fatigue damage models available in the literature. The tool includes several corrosion damage functions and corrosion rate histories based on surveys from literature. Moreover, in this research, a new strain-life corrosion-fatigue life prediction model is proposed and implemented in the program where it showed good predictions of experimental test results.

This tool is seen to be practical for engineers in industry; where it could be used for rating existing bridges under current loading and under different expected loading scenarios in the future, so that the designers could propose different rehabilitation scenarios and get an estimation of the expected corresponding fatigue life and the current damage level. Moreover, this tool is programmed using a powerful object oriented design

using the C# language to facilitate extensions and adding of new models and rules for interaction between input parameters.

6.4 Conclusions

1. The proposed VTLC method captures different ratios of low to high (L-H) loading patterns with a relatively small error, and showed better predictions than the non-conservative results obtained using Miner's LDR rule.
2. Miner's LDR rule has good predictions for loading patterns with block stress ratio $r_b = S_2/S_1$ which is very close to constant amplitude loading (close to unity). [Where S_2 is the block's low stress level and S_1 is the block's high stress level, respectively]
3. Although the VTLC method takes a linear (thus a more simple) trend in modeling fatigue damage, it proved to result in very good fatigue life predictions (comparable to those obtained by Corten's rule) just by taking into account the nonlinear effects of overloading.
4. Analysing the experimental results of fatigue lives of different riveted connections details showed that they have scattered fatigue lives at the same stress levels. Therefore, riveted steel connections need to be further classified into subcategories as classifying them into category D is conservative in many cases, as was the case of the analysed bridge in Croatia.
5. Using the theory of critical distances along with a $\pm 15\%$ variation in the calculated critical length proved to be a good approach to get a range for the expected fatigue life. This assumption is compatible with the probabilistic nature of fatigue, proven by the scatter of the test results of replica girders under the same test conditions.

6. As CorrFLP uses the concept of physical propagation of damage to a certain portion of the critical length L , thus in order to have relatively accurate fatigue life estimates, the critical surface elements should be meshed to have elements of sizes close to 0.01 mm. This is automatically done in CorrFLP using the Parent-Child element sub-meshing.
7. The reduced integration elements C3DR of ABAQUS give more numerically realistic fatigue life predictions than fully integrated solid elements C3D.
8. The augmented Lagrange method is recommended for modeling the interaction surfaces between steel components. Modeling the surfaces with no friction taken into consideration is preferred as this gives a more conservative life estimate.
9. The newly proposed strain-life corrosion fatigue model along with using $\gamma_{corr} \pm 0.05$ has very good agreement with reported experimental results of twenty-four beams tested under various fatigue and weathering conditions.
10. The effect of the maximum applied stress was found to be of significant importance in this study and was taken into account by the factor $\gamma_{corr} \gamma_\sigma$ which is a function in the ratio σ_{max} / σ_u . The relation between the ratio σ_{max} / σ_u and the factor $\gamma_{corr} \gamma_\sigma$ was found to be inversely proportional with a linear trend.
11. Analysing the experimental results available for fatigue lives of corroded beams, it was found that modeling corrosion just by geometrically reducing the steel section is not reliable. It is important to implement the newly proposed strain-life model to account for the effect of corrosion and different levels of maximum applied stresses.

6.5 Recommendations for future work

1. The proposed overloading factor in the proposed stress-life VTLC model needs to be investigated for other types of steel. It can also be extended to account for the crack closure phenomenon.
2. An experimental research program should be carried out to further investigate the proposed standardized procedure for determining the corrosion material constants for several types of steel.
3. In this study, the proposed material-environment properties α_b and α_c where assumed to be constant. Provided enough experimental data becomes available, a sensitivity analysis is required to determine how these two factors may vary based on the material's elastic and plastic properties.
4. The environmental corrosivity intensity factor γ_{corr} should be correlated to the categories provided by the ISO-9223 (1992) and the ISO-9224 (1992) to standardize this factor.
5. Further experimental work is needed to calibrate the proposed function for $\gamma_{corr} \gamma_\sigma$ to check if the behaviour interpreted in the current research would be applicable to other types of steel.
6. The effect of pitting on the acceleration of the process of fatigue life deterioration should be further investigated.
7. The guidelines provided for generation of environmentally dependant S-N curves should be implemented to create more precise categories for different riveted connections and assemblies.

REFERENCES

- AASHTO** AASHTO LRFD BRIDGE DESIGN SPECIFICATIONS (SI). Washington, D.C. : American Association of State Highway and Transportation Officials, 2007.
- AASHTO** Manual for Maintenance Inspection of Bridges (1983, Interim 1989) Washington, D.C. : American Association of State Highway and Transportation Officials, 1989.
- Abe H.** Fatigue Strength of Corroded Steel Plates from Old Railway Bridges. IABSE Symposium. Lisbon, 1989: 205-210.
- Adamson D.E. and Kulak G.L.** Fatigue Test of Riveted Bridge Girder. Structural Engineering Report No. 210. Department of Civil Engineering, University of Alberta, 1995.
- Albrecht P. et al.** Guidelines for the use of weathering steel in bridges. Washington : National Cooperative Highway Research Program (NCHRP - Report 314), 1989.
- Albrecht P. and ShabShab C.** 1994. Fatigue Strength of Weathered Rolled Beam Made of A588 Steel. Journal of Materials in Civil Engineering: Vol. 6, Issue 3.
- Albrecht P.** Fatigue Design Stresses for weathering steel structures. Corrosion Fatigue: Mechanics, Metallurgy, Electrochemistry, and Engineering (Book auth. Crooker T., W., Leis B., N. and Eds.) ASTM STP 801, 1983.
- Al-Emrani M.** Fatigue in Riveted Railway Bridges. Göteborg, Sweden : Steel and Timber Structures, Chalmers University of Technology, 2002. Doctoral Thesis.
- Ansys** 2011.
<http://www.ansys.com/Products/Simulation+Technology/Structural+Mechanics/ANSYS+nCode+DesignLife>. (accessed 2011)
- AREA** "Steel Structures," Manual for Railway Engineering, Chapter 15. American Railway Engineering Association, 1987.
- AREMA** Manual for Railway Engineering. American Railway Engineering and Maintenance-of-Way Association, 2011.
- Argon A. S.** Effect of Surface on Fatigue Crack initiation. Connecticut : Corrosion Fatigue: Chemistry, Mechanics and Microstructure, NACE and AIME, 1971: 176-210.
- ASCE** Infrastructure Report Card 2005. ASCE, 2005.
<http://www.asce.org/reportcard/2005/page.cfm?id=22>. (accessed 2011)
- Baker K.A. and Kulak G.L.** 1985. Fatigue of Riveted Connections. Canadian Journals of Civil Engineering: 184-191.
- Bannantine J. A. and Socie D. F.** A variable Amplitude multiaxial fatigue life prediction method. Fatigue under biaxial and multiaxial loading, Proc. Third International Conference on Biaxial/Multiaxial Fatigue. Stuttgart, 1989.

- Barsom J.M. and Rolfe S.T.** MNL41-3RD : Fracture and Fatigue Control in Structures: Applications of Fracture Mechanics, Third Edition, 1999.
- Baumel A. Jr. and Seeger T.** Materials data for cyclic loading, supplement 1. El Sevier Science Publisher BV, 1990.
- Bluhm J. I.** A note on fatigue damage. Materials Research and Standards, 1962.
- Boden Harald** Approaches in Modeling the Impact of Air Pollution-Induced Material Degradation, 1989.
- Brown M. W. and Miller K. J.** 1973. A theory of fatigue under multiaxial strain conditions. Proc. Inst. Mech. Eng.: Vol. 187: 745-755.
- Brühwiler E., Smith I. F. C. and Hirt M. A.** 1990. Fatigue and Fracture of Riveted Bridge Members. Journal of Structural Engineering: Vol. 116, Issue 1: ISSN 0733-9445/90/0001-0198.
- Cerit M., Genel K. and Eksi S.** 2009. Numerical investigation on stress concentration of corrosion pit. Engineering Failure Analysis: Vol. 16, Issue 7: 2467-2472.
- CHBDC CAN/CSA-S6-06 - Canadian Highway Bridge Design Code**, 2006.
- Chen Huating, Grondin Gilbert Y. and Driver Robert G.** Fatigue Resistance of High Performance Steel. Structural Engineering Report No. 258. University of Alberta, 2005.
- Cochrane V. H.** Rules for rivet hole deductions in tension members. Engineering News-Record, 1922. - Vol. 89. 847-848.
- Cojocaru D. and Karlsson A.M.** 2008. An object-oriented approach for modeling and simulation of crack growth in cyclically loaded structures. Advances in Engineering Software: Vol. 39: 995–1009.
- Corten H. T. and Dolan T. J.** 1956. Cumulative Fatigue Damage. International Conference on Fatigue of Metals, Institute of Mechanical Engineering. London: 235-246.
- Cui Weicheng** 2002. A state-of-the-art review on fatigue life prediction methods for metal structures. Journal of Marine Science and Technology: Vol. 7: 43-56.
- D. Cojocaru A.M. Karlsson** 2006. A simple numerical method of cycle jumps for cyclically loaded structures. International Journal of fatigue: Vol. 28: 1677-1689.
- DeJong S. J. and Heffernan P. J., MacDougall, C.** 2009. Periodic Overload Corrosion Fatigue of MMFX and Stainless Reinforcing Steels. J. Mater. Civ. Eng.: Vol. 21, Issue 1.
- Dessault-Systems** Abaqus 6.10 User Documentation, Dessault Systems, 2010.
- DiBattista J.D. and Kulak G.L.** Fatigue of Riveted Tension Members. Structural Engineering report No. 211. University of Alberta, Department of Civil Engineering, 1995.

- Dowling N. E.** A Discussion of Methods for Estimating Fatigue Life. Proceedings of the SAE Fatigue Conference, Dearborn, Mich., Society of Automotive Engineers. - Warrendale, PA, 1999: 161-174.
- Dowling N. E. and Begley J. A.** 1976. Fatigue Crack Growth during Gross plasticity and the J-integral. Mechanics of Crack Growth, ASTM: Vol. STP 590: 82-103.
- Downing S. D. and Socie D. F.** 1982. Simplified Rainflow Cycle Counting Algorithms. Int. J. Fatigue: Vol. 4, Issue 1: 31-40.
- Doyle J. L., Wood G. R. and Bondurant D. P.** 1990. Using Laser-based profilometry to locate and measure Corrosion fatiguecracking in boiler tubes. Materials Evaluation: 556-560.
- Drapper John** Modern Metal Fatigue Analysis, 2008.
- Du Ming Liang** Study of fatigue Proces in Air and Corrosive Environments using Optical Methods, Ph.D. Dissertation, New York, 1998.
- Duquette D.** 1998. Corrosion Fatigue Crack Initaltion Processes: A State-of-the-art Review. Environment-Induced Cracking of metals: 45-54.
- ECCS** Recommendations for the Fatigue Design of Steel Structures. Brussels, Belgium : European Convention for Constructional Steelwork, ECCS Technical Committee 6, 1985.
- El Haddad M. H., Smith K. N. and Topper T. H.** 1979. Fatigue crack propagation of short cracks. Journal of Engineering Materials and Technology (Trans. ASME): Vol. 101: 42-46.
- Elber W.** 1970. Fatigue Crack Closure under Cyclic Tension. Engineering Fracture Mechanics: Vol. 2: 37-45.
- Ellyin F.** Fatigue Damage, Crack Growth and Life Prediction. New York : Chapman & Hall, 1997.
- El-Sisi A.A.** Behaviour of Steel connections under fatigue loading, Ph.D. Thesis, 2009.
- Engelstad Stephen P. and Haj-Ali Rami M.** Cracked Hole Finite Element Modeling. Georgia Institute of technology, Atlanta, 2001.
- Eurocode3** prEN 1993-1-9: Eurocode 3 : Design of steel structures, Part 1.9 : Fatigue, May 2003.
- Everett R. A.** 1992. Comparison of Fatigue Life Prediction Methodologies for Rotorcraft. Journal of the American Helicopter Society: Vol. 37, Issue 2: 54-60.
- Fatemi A. and Yang L.** 1998. Cumulative fatigue damage and life prediction theories: a survey of the state of the art for homogeneous materials. Int. J Fatigue: Vol. 20: 9-34.
- FemFat** 2011.
- <http://www.femfat.com> (accessed 2011)

Fe-Safe - Safe Technology, 2011.

<http://www.safetechnology.com>. (accessed 2011)

Fisher J. W. et al. Fatigue and Fracture Evaluation for rating riveted bridges. Pennsylvania : NCHRP (National Cooperative Highway Research Program), 1988.

Fisher J. W. et al. Fatigue and Fracture Evaluation for Rating Riveted Bridges. Washington, D.C. : National Cooperative Highway Research Program Report 302, Transportation Research Board, National Research Council, 1987.

Fisher J. W., Yen B. T. and Wang D. Fatigue of Bridge Structure -A Commentary and Guide For Design, Evaluation and Investigation of Cracking. Bethlehem, Pennsylvania : ATLSS Report No.89-02, Lehigh university, 1989.

Fisher J.W. Bridge Fatigue Guide. New York: American Institute of Steel Construction, 1977.

Fisher J.W., Yen B.T. and Wang D. 1990. Fatigue Strength of Riveted Bridges Members. Journal of structural Engineering: Vol. 116, Issue 11: 2986-2981.

Forsberg B. Utmattningshållfasthet hos äldre konstruktionsstål med korrosionsskador. Master thesis 1993:064E. Division of Steel Structures Luleå University of Technology, 1993. ISSN: 0349-6023.

Freudenthal A. M. and Heller R. A. 1959. On Stress interaction in fatigue and cumulative damage rule. Journal of Aero/Space Science: Vol. 26: 431-442.

Frost N. E., March K. J. and Pook L. P. Metal Fatigue. Clarendon Press, Oxford., 1974.

Gangloff R. 1990. Corrosion Fatigue Crack Propagation in Metals. Environment-Induced Cracking of Metals, NACE-10: 55-110.

Gatts R. R. 1961. ASME Journal of Basic Engineering: Vol. 83: 529-540.

Goodman J. Mechanics Applied to Engineering (Book Section). London : Longmans Green, 1899.

Hancq D. Alfred, Walters Andrew J. and Beuth Jack L. 2000. Development of an Object-Oriented Fatigue Tool. Engineering with Computers: Vol. 16: 131-144.

Hashin Z. and Rotem A., A. 1978. A cumulative damage theory of fatigue failure. Materials Science and Engineering: Vol. 34, Issue 2: 147-160.

Helmerich R., Brandes K. and Herter J. Full Scale Laboratory Fatigue Tests on Riveted Railway Bridges. Evaluation of Existing Steel and Composite Bridges, IABSE Workshop. Lausanne, 1997: 191-200.

Henry D. L. 1955. A theory of fatigue damage accumulation in steel. Transactions of the ASME: Vol. 77: 913-918.

Hunsche A. and Neumann P. 1988. Crack Nucleation Persistent Siipbands. Philadelphia: ASTM STP 924: Vol. Basic Questions in Fatigue: I: 26-38.

- Hwang W. and Han K. S.** 1986. Cumulative Damage Models and Multi-stress Fatigue Life Prediction. *Journal of Composite Materials*: Vol. 20, Issue 125.
- ISO9223** Corrosion of metals and alloys- Classification of corrosivity of atmospheres.
- ISO-9223** Corrosion of metals and alloys-Corrosivity of atmospheres-Classification. Geneva, 1992.
- ISO-9224** Corrosion of metals and alloys-Corrosivity of atmospheres-Guiding for the corrosivity categories. Geneva, 1992.
- Josi G., Grondin G. Y. and Kulak G. L.** Fatigue of Bearing-Type Shear Splice. University of Alberta, 1999. Structural Engineering Report No. 227.
- Josi Georg, Grondin Gilbert Y. and Kulak Geoffrey L.** Fatigue of Bearing-Type Shear Splice. Structural Engineering Report No. 227. University of Alberta, 1999.
- Kandil F. A., Brown M. W. and Miller K. J.** 1982. Biaxial low cycle fatigue fracture of 316 stainless steel at elevated temperatures. London : The Metals Society: Vol. 280 :745-755.
- Kawahara M. et al.** 1988. Corrosion fatigue Crack initiation of carbon steels in Seawater. *ASTM STP 924*: Vol. II: 145-163.
- Koch G. H. et al.** Corrosion cost and prevention strategies in the United States. McLean, Va. : Report No. FHWA-RD-01-156, Office of Infrastructure Research and Development, Federal Highway Administration, 2002.
- Kramer I. R.** 1974. A mechanism of fatigue failure. *Metallurgical Transactions*: Vol. 5: 1735-1742.
- KTS** Corrosion Doctors. Kingston Technical Software, 2010.
<http://corrosion-doctors.org>. (accessed 2011)
- Kühn B. et al.** Assessment of Existing Steel Structures - Recommendations for Estimation of the Remaining Fatigue Life. Luxembourg : EUR 23252 EN.: Office for Official Publications of the European Communities, 2008.
- Kulak G. L.** High Strength Bolting. CISC, 2005.
- Kulicki J.,M. et al.** Guidelines for Evaluating Corrosion Effects In Existing Steel Bridges. National Cooperative Highway Research Program (NCHRP) Report 333, 1990.
- Kunihiro T., Inove K. and Fukuda T.** Atmospheric exposure study of weathering steel. Tokyo, Japan : Research Lab. Report Br. 71-08, Ministry of Construction, 1972. (In Japanese).
- Leipholtz H.H. E.** 1986. On the modified S-N curve for metal fatigue prediction and its experimental verification: Vol. 23, Issue 3: 495-505.
- Leis B. N., Gowda C. V. B. and Topper T. H.** 1973. Cyclic Inelastic Deformation and the Fatigue Notch Factor. Symposium on Cyclic Stress–Strain Behavior Analysis, Experimentation, and Failure Prediction, Bal Harbour, Fla.. - Philadelphia: ASTM STP 519: 133-150.

- Li Z. X., Ko J. M. and Chan T. H. T.** 2001. Modelling of load interaction and overload effect on fatigue damage of steel bridges. *Fatigue & Fracture of Engineering Materials & Structures*, (June): Vol. 24, Issue 6: 379–390.
- Lounis Z.** 2007. Aging highway bridges. *Canadian Consulting Engineer*: 30-34.
- Mang F. and Bucak O.** Application of the S-N line concept for the assessment of the remaining fatigue life of old bridge structures. *Bridge Management 2. Inspection, maintenance*, 1993. ISBN: 0 7277 1926 2.
- Manson S. S. and Halford G. R.** 1981. Practical implementation of double linear damage rule and damage curve approach for treating cumulative fatigue damage. *International Journal of Fracture*: Vol. 17, Issue 2.
- Manson S. S., Freche J. C. and Ensign S. R.** 1967. Application of double linear damage rule to cumulative fatigue. In *Fatigue Crack Propagation*: Vol. ASTM STP 415: 384-412.
- Marco S. M. and Starkey W. L.** 1954. A concept of fatigue damage. *Transactions of the ASME*: Vol. 76: 627-632.
- Miner M. A.** 1945. Cumulative damage in Fatigue. *Journal of Applied Mechanics*: Vol. 67: A159-A164.
- Morrow J. and Socie D. F.** Evolution of Fatigue Crack Initiation Life Prediction Methods. *Materials, Experimentation and Design in Fatigue. Proceedings of Fatigue '81*, Warwick University, England, Sherratt, F., and Sturgeon, J.B. (Editors), Westbury House. - Guildford, 1981. 3-21.
- Moses E. Schilling, E. A., and Raju, K. S.** Fatigue Evaluation Procedures for Steel Bridges. Washington, D.C. : National Cooperative Highway Research Program Report 299, Transportation Research Board, National Research Council, 1987.
- MSC** 2011.
<http://www.mscsoftware.com/Products/CAE-Tools/MSC-Fatigue.aspx>.
 (accessed 2011)
- NACE** Atmospheric Corrosion 2011.
<http://events.nace.org/library/corrosion/AtmCorros/iso9223.asp>. (accessed 2011)
- nCode**, 2011.
<http://www.ncode.com>. (accessed 2011)
- Neuber H.** Theory of notch stresses: principles for exact calculation of strength with reference to structural form and material. 2nd Edition. Berlin : Springer, 1958.
- Novak S., R.** Corrosion Fatigue crack initiation behaviour of four structural steels. *Corrosion Fatigue: Mechanics, Metallurgy, Electrochemistry, and Engineering*, ASTMSTP 801, (Book auth. Crooker T. W., Leis B., N. and Eds.). American Society for Testing and Materials, 1983.
- Out J.M.M., Fisher J.W. and Yen B.T.** 1984. Fatigue Strength of Weathered and Deteriorated Riveted Members. *Transportation Research Record* 950: Vol. 2: 10-20.

- Paepegem W. Van and Degrieck J.** 2002. Effects of Load Sequence and Block Loading on the Fatigue Response of Fibre-reinforced Composites. *Mechanics of Advanced Materials and Structures*: Vol. 9, Issue 1: 19-35.
- Paepegem W. Van, Degrieck J. and De Baets P.** 2001. Finite Element approach for modelling fatigue damage in fibre-reinforced composite materials. *Composites: Part B*: Vol. 32: 575-588.
- Palmgren** 1924. A Die Lebensdauer von Kugellagern. Verfid-mwsrrchinik. Berlin: Vol. 68: 339-341.
- Papuga Jan** Mapping of Fatigue Damages - Program Shell of FE-Calculation, Ph.D. Thesis. Prague, 2005.
- Paris P. C., Gomez M. P. and Anderson W. P.** 1961. A Rational Analytic Theory of Fatigue. *The Trend in Engineering*: Vol. 13: 9-14.
- Peterson RE.** Notch sensitivity. Metal Fatigue (Book auth. Sines G. and Waisman JL). New York : McGraw Hill, 1959.
- Radaj D. and Sonsino C. M.** Fatigue Assessment of Welded Joints by Local Approaches. Cambridge, England : Abington Publishing, 1998.
- Reemsnyder H. S.** 1975. Fatigue Life Extension of Riveted Connections. *Journal of the Structural Division*. Proceedings of the American Society of Civil Engineers: Vol. 101, No. ST12: 2591-2608.
- Rice R. C., Leis B. N. and Nelson D. V.** Fatigue Design Handbook, Second Edition. Warrendale, PA : Society of Automotive Engineers, 1988.
- Schutz W.** 1996. A History of fatigue. *Engineering fracture mechanics*: Vol. 54: 263-300.
- Sehitoglu H.** 1983. Fatigue Life Prediction of Notched Members Based on Local Strain and Elastic-Plastic Fracture Mechanics Concepts. *Engineering Fracture Mechanics*. Vol. 18, Issue 3: 609-621.
- Smith K. N., Watson P. and Topper T. H.** 1970. A stress-strain function for the fatigue of metals. *J. Mater*: Vol. 5, Issue 4: 767-778.
- Subramanyan S.** 1976. A Cumulative Damage Rule Based on the Knee Point of the S-N Curve. *ASME Journal of Engineering Materials*: Vol. 98, Issue 4: 316-321.
- Taylor D.** A Compendium of Fatigue Thresholds and Growth Rates. EMAS, 1985.
- Taylor D.** 2008. The theory of critical distances: Vol. 75: 1696-1705.
- Trethewey K. R. and Chamberlain J.** Corrosion for students of science and engineering. New York : Wiley, 1988.
- USACE(EM) US Army Corps of Engineers Engineer Manual** Inspection, Evaluation, and Repair of Hydraulic Steel Structures, 2001: 1110-2-6054.
- Vernon W.H.J.** 1935. A Laboratory Study of the Atmosphere Corrosion of Metals. *Trans.*

Xiulin et al. 1996. Fatigue Performance of Old Bridge Steel and the Procedures For Life Prediction With Given Survivability. Engineering Fracture Mechanics: Vol. 53, Issue 2: 251-262.

Zhou et al. 1995. Examination of Fatigue Strength (Sr-N) Curves for Riveted Bridge Members. Engineers Society of Western Pennsylvania. - Pittsburg : 12th International Bridge Conference.

APPENDIX A

This section provides a sample C# code used for derivation of the VTLC parameters using the data provided by Corten et al.

```
struct CaseStudy
{
    public double TotalCyclesPerBlock;
    public double Alpha;
    public double S1;
    public double S2;
    public double Nactual;
    public double BasquinExponent;
    public double FatigueStrength;

    public CaseStudy(    double FirstStress,
                        double SecondStress,
                        double CyclesToFailure,
                        double Ratio,
                        double TotalCyclesInBlock,
                        double Basquin,
                        double Sf)
    {
        TotalCyclesPerBlock = TotalCyclesInBlock;
        Alpha = Ratio;
        S1 = FirstStress;
        S2 = SecondStress;
        Nactual = CyclesToFailure;
        BasquinExponent = Basquin;
        FatigueStrength = Sf;
    }

    public double n1
    {
        get { return Alpha * TotalCyclesPerBlock; }
    }

    public double n2
    {
        get { return (1 - Alpha) * TotalCyclesPerBlock; }
    }
}

class Program
{
    static void Main(string[] args)
    {
        // Create an array of case studies
        CaseStudy[] c = new CaseStudy[31];

        // 96000 .. 76000 (Series B, R = 0.79, Rr = 0.2) b = 0.28
        c[0] = new CaseStudy(96000, 76000, 55348, 0.4, 10000, -0.13137, 369200);
        c[1] = new CaseStudy(96000, 76000, 97499, 0.1, 10000, -0.13137, 369200);
        c[2] = new CaseStudy(96000, 76000, 121423, 0.04, 10000, -0.13137, 369200);
        c[3] = new CaseStudy(96000, 76000, 129509, 0.01, 10000, -0.13137, 369200);
    }
}
```

```

// 96000 .. 66000 (Series A, R = 0.69, Rr = 0.3125) b = 0.10
c[4] = new CaseStudy(96000, 66000, 60187, 0.4, 10000, -0.136314, 381640);
c[5] = new CaseStudy(96000, 66000, 133567, 0.1, 10000, -0.136314, 381640);
c[6] = new CaseStudy(96000, 66000, 221055, 0.04, 10000, -0.136314, 381640);
c[7] = new CaseStudy(96000, 66000, 269650, 0.01, 10000, -0.136314, 381640);
c[8] = new CaseStudy(96000, 66000, 297440, 0.047, 10000, -0.136314, 381640);

// 96000 .. 46000 (Series B, R = 0.48, Rr = 0.52) b = 0.019
c[9] = new CaseStudy(96000, 46000, 83560, 0.4, 10000, -0.13137, 369200);
c[10] = new CaseStudy(96000, 46000, 293900, 0.1, 10000, -0.13137, 369200);
c[11] = new CaseStudy(96000, 46000, 599100, 0.04, 10000, -0.13137, 369200);
c[12] = new CaseStudy(96000, 46000, 974990, 0.01, 10000, -0.13137, 369200);

// 86000 .. 76000 (Series C, R = 0.88, Rr = 0.116) b = 0.146
c[13] = new CaseStudy(86000, 76000, 115378, 0.1, 10000, -0.13137, 375000);
c[14] = new CaseStudy(86000, 76000, 172902, 0.04, 10000, -0.13137, 375000);
c[15] = new CaseStudy(86000, 76000, 183992, 0.01, 10000, -0.13137, 375000);

// 86000 .. 66000 (Series B, R = 0.77, Rr = 0.233) b = 0.106
c[16] = new CaseStudy(86000, 66000, 127174, 0.4, 10000, -0.13137, 369200);
c[17] = new CaseStudy(86000, 66000, 235288, 0.1, 10000, -0.13137, 369200);
c[18] = new CaseStudy(86000, 66000, 290670, 0.04, 10000, -0.13137, 369200);
c[19] = new CaseStudy(86000, 66000, 333273, 0.01, 10000, -0.13137, 369200);

// 86000 .. 56000 (Series B, R = 0.65, Rr = 0.35) b = 0.0096
c[20] = new CaseStudy(86000, 56000, 458142, 0.1, 10000, -0.13137, 369200);
c[21] = new CaseStudy(86000, 56000, 648485, 0.04, 10000, -0.13137, 369200);
c[22] = new CaseStudy(86000, 56000, 864172, 0.013, 10000, -0.13137, 369200);

// 86000 .. 46000 (Series B, R = 0.53, Rr = 0.47) b = 0.0001
c[23] = new CaseStudy(86000, 46000, 175227, 0.4, 10000, -0.13137, 369200);
c[24] = new CaseStudy(86000, 46000, 611646, 0.1, 10000, -0.13137, 369200);
c[25] = new CaseStudy(86000, 46000, 1122536, 0.04, 10000, -0.13137, 369200);
c[26] = new CaseStudy(86000, 46000, 1809256, 0.013, 10000, -0.13137, 369200);

// 76000 .. 66000 (Series A, R = 0.87, Rr = 0.132)
c[27] = new CaseStudy(76000, 66000, 220850, 0.40, 10000, -0.136314, 381640);
c[28] = new CaseStudy(76000, 66000, 282358, 0.10, 10000, -0.136314, 381640);
c[29] = new CaseStudy(76000, 66000, 338532, 0.04, 10000, -0.136314, 381640);

int Counter = 0;
bool AllSatisfied = true;

double MinSumError = 100000;

#region VTLC1

//for (double c1 = -100; c1 <= -4; c1 -= .5)
//    for (double c2 = 1.0; c2 <= 1; c2 += .5)
//        //for (double bi = 0.0001; bi <= 0.002; bi += 0.0001) // 0.0037
//        //    //for (double p = 0.02; p <= 0.1; p += 0.001) // 0.0037
//        for (double d = 100; d <= 100; d += 20) // 0.0037
//        for (double p = .3; p <= .3; p += .1) // 0.0037
//        for (double B = 2.7; B <= 2.7; B += 0.1) // 0.0037
//        for (double D = 05; D <= 05; D += 10) // 0.0037
//        {
//            double SumError = 0;
//            double MinError = 100, MaxError = 0;
//            double N = 0;
//
//            double c1 = 0 ; //, c2 = 2.6;
//            //double bi = 0; // 0.0016;
//            //double p = 0.04;
//
//            // double d = 460;
//            // double p = 1;
//            //double B = 2.7; with c1 = a = 1 // gave best results

```

```

        AllSatisfied = true;

        for (int i = 0; i <= 29; i++)
        {
            double Nact = c[i].Nactual;
            N = VTLC2(c1, c2, B, d, c[i], D, false, false, p);

            double Error = (Math.Abs(N - c[i].Nactual)/c[i].Nactual)*
100;

            if (Error > MaxError)
                MaxError = Error;

            if (Error < MinError)
                MinError = Error;

            Counter++;
        }

//if (AllSatisfied) //&& MinSumError >= SumError
{
    MinSumError = SumError;

    System.IO.StreamWriter fout =
        new StreamWriter("C:\\\\Numbers.txt");

    for (int i = 0; i <= 29; i++)
    {
        N = VTLC2(c1, c2, B, d, c[i], D, false, false, p);

        double Error = (Math.Abs(N - c[i].Nactual)/c[i].Nactual)*
100;
        fout.WriteLine(N.ToString("N0"));

    }

    Console.WriteLine("B = " + B
+ ", d = " + d
+ ", D% = " + D
+ ", p = " + p
+ ", Max Error = " + MaxError);

    fout.Close();
}
}

#endif

}

// Damage Using Linear Loss in Life with
// Constant Jump magnitude based on the S2/S1 ratio
static double VTLC1( double c1,
                      double c2,
                      double B,
                      double BjumpInitial,
                      CaseStudy Case,
                      double Dcritical,
                      bool ConservativeOnly,
                      bool PrintError,
                      double power)
{
    // Some variables
    int n1, n2, Nact;
    double S1, S2, Alpha;
}

```

```

    double b, Sf;
    double Nf1, Nf2;
    double Increment = 100; // Cycles
    double TotalCycles = 0;

    // Initialization
    b = Case.BasquinExponent;
    Sf = Case.FatigueStrength;
    S1 = Case.S1;
    S2 = Case.S2;
    Alpha = Case.Alpha;
    Nactual = (int)Case.Nactual;

    // Cycles per block
    n1 = (int)(10000 * Alpha);
    n2 = (int)(10000 * (1 - Alpha));

    // Slopes
    double m = -1 / b; // S-N Slope at failure
    double mv0 = B*m; // Slope of Virgin (virtual Life Curve)
    double mv = mv0; // Slope of S-N curve at any time (Very IMPORTANT)
    double Dm0 = mv - m; // Reference change in slope

    // Failure Lives
    Nf1 = Math.Pow(S1 / Sf, -m);
    Nf2 = Math.Pow(S2 / Sf, -m);

    // Virtual target Lives
    double NVTL1 = Math.Pow((S1 / Sf), -mv);
    double NVTL2 = Math.Pow((S2 / Sf), -mv);

    // Loss in Life (dN)
    double dN1 = NVTL1 - Nf1;
    double dN2 = NVTL2 - Nf2;

    double Level1Ratio = dN1 / Nf1;
    double Level2Ratio = dN2 / Nf2;

    int n = 0;
    double Bjump = 0;

    double FatigueLimit = 0;
    double DamagePercentage = 0;
    bool Terminate = false;

    // Stage 1
    while (true)
    {
        n = 0;

        Terminate = false;

        // Stress Level 1
        while (n < n1)
        {
            // Damage curves constants (ai , ri)
            double ai = c1 * (S1 / Sf) + c2;
            double ri = Dm0 / Math.Pow(dN1, ai);

            int Partial = n1 - n;

            if (Partial >= Increment)
            {
                n += (int)Increment;

                // Extra initial Jump
                if (n == Increment && S1 > S2 && TotalCycles != 0 )

```

```

    {
        double R = S2/S1;

        power = 60*R*R - 65*R + 17.1; // equation 1
        power = 100 * R * R - 120 * R + 36; // equation 2

        double power2 = 18.43 * R - 11.8; // equation 3

        power = 0;

        double StressRatioModifier = 1-(Math.Pow(S2/ S1, power));

        double dDmj = Dm0 / BjumpInitial * StressRatioModifier;

        mv -= dDmj;

    }

    // Count additional cycles
    TotalCycles += Increment;
}
else
{
    n += Partial;

    TotalCycles += Partial;
}

// Get the change in slope due to accumulated cycles
double dDm = ai * ri * Math.Pow(TotalCycles + Increment / 2, ai - 1)
*
Increment * Math.Pow(Level1Ratio, 1/ai);

// Get the updated slope
mv -= dDm;

// Calculate Virtual Life
NVTL1 = Math.Pow((S1 / Sf), -mv );

if (TotalCycles >= NVTL1)
{
    Terminate = true;
    break;
}

}

if (Terminate)
break;

n = 0;

// Stress Level 2
while (n < n2)
{
    // Damage curves constants (ai , ri)
    double ai = c1 * (S2 / Sf) + c2;
    double ri = Dm0 / Math.Pow(dN2 , ai);

    int Partial = n2 - n;

    if (Partial >= Increment)
    {
        n += (int)Increment;

        // Extra initial Jump
        if (n == Increment && S2 > S1 && TotalCycles != 0)
        {
            //Bjump += BjumpInitial;
        }
    }
}

```

```

                //Db += Bjump;
            }

            // Count additional cycles
            TotalCycles += Increment;
            //Nacc = Math.Pow((Dm / ri), (1 / ai)) + Increment;
        }
        else
        {
            n += Partial;

            if (n == Increment && S2 > S1 && TotalCycles != 0)
            {
                //Bjump += BjumpInitial;
                //Db += Bjump;
            }

            // Count additional cycles
            TotalCycles += Partial;
            //Nacc = Math.Pow((Dm / ri), (1 / ai)) + Partial;
        }

        double dDm = ai * ri * Math.Pow(TotalCycles + Increment / 2, ai - 1)
*
Increment * Math.Pow(Level2Ratio, 1/ai);

// Get the change in slope due to accumulated cycles
//Dm = ri * Math.Pow(Nacc, ai); ;

// Get the updated slope
//mv = mv0 - Dm;
mv -= dDm;

// Calculate Virtual Life
NVTL2 = Math.Pow((S2 / Sf), -mv);
//RemainingLife = NVTL2 - Nacc;

if (TotalCycles >= NVTL2)
{
    Terminate = true;
    break;
}
}

if (Terminate)
{
    break;
}

// Console.WriteLine("Nacc2 = " + Nacc + ", NVTL = " + NVTL + ", "
TotalCycles Until Now = " + TotalCycles);

}

//double PosError = (Nact - TotalCycles)/(double)Nact;

//if (PrintError && Error < ErrorPercent / 100)
//    Console.WriteLine("At S1 = " + S1 + ", S2 = " + S2 + ", c1 = " + c1 +
", c2 = " + c2 + ", Binit = " + BjumpInitial + ", B = " + B + ", Nexp/Nact = (" +
(int)TotalCycles + "/" + (int)Nact + ")" + ", Error = " + (Error * 100).ToString("N2") +
"%");

return TotalCycles;
}

// Damage Using Linear Loss in Life with
// Constant Jump magnitude based on the S2/S1 ratio

```

```

    static double VTLC2(double c1, double c2, double B, double BjumpInitial,
CaseStudy Case, double Dcritical, bool ConservativeOnly, bool PrintError, double power)
{
    B = 2;

    // Some variables
    int n1, n2, Nact;
    double S1, S2, Alpha;
    double b, Sf;
    double Nf1, Nf2;
    double Increment = 100; // Cycles
    double TotalCycles = 0;

    // Initialization
    b = Case.BasquinExponent;
    Sf = Case.FatigueStrength;
    S1 = Case.S1;
    S2 = Case.S2;
    Alpha = Case.Alpha;
    Nact = (int)Case.Nactual;

    Alpha = 1;

    // Cycles per block
    n1 = (int)(10000 * Alpha);
    n2 = (int)(10000 * (1 - Alpha));

    // Slopes
    double m = -1 / b; // S-N Slope at failure
    double mv0 = B * m; // Slope of Virgin (virtual Life Curve)
    double mv = mv0; // Slope of S-N curve at any time (Very IMPORTANT)
    double Dm0 = mv - m; // Reference change in slope

    // Failure Lives
    Nf1 = Math.Pow(S1 / Sf, -m);
    Nf2 = Math.Pow(S2 / Sf, -m);

    // Virtual target Lives
    double NVTLo1 = Math.Pow((S1 / Sf), -mv);
    double NVTLo2 = Math.Pow((S2 / Sf), -mv);

    double x = Math.Pow(Nf1, B);

    double NVTL1 = NVTLo1;
    double NVTL2 = NVTLo2;

    // Loss in Life (dN)
    double dNo1 = NVTLo1 - Nf1;
    double dNo2 = NVTLo2 - Nf2;

    double Level1Ratio = dNo1 / Nf1;
    double Level2Ratio = dNo2 / Nf2;

    int n = 0;
    double Bjump = 0;

    double FatigueLimit = 0;
    double DamagePercentage = 0;
    bool Terminate = false;

    // Stage 1
    while (true)
    {
        n = 0;
        Terminate = false;

```

```

// Stress Level 1
while (n < n1)
{
    // Damage curves constants (ai , ri)
    double ai = c1 * (S1 / Sf) + c2;
    double ri = Dm0 / Math.Pow(dNo1, ai);

    int Partial = n1 - n;

    if (Partial >= Increment)
    {
        n += (int)Increment;

        // Extra initial Jump
        if (n == Increment && S1 > S2 && TotalCycles != 0)
        {

            power = 60*R*R - 65*R + 17.1; // equation 1
            power = 100 * R * R - 120 * R + 36; // equation 2

            double power2 = 18.43 * R - 11.8; // equation 3

            power = 0;

            double StressRatioModifier = 1-(Math.Pow(S2/ S1, power));

            double dDmj = Dm0 / BjumpInitial * StressRatioModifier;

            mv -= dDmj;

        }

        // Count additional cycles
        TotalCycles += Increment;
    }
    else
    {
        n += Partial;

        TotalCycles += Partial;
    }

    // Calculate Virtual Life
    NVTL1 = NVTL1 / Increment;

    if (TotalCycles >= NVTL1)
    {
        Terminate = true;
        break;
    }
}

if (Terminate)
    break;

n = 0;

// Stress Level 2
while (n < n2)
{
    // Damage curves constants (ai , ri)
    double ai = c1 * (S2 / Sf) + c2;
    double ri = Dm0 / Math.Pow(dNo2, ai);

    int Partial = n2 - n;

    if (Partial >= Increment)

```

```

        {
            n += (int) Increment;

            // Count additional cycles
            TotalCycles += Increment;
        }
        else
        {
            n += Partial;

            // Count additional cycles
            TotalCycles += Partial;
        }

        // Calculate Virtual Life
        NVTL2 = NVTL2/Increment;

        if (TotalCycles >= NVTL2)
        {
            Terminate = true;
            break;
        }
    }

    if (Terminate)
        break;

}

//double PosError = (Nact - TotalCycles)/(double)Nact;

//if (PrintError && Error < ErrorPercent / 100)
//    Console.WriteLine("At S1 = " + S1 + ", S2 = " + S2 + ", c1 = " + c1 +
", c2 = " + c2 + ", Binit = " + BjumpInitial + ", B = " + B + ", Nexp/Nact = (" +
(int)TotalCycles + "/" + (int)Nact + ")" + ", Error = " + (Error * 100).ToString("N2") +
"%");

return TotalCycles;
}

static double CortenDolan(    double Ra,
                                ref double CorrespondingA,
                                CaseStudy Case,
                                double ErrorPercent,
                                bool ConservativeOnly,
                                bool PrintError)
{
    double B = 0.5;
    int n1, n2, Nact;
    double S1, S2, Alpha;
    double b, Sf;
    double Nf1, Nf2;
    double TotalCycles = 0;
    double Error = 0;

    // Initialization
    b = Case.BasquinExponent;
    Sf = Case.FatigueStrength;
    S1 = Case.S1;
    S2 = Case.S2;
}

```

```

Alpha = Case.Alpha;
Nact = (int)Case.Nactual;

Nf1 = Math.Pow(S1 / Sf, 1 / b);
Nf2 = Math.Pow(S2 / Sf, 1 / b);

double RHS, LHS;
double A = 0.01;

double MinError = 10000000;

do
{
    RHS = Nact * Alpha + Ra * (1 - Alpha) * Math.Pow(Nact, A);

    LHS = Nf1;

    Error = (Math.Abs(LHS - RHS) / LHS) * 100;

    if (MinError >= Error)
    {
        MinError = Error;
        CorrespondingA = A;
        // Calcualte CorrespondingN = Nact;
    }

    A += 0.0001;

} while (A <= 4);

return MinError;
}

}

```

APPENDIX B

This appendix lists the materials database available in CorrFLP:

- Stainless_Steel_30304_Cold_Rolled_BHN_327
- Stainless_Steel_30304_Hot_Rolled_BHN_160
- Stainless_Steel_30304_Su_650
- Stainless_Steel_30310_Hot_Rolled_BHN_145
- Steel_1005_HR_Sheet_Su_359
- Steel_1008_HR_Sheet_Su_363
- Steel_1015_Normalized_Su_414
- Steel_1018_BHN_120
- Steel_1020_HR_Plate_BHN_108
- Steel_1020_BHN_120
- Steel_1020_Su_455
- Steel_1040_Cold_Drawn_BHN_225
- Steel_1045_Normalized_BHN_153
- Steel_1045_Annealed_BHN_225
- Steel_1045_Q_T_BHN_277
- Steel_1045_Q_T_BHN_336
- Steel_1045_Q_T_BHN_390
- Steel_1045_Q_T_BHN_410
- Steel_1045_Q_T_BHN_500
- Steel_1045_Q_T_BHN_563
- Steel_1045_Q_T_BHN_595
- Steel_4130_BHN_259
- Steel_4130_Q_T_BHN_366
- Steel_4140_Q_T_BHN_293
- Steel_4140_Q_T_BHN_475
- Steel_4142_As_Quenched_BHN_670
- Steel_4142_Q_T_BHN_380
- Steel_4142_Q_T_BHN_400
- Steel_4142_Q_T_BHN_450_b_0_076
- Steel_4142_Q_T_BHN_450_b_0_086
- Steel_4142_Q_T_BHN_475
- Steel_4340_Hot_Rolled_BHN_243
- Steel_4340_Q_T_BHN_275
- Steel_4340_Q_T_BHN_409
- Steel_4340_Su_1172
- Steel_5160_Q_T_BHN_430
- Steel_8630_Cast_BHN_254
- Steel_9262_BHN_260
- Steel_9262_BHN_275
- Steel_9262_BHN_405
- Steel_Maraging_18Ni_250_BHN_500
- Steel_300M_Su_1958
- Steel_4130_sheet_Su_806
- Steel_4130_sheet_Su_1241
- Steel_4340_bar_Su_862
- Steel_4340_bar_Su_1090
- Steel_4340_bar_Su_1482
- Steel_4340_bar_Su_1896
- Steel_8620H_Case_Su_1600
- Steel_8620H_Core_Su_1510
- Steel_A27_Cast_BHN_135
- Steel_A36_HAZ_BHN_243
- Steel_A36_BHN_160
- Steel_A36_Su_540

- Steel_A514_HAZ_BHN_461
- Steel_A514_BHN_303
- Steel_A_517_Grade_F_BHN_256
- Steel_E110_WM_1P_Weld_Metal_BHN_362
- Steel_E110_WM_2P_Weld_Metal_BHN_310
- Steel_E60S_3_WM_1P_Weld_Metal_BHN_233
- Steel_E60S_3_WM_2P_Weld_Metal_BHN_201
- Steel_H1000_Su_1448
- Steel_H1000_bar_Su_1414
- Steel_H1050_sheet_Su_1386
- Steel_H900_bar_Su_1393
- Steel_H950_bar_Su_1689
- Steel_HY130_Su_1103
- Steel_IN787_BHN_188
- Steel_ManTen_Su_565
- Steel_RQC_100_Su_863
- Steel_TH1050_sheet_Su_1386
- Steel_TH1050_sheet_Su_1207
- Aluminum_1100_Su_110
- Aluminum_5454_Forged_Su_334
- Aluminum_2014_T6_Su_510
- Aluminum_2014_T6_Hand_Forged_Su_483
- Aluminum_2014_T6_Su_496_44
- Aluminum_2024_T3_Su_490
- Aluminum_2024_T3_Su_496
- Aluminum_2024_T4_Su_476
- Aluminum_2024_T6_Su_475
- Aluminum_5083_0_BHN
- Aluminum_5083_H12_Su_385
- Aluminum_5183_0_Weld_metal_BHN_92
- Aluminum_5456_H311_Su_400
- Aluminum_6061_T6_Forged_Su_389
- Aluminum_6061_T6_Sheet_Su_314
- Aluminum_6061_T6_Hand_Forged_Su_340
- Aluminum_6061_T6_Su_310
- Aluminum_7049_T73_Su_537
- Aluminum_7049_T73_Su_517
- Aluminum_7050_T7351X_Su_517
- Aluminum_7050_T7451_plate_Su_544
- Aluminum_7050_T7451_plate_Su_530
- Aluminum_7050_T7452_Su_537
- Aluminum_7050_T7452_Su_524
- Aluminum_7050_T7651X_Su_599
- Aluminum_7075_T6_Su_572
- Aluminum_7075_T6_Su_579
- Aluminum_7075_T6_Su_565_b_0_105
- Aluminum_7075_T6_Su_565_b_0_172
- Aluminum_7075_T651_Su_580
- Aluminum_7149_T73_Su_503
- Aluminum_7175_T73_Hand_Forged_Su_524
- Aluminum_7175_T73611_Su_524
- Aluminum_7175_T74_Su_510
- Aluminum_7475_T7351_plate_Su_482
- Aluminum_Cast_A356_T6_Su_252
- Aluminum_Cast_A356_T6_Su_266
- Aluminum_Cast_A356_T6_Su_283

APPENDIX C

The regression analysis performed in this section was adopted from the method used by Josi et al. (1999). Regression analysis of the test data was used to derive S-N curves that can be described using the following equation:

$$\log(\Delta\sigma) = \frac{\log(C)}{m} - \frac{\log(N_f)}{m} \quad (C-1)$$

For simplicity, the notation $\log(\Delta\sigma)$ will be replaced by y , $\log(N_f)$ by x , $\log(C)/m$ by a and $-1/m$ by b to have the following form:

$$y = a + bx \quad (C-2)$$

Using the least squares fitting method, the slope b and the intercept a of the best fit line with "n" test results can be obtained from:

$$b = \frac{S_{xy}}{S_{yy}} \quad (C-3)$$

where

$$S_{xy} = \sum_{i=1}^n (x_i - \bar{x})(y_i - \bar{y}) \quad (C-4)$$

$$S_{yy} = \sum_{i=1}^n (y_i - \bar{y})^2$$

and "a" can be obtained from :

$$a = \bar{y} - b\bar{x} \quad (C-5)$$

To measure the goodness of fit of the regression model, the correlation coefficient R^2 can be used:

$$R^2 = \frac{S_{xy}^2}{S_{xx} S_{yy}} \quad (C-6)$$

where

$$S_{xx} = \sum_{i=1}^n (x_i - \bar{x})^2 \quad (C-7)$$

A statistical comparison of mean values of two sets of test results (y_1 and y_2) can be carried out using Student's t test :

$$t = \frac{|\bar{y}_1 - \bar{y}_2|}{\sqrt{\frac{\sum (y_1 - \bar{y}_1)^2 + \sum (y_2 - \bar{y}_2)^2}{(n_1 - 1) + (n_2 - 1)} \times \left(\frac{n_1 + n_2}{n_1 n_2}\right)}} \quad (C-8)$$

If a 95 percent level of confidence is defined, then t should not be greater than 2.776 in order to conclude there is no significant difference between the two variances.